AFRL-ML-TY-TR-2006-4521

SELECTION OF A MATERIAL MODEL FOR SIMULATING CONCRETE MASONRY WALLS SUBJECTED TO BLAST

James S. Davidson and Lee Moradi
University of Alabama at Birmingham
Department of Civil and Environmental Engineering
140 Hoehn Building, 1075 13th Street South
Birmingham, AL 35294-4440

Robert J. Dinan
Air Force Research Laboratory
139 Barnes Drive, Suite 2
Tyndall AFB, FL 32403-5323

Interim Report, Feb 2004

Air Force Research Laboratory
Materials and Manufacturing Directorate
Airbase Technologies Division
139 Barnes Drive, Suite 2
Tyndall AFB, FL 32403-5323

REPORT DOCUMENTATION PAGE

Form Approved
OMB No. 0704-0188

PLEASE DO NOT RETURN YOUR FORM TO THE ABOVE ORGANIZATION.

1. REPORT DATE *(DD-MM-YYYY)*	2. REPORT TYPE	3. DATES COVERED *(From - To)*
01-02-2004	Interim Technical Report	01-09-2002 - 31-05-2003

4. TITLE AND SUBTITLE

Selection of a Material Model for Simulating Concrete Masonry Walls Subjected to Blast

5a. CONTRACT NUMBER

F08637-02-C-7027

5b. GRANT NUMBER

5c. PROGRAM ELEMENT NUMBER

63112F

6. AUTHOR(S)

Davidson, James S.; Moradi, Lee; Dinan, Robert J.

5d. PROJECT NUMBER

4918

5e. TASK NUMBER

C10B

5f. WORK UNIT NUMBER

4918C10B

7. PERFORMING ORGANIZATION NAME(S) AND ADDRESS(ES)

University of Alabama at Birmingham
Department of Civil and Environmental Engineering
140 Hoehn Building, 1075 13th Street South
Birmingham, AL 35294-4440

8. PERFORMING ORGANIZATION REPORT NUMBER

9. SPONSORING/MONITORING AGENCY NAME(S) AND ADDRESS(ES)

Air Force Research Laboratory, Materials and Manufacturing Directorate
Airbase Technologies Division, Force Protection Branch
139 Barnes Drive, Suite 2
Tyndall AFB, FL 32403-5323

10. SPONSOR/MONITOR'S ACRONYM(S)

AFRL/MLQF

11. SPONSOR/MONITOR'S REPORT NUMBER(S)

AFRL-ML-TY-TR-2006-4521

12. DISTRIBUTION/AVAILABILITY STATEMENT

Distribution Statement A: Approved for public release; distribution unlimited.

13. SUPPLEMENTARY NOTES

Technical contact: Dr. Robert J. Dinan, AFRL/MLQF, 850-283-3605. Report contains color images.

14. ABSTRACT

One of the most common methods of construction is the use of concrete masonry units (CMU) in the walls of buildings. However, they are vulnerable to blast, and result in collapse, fragmentation, and severe injury to occupants. An understanding of the behavior of CMU walls during blast is key to developing mitigation techniques. Research has been conducted using the finite element method to simulate structural failure due to blast. A common problem faced by model developers is the selection of constitutive relationships that appropriately simulate the behavior of materials subjected to shock loading. This project examined the effect of blast impulse loading on CMU blocks. Finite element models were used to perform direct transient analysis using various material cards available in LS-DYNA, and the results were compared to the results of full-scale blast tests conducted by AFRL. The material card that best agreed with the test results was recommended for use in the models of polymer reinforced masonry walls.

15. SUBJECT TERMS

finite element, concrete masonry units, blast reponse, LS-DYNA material card, polymer reinforced

16. SECURITY CLASSIFICATION OF:			17. LIMITATION OF ABSTRACT	18. NUMBER OF PAGES	19a. NAME OF RESPONSIBLE PERSON
a. REPORT	b. ABSTRACT	c. THIS PAGE			Elizabeth Trawinski
U	U	U	UU	147	19b. TELEPHONE NUMBER *(Include area code)* 850-283-3605

NOTICE

Using Government drawings, specifications, or other data included in this document for any purpose other than Government procurement does not in any way obligate the U.S. Government. The fact that the Government formulated or supplied the drawings, specifications, or other data does not license the holder or any other person or corporation; or convey any rights or permission to manufacture, use, or sell any patented invention that may relate to them.

This technical report was reviewed and cleared for public release by the Air Force Research Laboratory Tyndall Site (AFRL/MLQ) Public Affairs Office (PAO) and is releasable to the National Technical Information Service (NTIS). Reference PAO Case Number: 06-019

This report is releasable to the National Technical Information Service (NTIS) where it will be available to the general public, including foreign nationals.

5285 Port Royal Road
Springfield VA 22161
Telephone (703) 487-4650, (703) 487-4639 (TDD for the hearing impaired)
e-mail: orders@ntis.fedworld.gov
http://www.ntis.gov/index.html

This technical report is approved for publication.

/s/
ELIZABETH TRAWINSKI, 1st Lt, USAF
Work Unit Manager

/s/
AL D. NEASE
Chief, Force Protection Branch

/s/
JIMMY L. POLLARD, Colonel, USAF
Chief, Airbase Technologies Division

This report is published in the interest of scientific and technical information exchange and its publication does not constitute the Government's approval or disapproval of its ideas or findings.

ABSTRACT

Building material fragmentation is a major cause of human injury during intentional or unintentional explosions. One of the most common methods of construction is the use of concrete masonry units (CMU) in the walls of buildings. CMUs provide a fast and inexpensive way to construct building facilities of various heights. However, they are vulnerable to blast, and result in collapse, fragmentation, and severe injury to occupants. An understanding of the behavior of CMU walls during blast is key to developing mitigation techniques. Research has been conducted using the finite element method to simulate structural failure due to blast. A noteworthy effort in this area is the research performed by the University of Alabama at Birmingham (UAB) for the Force Protection Branch of the Air Force Research Laboratory (AFRL), Tyndall Air Force Base (AFB), which uses LS-DYNA finite element software to simulate CMU walls. A common problem faced by model developers is the selection of constitutive relationships that appropriately simulate the behavior of materials subjected to shock loading. This project examined the effect of blast impulse loading on CMU blocks. Finite element models were used to perform direct transient analysis using various material cards available in LS-DYNA. The results were compared to the results of full-scale blast tests conducted by AFRL. The material card that best agreed with the test results was recommended for use in the models of polymer reinforced masonry walls.

TABLE OF CONTENTS

Page

LIST OF FIGURES

Figure **Page**

LIST OF ACRONYMS

AFB	Air Force Base
AFRL	Air Force Research Laboratory
ANFO	Ammonium Nitrate and Fuel Oil
CFRP	Carbon Fiber-Reinforced Plastics
CMU	Concrete Masonry Unit
CONWEP	Conventional Weapon Effect
ERDC	Engineering Research and Development Center
FE	Finite Element
ft	Foot
in	Inch
ln	Natural logarithm
m-sec	Milli-seconds
psi	Pounds per square inch
SDOF	Single Degree of Freedom System
TCCMAR	Technical Coordinating Committee for Masonry Research
UAB	University of Alabama at Birmingham
WAC	Wall Analysis Code

CHAPTER 1

INTRODUCTION

In today's society, there is an increasing risk of terrorist attacks by radical groups, political separatists, and those people who intend to injure, and even kill, innocent people. Attacks of this nature can be carried out with relative ease by anyone who has such intent. The most widely used type of device in such an attack is the bomb. The simplest of bombs may consist only of a container carrying fuel, an oxidizer, and a detonation device. Bombs are easily concealed and are commonly delivered by vehicles, in postal packages, and even on foot.

Terrorist attacks commonly target crowded facilities, such as office buildings and restaurants, not to mention military installations. Most casualties and injuries sustained in such attacks are not caused by the blast itself, but rather by the disintegration and fragmentation of walls, the shattering of windows, and by non-secured objects that can be propelled at high velocities by the blast. Ensuring that the exterior walls of a structure are able to withstand a blast and not produce deadly fragments is an important part of minimizing injuries to building occupants.

Most civilian structures are constructed with lightly reinforced or un-reinforced exterior walls without any consideration to blast loading (Crawford et al. 1997a). These exterior walls must therefore be strengthened to increase the resistance to blast loads. One of the most common ways to reinforce a wall for blast loading is to increase the mass of the wall. This can be achieved by applying additional concrete and steel reinforcement. Reinforcing an existing wall with additional concrete and steel is not only time-consuming and expensive, but provides little insurance for containment of deadly fragments and projectile. For this reason, a need has risen for an expedient and efficient method for reinforcing existing concrete and masonry walls.

One of the most common methods of construction is the use of Concrete Masonry Units (CMU) in the walls of buildings. CMUs provide a fast and inexpensive way to construct building facilities of various heights. However, they are extremely vulnerable to the high pressures induced by blast, and result in collapse, fragmentation, and severe injury to occupants. An understanding of structural behavior of CMU walls during blast is key to developing mitigation techniques. Much research has been conducted using explosive tests as well as finite element methods to examine structural failure due to blast. The Air Force Research Laboratory (AFRL) at Tyndall Air Force Base, Florida, has been testing the effectiveness of polymer reinforcement for protection against blast loadings through full-scale explosive testing. This type of testing is expensive and requires much preparation. However, the explosive testing can be supplemented with computer models. The use of finite element models allows a variety of structures and retrofit materials to be evaluated with relatively low expense in a much shorter time frame.

A noteworthy effort in this area is the research performed at the University of Alabama at Birmingham (UAB), Department of Civil and Environmental Engineering,

under the direction of Dr. Jim Davidson. This research makes use of LS-DYNA finite element software to simulate full-scale models of CMU walls. One common problem faced by UAB researchers and other researchers in this field is the selection of constitutive relationships for the elements used in these models that yield accurate results under blast-impulsive loading.

1.1 Objectives

The objective of this project was to determine the most appropriate LS-DYNA material model for simulating concrete masonry units subjected to blast. A finite element model of the CMU was used to perform direct transient analysis for the various material cards available in LS-DYNA. The results of full scale blast tests conducted by the Air Force Research Laboratory (AFRL) at Tyndall Air Force Base (AFB) were used as one measure of evaluation.

1.2 Scope and Methodology

Explosive tests were planned with AFRL engineers and conducted at Tyndall Air Force Base. Painted CMUs were placed on a radius at various distances from the blast source. Each color designated the distance of the CMU from the source. After the test, image data and failure description data was obtained from each test specimen and provided to UAB for analysis. High-fidelity finite element models were developed using the DYNA-3D finite element software (LS-DYNA 1999). Eight material cards were initially considered. The simulated blast loads were checked for accuracy in application, and the model was analyzed using four material cards. The results were compared to the test data provided by AFRL to examine the performance of each constitutive model. The model and the MAT card inputs were adjusted until results matched.

1.3 Report Organization

This report is organized into five chapters. Chapter 1 is an introduction that gives an overview of the objectives, scope, methodology, and organization of the report. Chapter 2 is a review of previously published literature concerning the strength of masonry walls exposed to blast loads and modeling. Chapter 3 presents the discussion of the full-scale explosive tests performed at Tyndall AFB, Florida, using single CMUs. The test setup, test results, and a discussion of the results are also included in Chapter 3. Chapter 4 discusses the development of the high-fidelity finite element model in conjunction with four constitutive relationships provided by LS-DYNA for concrete structures to examine the behavioral characteristics of a single CMU during the actual blast tests. Chapter 5 discusses the results of the analyses for various constitutive models, and compares these results with the blast tests. Chapter 6 provides an overall summary for the report, highlights the conclusions derived from the research, and sets forth recommendations for further research.

CHAPTER 2

LITERATURE REVIEW

The largely empirical design of masonry structures does not "rely extensively on the rational application of engineering principles," which can result in the designer not fully recognizing all of the relevant design variables (Yokel and Dikkers 1971). Design variables such as loading geometry, end fixity, wall stiffness, and cross-sectional properties can have significant effects on the overall strength of masonry walls. In May of 1971, Yokel and Dikkers reported a study on the strength of load bearing masonry walls based on 192 full-scale masonry wall tests previously conducted by the National Bureau of Standards and the Structural Clay Products Institute. This study used rational analysis methods, which were based upon established theory, to predict the strength of load bearing masonry walls (Yokel and Dikkers 1971).

2.1 Retrofit Measures for Seismic Loads

Masonry walls normally have predictable and adequate performance when subjected to static in-plane loading. However, masonry walls tend to perform poorly when subjected to out-of-plane loading, such as the loading caused by an earthquake. Extensive research has been conducted in the out-of-plane behavior of masonry walls. In-depth dynamic studies arose as part of an investigation into the renovation of unreinforced masonry buildings in Los Angeles (Martini 1996). In earthquake regions, typical unreinforced masonry walls lack the strength and ductility to survive seismic loads. Carbon overlays have been investigated as a repair and retrofit technique for masonry walls during tests of single-story masonry walls (Laursen et al. 1995). The carbon overlays were used in an attempt to enhance shear and flexural strength. The test results indicated "significant strength and deformation capacities increases" (Laursen et al. 1995).

Strengthening of individual structural components for seismic loading has also been the subject of numerous experimental tests. The retrofit of structural components with advanced composite materials has become popular in light of recent earthquakes. Bridge columns were the focus of an advanced composite material seismic retrofit study by Seible and Karbhari. Both circular and rectangular bridge columns were retrofitted with composite jackets of glass fiber reinforcement and resin. Resin systems such as polyesters, vinylesters, and epoxies were used as the matrix of the composite materials (Seible and Karbhari 1996). The composite jacket designs were determined to be as effective as steel jackets in improving deformation capacity levels of columns subjected to seismic loading.

Other structural components, such as reinforced concrete beams, have also been retrofitted and tested. In 1994, C. Allen Ross performed a study looking into the hardening and rehabilitation of concrete structures using carbon fiber-reinforced plastics (CFRP). The application of CFRP panels to the tension side of conventional reinforced concrete beams resulted in an increase in maximum load carrying capacity (Ross et al. 1994). The CFRP performed well on beams with less than 1% tensile steel

reinforcement. However, beams with more than one percent tensile steel reinforcement experienced delamination of the CFRP panels due to the low bond strength between the panels and the adhesive (Ross et al. 1994).

Experimental testing of retrofit techniques has also been applied to full-scale structures. The Technical Coordinating Committee for Masonry Research (TCCMAR) constructed a full-scale five-story building and performed simulated seismic load tests on the structure. After the original test, repair and retrofit techniques were applied to damaged and undamaged components of the structure. "The principal objective was to increase the deformation capacity of the building without increasing the flexural stiffness or strength since the latter would increase the shear demand" (Weeks et al. 1994). Carbon fiber overlays, polymer-concrete repairs, and epoxy injection techniques were used to enhance the shear transfer in walls, beams, and floor panels. The repair and retrofit test results were compared to the results from the original test. The test results indicated "that the individual repair measures and components of the repaired five-story building performed very well" (Weeks et al. 1994). The repaired building exhibited an increase in load carrying capacity, along with an increased capacity for deformation.

2.2 Retrofit Measures for Explosive Loads

Retrofit techniques that were originally designed for seismic loading have also been investigated for their use in strengthening concrete masonry structures against explosive, or blast, loading. For instance, column-jacketing techniques that have been used to improve the response of seismically loaded reinforced concrete columns have also been analyzed for effectiveness in reducing explosive-induced damage. It has been found that multi-story reinforced concrete structures typically collapse with the failure of just a small number of outer support columns. Outer support columns tend to fail "in shear near the supports" when subjected to blast loadings (Crawford et al. 1997b). These columns can be retrofitted and strengthened by the use of steel or composite material jackets. Finite element analysis of explosively loaded columns has shown that jacketing techniques can increase the "strength and ductility of concrete" (Crawford et al. 1997b).

During the summer of 1994, the United States participated in a composite retrofit material study with the Israeli Home Front Command. This study was performed to better understand the effects of blast loadings on concrete and masonry structures strengthened with composite retrofit materials. Based upon dynamic testing conducted at Tyndall Air Force Base, Florida, two retrofit materials were selected for the first phase of the study: an autoclaved 3-ply carbon fiber composite laminate, and a knitted biaxial fiberglass fabric (Purcell et al. 1995). Phase I of the test series consisted of full-scale explosive tests against structures retrofitted with the composite materials. This phase was conducted in Qiryat Gat, Israel. Israeli civil engineers constructed the structures used in the test. Each structure had 8 in. thick wall panels that were reinforced with 3/8 in. rebar spaced 12 in. center to center. The retrofit materials were bonded to the wall surfaces in order to maximize their effects. To ensure a proper bond, the wall panels were cleaned and then primed with Sikadur 62. The carbon fiber laminate and the knitted fiberglass fabric were bonded to the wall panels using HYSOL 9460 epoxy adhesive (Purcell et al. 1995).

Conventional Weapon Effect (CONWEP) software was used to calculate a standoff distance for a cylindrically shaped explosive charge of TNT (Purcell et al. 1995).

This standoff distance was calculated to ensure breaching of the wall panels. The results of the tests showed that the retrofit materials had a significant effect on the amount of wall displacement caused by the explosive charge. The knitted fiberglass fabric outperformed the carbon fiber composite during this test. In fact, the carbon fiber composite seemed to be minimally effective. The reduced performance of the carbon fiber composite can be attributed in part to a poor bond between the material and the concrete that resulted in delamination. These tests also resulted in a recommendation for the development of a finite element analysis to predict retrofitted wall response to explosive charges (Purcell et al. 1995).

In September 1995, a blast response experiment was conducted at Eglin Air Force Base, FL. A three-story reinforced concrete building was used to evaluate the effectiveness of externally applied reinforcement. A Kevlar fabric was used to retrofit the interior side of four wall panels facing the detonation of an explosive device. The fabric was applied to the concrete walls, using HYSOL 9460 epoxy, in much the same way as the previous United States/Israeli test conducted in 1994 (Taun et al. 1995).

The test structure had the following general dimensions: 40 ft wide, 40 ft deep, and 30 ft tall. The building had 10 in. thick center walls and nine 14 in x 14 in square sectioned columns. The floors and exterior walls were 6 in. thick. The exterior walls were approximately 7.2 ft wide and 8.5 ft tall. The walls contained number 4 rebar at 18 in. spacing on center. Testing of the concrete showed an average compressive strength of 4,600 psi.

An explosive charge of Tritonal, having a TNT equivalency factor of 1.19, was used for this test. The explosive was compacted into a cylindrical container and placed at a predetermined standoff from the center wall of the building.

One major difference between this test and the United States/Israeli test was the pre-test prediction using DYNA-3D finite element code. Each wall panel was modeled neglecting the contribution from the rebar for carrying tensile stress in the concrete. The behavior of the concrete was assumed to be elastic with failure in tension (Taun et al. 1995). The Kevlar material was modeled as linearly elastic and fully bonded to the concrete walls. The models were used to predict the level of failure for the retrofitted walls.

The results of the test showed that the structural response predictions by DYNA-3D were not accurate (Taun et al. 1995). The accelerations of the walls due to the blast loading were greatly underestimated, due to the absence of reliable models for concrete behavior. Three of the four retrofitted exterior walls failed completely. It was suggested that further work be done on the optimization of the layering and fiber orientation of the retrofit materials.

The lack of usable data and reliable conclusions from the experiment greatly emphasized the need for more accurate computer models. In order to obtain higher levels of accuracy, the computer models had to become more complex so that the actual material behaviors could be simulated.

In October 1996, explosive tests were conducted to evaluate retrofit measures for conventional concrete masonry unit buildings. These tests were a continuation of the Israeli Home Front Command's research into strengthening civilian structures against terrorist threats. The tests were performed on a 5-story building and two additional test cubicles. Whiting and Coltharp, members of the US Army Engineer Waterways

Experiment Station research team, produced a paper concentrating on the two test cubicles and CMU retrofit techniques (Whiting and Coltharp 1996).

The test cubicles were constructed with load-bearing CMU frames with the assumption that the walls were part of a generic 2-story building. The CMU walls were constructed with post-tensioned steel bars in ungrouted CMU void spaces. This was done to simulate the additional weight that would be present in the 2-story structure. Several mechanical/structural retrofit techniques that had been previously used for seismic retrofit of load-bearing masonry walls were selected and evaluated for effectiveness in resisting blast loadings (Whiting and Coltharp 1996). Pilasters, shotcrete, and knee bracing were the specific retrofit measures used during the tests.

Pretest predictions were performed using SDOF applications, semi-empirical blast load calculations, and finite element analysis. The SDOF applications consisted of the Single Degree of Freedom Code and the Wall Analysis Code (WACv2). The blast load predictions and finite element analysis were performed using CONWEP and DYNA-3D, respectively. SDOF and finite element analysis was performed for each type of retrofit wall panel and a control (unretrofit) wall panel. The pre-test predictions seemed to "compare favorably with the test results" (Whiting and Coltharp 1996). Post-test photos of the wall panels were compared to DYNA-3D damage predictions, and it was concluded that "finite element code is the most accurate means of damage prediction" for complex masonry cross-sections (Whiting and Coltharp 1996).

In the fall of 1999, researchers at the AFRL began looking for retrofit techniques to increase the blast resistance of common exterior walls. One of the researcher's goals was to develop a retrofit technique that did not have difficult application processes and the high expense of commonly used methods for strengthening walls, such as increasing the mass with reinforced concrete. The need arose for a "lighter weight solution" that would "introduce ductility and resilience into building walls" (Knox et al. 2000). An elastomeric polymer, with a polyurea base, was chosen for use as a retrofit material based upon the results of material testing performed at Tyndall AFB. The material was selected based on "its strength, flammability, and cost" (Knox et al. 2000). The application method for this material was a relatively straightforward spray-on process. Proof-of-concept tests were performed using blast-loaded masonry walls and lightweight structures retrofitted with the polymer material. The material was easily sprayed onto the interior and exterior wall surfaces while maintaining control over the application thickness. The proof-of-concept tests showed that the masonry and the lightweight structure walls experienced large deflections without breaching, and that no debris entered the interior of the test structures. The lightweight structure used in the proof-of-concept tests stayed intact, but the structure experienced severe ceiling crushing which needed to be mitigated.

The successful proof-of-concept tests performed by the AFRL quickly led to the development of a lightweight structures program. Lightweight structures are generally "characterized by timber stud walls, exterior aluminum siding, and interior veneer-plywood paneling" (Knox et al. 2000). Three explosive tests were performed on structures retrofitted with the polymer material. The first test consisted of two lightweight constructed wall panels. This test was used to study the performance of the retrofit material when subjected to high rates of strain caused by explosive loading. The following two tests were conducted using "single-wide construction and house trailers"

(Knox et al. 2000). For the single-wide construction trailer, additional strengthening measures were tested along with the polymer retrofit material. Frames constructed from thin steel tubing were installed in an attempt to reduce ceiling crushing seen in the proof-of-concept tests. It was predicted that the steel frames would have little impact on wall deflections. The steel frames were installed and the spray-on polymer was applied to the interior wall surfaces and the steel frame to ensure a continuous layer of retrofit material. The house trailer was divided into three separate test sections. The right end section and the middle section of the house trailer had the same stud spacing for the steel frame and different thickness for the polymer retrofit. The left end section had a much shorter stud spacing for the steel frame with the same polymer retrofit thickness as the right end section. The house trailer test was designed to "push the envelope of the retrofit technique" by using a higher explosive yield (Knox et al. 2000).

The results of the first two tests showed that the polymer retrofit technique was successful. Even though the lightweight wall panels and structures sustained severe damage, the polymer retrofit kept significant amounts of debris out of the interior of the test structures. The higher explosive yield of the third test resulted in numerous tears in the retrofit material that were "significant enough to permit some debris fragments to enter the rooms" (Knox et al. 2000). The test structures equipped with the tubular steel frames experienced significant reductions in ceiling deflections compared to the proof-of-concept tests. The AFRL research team found that unsecured items inside the test structures, such as furniture and light fixtures, were a major source of potentially deadly flying debris. Based on the results of the tests, the research team concluded that the polymer retrofit technique would be an effective addition to a "comprehensive security program" (Knox et al. 2000).

The AFRL research team continued the development and testing of the polymer retrofit technique by shifting their focus to the retrofit of CMU walls. An overview and discussion of the CMU wall tests carried out by the AFRL, at Tyndall AFB, is presented by Connell in chapter 3.0 of his MS thesis (Connell 2002).

2.3 Computer Modeling of Masonry Walls and Retrofit Measures

In 1996, Karagozian & Case developed a number of candidate retrofit designs for increasing the blast resistance of concrete masonry walls. The retrofit designs were direct adaptations of existing seismic retrofit designs for increasing the out-of-plane load capacity of under-reinforced walls (Wesevich and Crawford 1996). Several of the retrofit designs were chosen for use as articles in explosive tests to be conducted in Israel during October of 1996. The choice of retrofit designs was based upon the availability of materials in third-world countries, ease of construction, and the feasibility of applying the designs to existing structures (Wesevich and Crawford 1996). Three retrofit designs were chosen: a single steel pilaster retrofit, a steel knee brace retrofit, and an interior shotcrete retrofit. Finite element models were developed for the chosen retrofit designs so that wall response predictions could be made prior to the explosive tests.

The finite element models for the retrofit designs were generated using DYNA-3D. Each model used 3-D continuum elements and material models that were formulated to account for the extensive nonlinear behaviors of material subjected to blast loads (Wesevich and Crawford 1996). The particular concrete material model used was developed for predicting the response of concrete to explosive loads. The material model

was also validated for the prediction of light and severe damage for reinforced concrete and masonry walls subjected to blast loading (Wesevich and Crawford 1996).

The results of the DYNA-3D analysis indicated that the knee brace and shotcrete options were the "best retrofit candidates in that the least amount of damage occurred to the wall panels for the two designs" (Wesevich and Crawford 1996). The structural integrity of the wall panels retrofit with these designs remained sound. The success of the shotcrete retrofit seems to indicate that the use of other materials, such as composites, that can be bonded to the wall surfaces may also provide positive results (Wesevich and Crawford 1996).

In April of 1997, a paper was presented at the *8th International Symposium on Interaction of the Effects of Munitions with Structures* that discussed the development of a finite element model for study of masonry walls subject to air blast loads. DYNA-3D was successfully used to model lightly reinforced and unreinforced masonry walls composed of concrete blocks (Crawford et al. 1997a). The models were used to study wall response mechanisms and several methods of reinforcement. Composite wraps, shotcrete, and the addition of pilasters were the reinforcement methods used. The study indicated that reinforcement techniques that provide uniform reinforcement are much more effective than those that discretely reinforce a wall (Crawford et al. 1997a). This study also compared DYNA-3D and simplified analysis tools such as SDOF models. It was determined that the finite element software provided a "significant improvement" in the calculation of wall responses over the simplified analysis tools (Crawford et al. 1997a).

Shope and Frank performed finite element analysis of blast-loaded concrete masonry unit walls in 1998. One-way action strip models and two-way action wall panel models subjected to blast loads were developed using the DYNA-3D software package.

For the one-way action models, two approaches were taken with regard to modeling the bond between the concrete masonry units and mortar layers. The first was the use of contact/sliding surfaces to represent the mortar joints, and the second was the use of continuum elements (Shope and Frank 1998). The contact/sliding surface approach yielded results that were "very sensitive" to a penalty stiffness factor that had "no physical basis" for selection (Shope and Frank 1998). It was determined that the contact surface approach was not an appropriate method for this type of analysis. However, the use of continuum elements showed "close agreement between DYNA-3D and theoretical single-degree-of-freedom results for one-way bending" (Shope and Frank 1998).

Significant differences in the results for two-way action wall panel models did arise between the finite element analysis and SDOF analysis. The greatest difference was seen between the fixed support condition and arching results for two-way bending (Shope and Frank 1998). It was noted that resistance functions generated by the SDOF models could be modified to give results that were closer to those from the finite element analysis. Recommendations resulting from this research included refining material models, performing failure mode comparisons, and updating the finite element models as actual physical test data becomes available (Shope and Frank 1998).

In May of 1999, a paper was presented at the *9th International Symposium on Interactions of the Effects of Munitions with Structures* that discussed the use of anchored fabrics for the retrofit of concrete masonry unit walls. SDOF and finite element models

were used in an attempt to validate test results from explosive tests conducted in Israel during May 1998 (Slawson et al. 1999).

The anchored fabric retrofit technique was not intended to strengthen the masonry walls. Its purpose was to catch hazardous debris caused by the disintegration of the wall (Slawson et al. 1999). Anchored to the roof and floor slabs of a structure, on the inside face of a wall, the fabric acts like a net that catches broken pieces of the wall and reduces the threat to occupants. Two commercially available geofabrics were used during the Israeli explosive tests. The geofabrics were successful in preventing debris from entering the interior of the test structure.

A total of six wall panel models were generated using the WAC SDOF software and the DYNA-3D finite element software. Each wall panel model was given a width of 120 in and a height of 104 in. (Slawson et al. 1999). For both the WAC and DYNA-3D models, there was one control wall and two walls that were retrofitted with the anchored fabric. The membrane resistance of the anchored fabric was added to the resistance function of the WAC-generated wall panels to account for the retrofit. The finite element models contained over 80,000 solid elements. The finite element retrofit models also contained a 40 x 40 mesh of linear-elastic membrane elements placed 0.1 in. behind the wall that represented the anchored geofabric (Slawson et al. 1999).

Results from the WAC and DYNA-3D models were compared to the data collected from the explosive tests. The results from the models did not coincide well with the results from the explosive tests. The results obtained from the models indicated that the maximum displacements for the retrofitted walls were being overestimated. It was recommended that additional experimental data would be required to fully validate the computation procedures (Slawson et al. 1999).

In June of 1999, a study of finite element modeling techniques for a CMU wall subjected to airblast loading was performed using the DYNA-3D software (Dennis 1999). A simplified modeling approach was used for this study. A simplified approach was used because of modeling difficulties that arise when complex algorithms are implemented without the fundamental characteristics being accurately known (Dennis 1999).

The finite element models were based upon nominal 8 in x 8 in x 16 in hollow concrete masonry units. Each masonry unit was comprised of 8-node solid elements. All masonry units were constructed as individual parts of a wall panel that were connected with slide surfaces that represented the mortar layers (Dennis 1999). The material properties for the concrete masonry units and the mortar were based upon the current ACI 530-95 and ASTM C 270-89 standards. These properties were used in conjunction with material models that incorporated failure and strain-rate strengthening criterion.

Model verification was performed to assure proper behavior of the models. A series of simple geometries and loadings verified the slide surface, material response, and strain-rate strengthening behavior of the DYNA-3D models (Dennis 1999). The study indicated that efficient finite element models could be generated using slide surfaces with failure criterion to represent the bond between concrete masonry units.

The U.S. Army Engineering Research and Development Center (ERDC) conducted experiments involving blast-loaded masonry walls in 1999. The goal of the experiments was to experimentally validate the finite element modeling method previously discussed. A series of five ¼-scale CMU wall experiments was performed to study the response of non-grouted, non-reinforced, one-way CMU walls to the blast

pressure from high explosives (Dennis et al. 2000). A single one-way ¼-scale CMU wall was also statically tested. Pre-test analysis and predictions were made for the ¼-scale experiments using the previously developed DYNA-3D modeling method.

The pre-test analysis was used, in part, to determine a standoff distance for the explosive charge that would ensure wall failure without the complete destruction of the test specimen. The originally calculated standoff distance was used for the first test. For the second and third tests, the standoff distance was reduced by 25%. The fourth test used the original standoff distance and was a repeat of the first test. The standoff distance for the final test was increased by 25% (Dennis et al. 2000).

Accelerometers and pressure gages were used to collect data for the five tests. Velocities and displacements for the ¼-scale walls were obtained by the integration of the recorded accelerometer data. Likewise, the recorded pressure histories were integrated to obtain the impulse history of the explosive load (Dennis et al. 2000). The test data was used to update the finite element models used for the dynamic analysis. The average pressure histories from each of the five experiments were used to load the same finite-element model used to model the static experiment and the pretest blast experiments (Dennis et al. 2000).

The results showed that the analysis method slightly overpredicted the maximum static capacity of the CMU wall (Dennis et al. 2000). The overprediction was attributed to the use of average CMU properties, and it was found that the use of lower-bound properties provided a very good estimate of the load-deflection function (Dennis et al. 2000). The use of average properties also led to the slight underprediction of the response of the walls in several of the blast-load tests (Dennis et al. 2000). For three of the five tests, the finite element analysis did not predict wall failure, even though it did predict moderate damage to the walls. Small adjustments to the applied pressure yielded results that more closely matched the failure of the experimental walls. The effects of small adjustments to the model indicate that considerable variability is to be expected in the results, and the effects also demonstrate that the analysis for both of these experiments provided reasonable, conservative results (Dennis et al. 2000).

CHAPTER 3

TEST SET-UP AND RESULTS

A variety of concrete masonry units are used in building construction. To accurately match the analysis with test results, the type of CMU that was used for the actual blast tests by the Air Force Research Laboratory at Tyndall AFB was acquired. This unit is 15.625 in long, 7.625 in wide, 7.625 in deep and has an average wall thickness of approximately 1.0 to 1.125 in. It weighs 32 lb, has a volume of 367 in^3, and has the following structural properties (Slawson et al 1999). Figure 3.0-1 shows a typical CMU.

CMU Properties
Mass Density = 0.0002247 lb s^2/in^4
Ultimate Compressive Strength (f'c) = 2000 psi
Ultimate Tensile Strength = 1/10 (f'c) = 200 - 250 psi
Ultimate Shear Strength = 100 psi

During one of the blast tests at AFRL, a total of eight (8) CMUs were colored and set-up around the blast source at various distances as shown in Figures 3.0-2 thru 3.0-4. Although Figure 3.0-3 indicates the source to be 500 lb of ANFO, the layout for the 1000 lb ANFO was the same. The coloration of the blocks made for easy identification of their distances from the source. Each colored block rested on top of a similar block

Figure 3.0-1 Typical Concrete Masonry Unit

and two small wood supports in a freestanding position to minimize boundary effects. The set-up was arranged in a circular configuration with one of the long sides of blocks facing the blast source. Refer to the notes on Figure 3.0-3 for a quick summary of test results. The AFRL tests indicated failure in the form of fracture and significant fragmentation for 500 lb ANFO at distances of 20 ft (cream in Figure 3.0-5), 25 ft (brown in Figure 3.0-6), 30 ft (purple in Figure 3.0-7) and 32 ft (pink in Figures 3.0-8 and 3.0-9). No failure was noted 35 ft (dark blue in Figure 3.0-10), 40 ft (light blue in Figure 3.0-11), 45 ft (yellow in Figure 3.0-12), and 50 ft (green in Figure 3.0-13), but the blocks would sometimes fall over as a rigid body mass. The test results for the 1000 lb ANFO showed failure and significant fragmentation at 40 ft. For distances of 45 ft and larger, no failure or fragmentation was noted, but the blocks would sometimes fall over as a rigid body mass similar to the 500 lb ANFO.

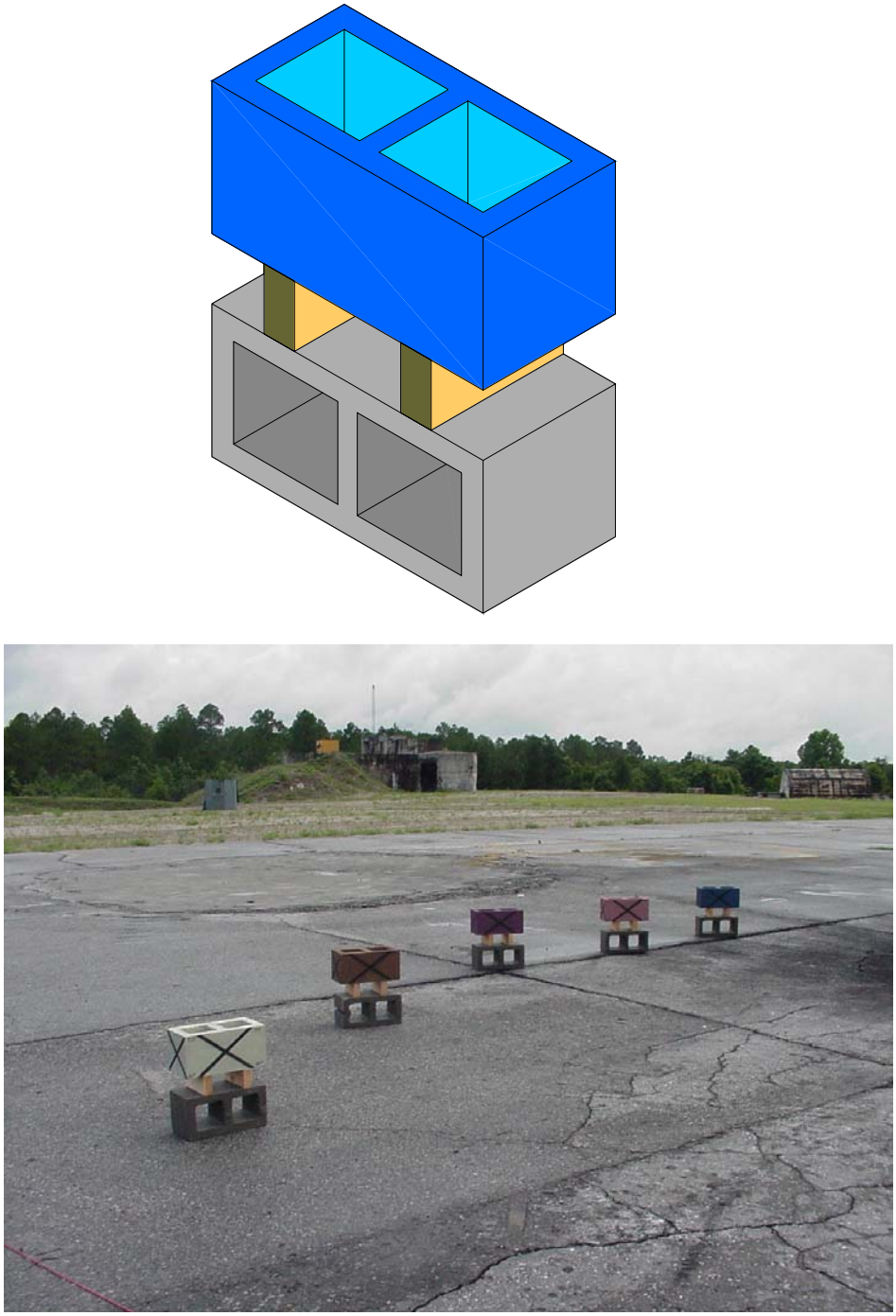

Figure 3.0-2 Test Set-up

NOTES:

1. **CMU blocks at 20', 25', 30' and 32' were broken into many pieces.**
2. **CMU block at 35', 40', 45', and 50' stayed intact. Block at 40' was broken, but appears to be from falling off support block.**
3. **The broken blocks appear to have similar failure.**
4. **The purple block had the greatest scatter area and it's pieces were found the furthest from the blast.**

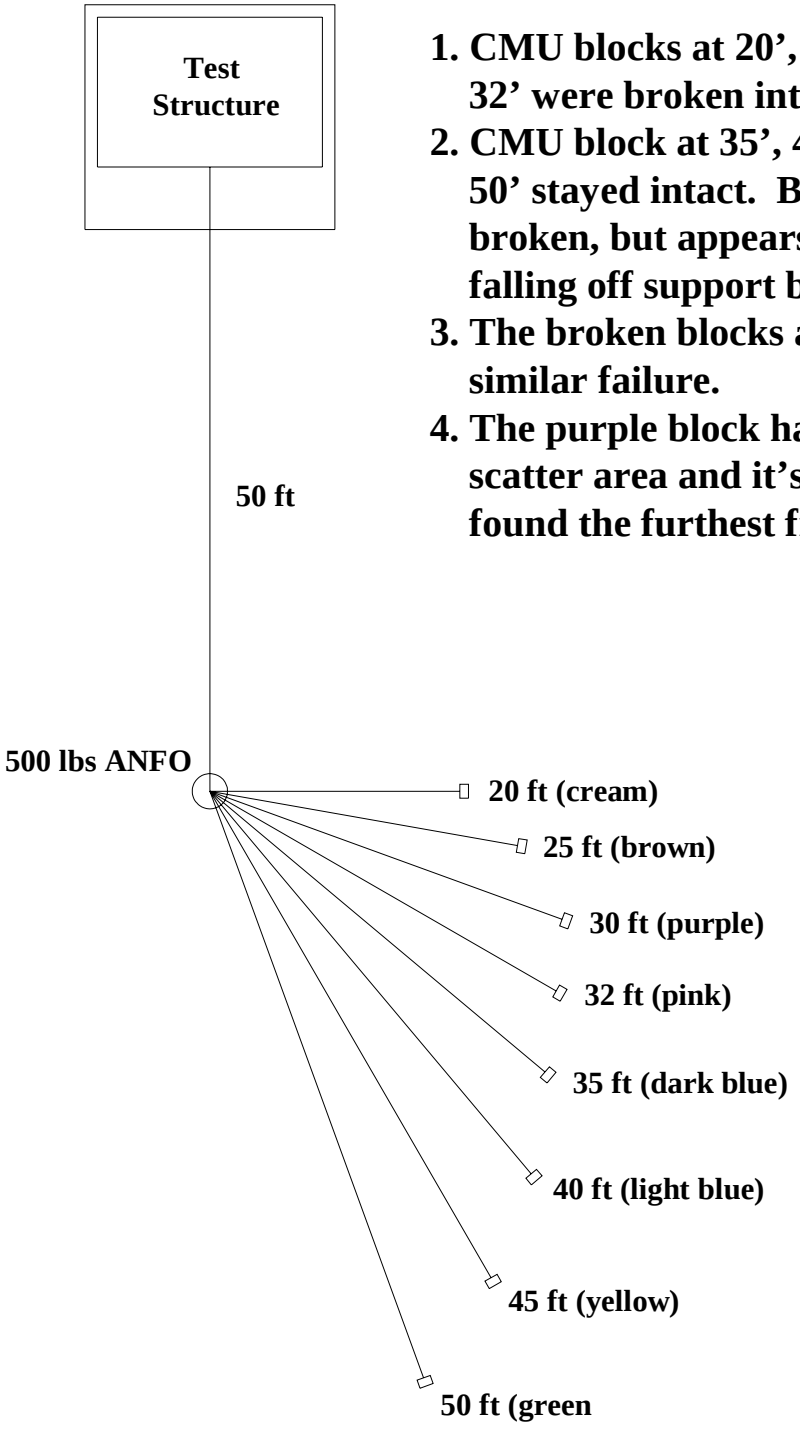

Figure 3.0-3 Test Layout for 500 lb ANFO

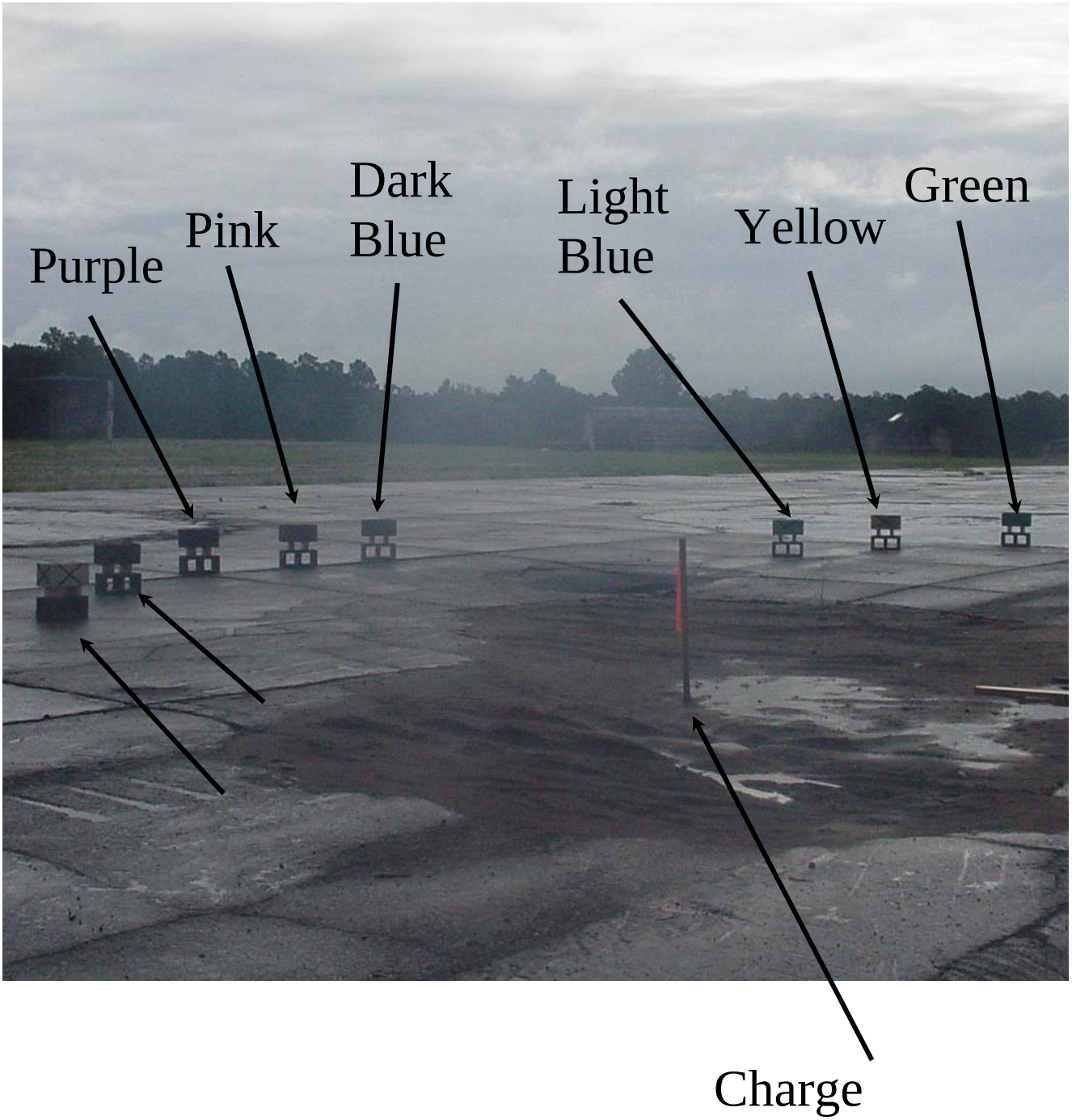

Figure 3.0-4 Test Set-up of All CMUs

Figure 3.0-5 Cream CMU at 20 ft

Figure 3.0-6 Brown CMU at 25 ft

Figure 3.0-7 Purple CMU at 30 ft

Figure 3.0-8 Pink CMU at 32 ft

Figure 3.0-9 Test #1 500 lb at 32 ft

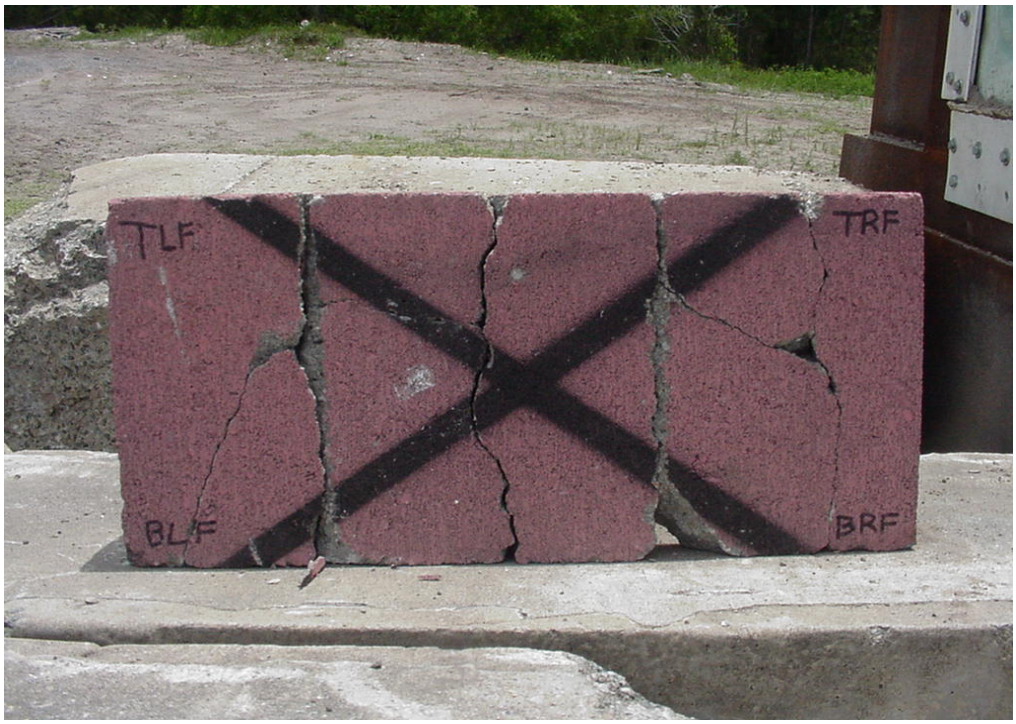

Figure 3.0-10 Test #9 500 lb at 32 ft

Figure 3.0-11 Dark Blue CMU at 35 ft

Figure 3.0-12 Light Blue CMU at 40 ft

Figure 3.0-13 Yellow CMU at 45 ft

Figure 3.0-14 Green CMU at 50 ft

CHAPTER 4

FINITE ELEMENT ANALYSIS

The model used for this project is finely meshed and incorporates 9027 nodes and 6656 elements as shown in Figure 4.0-1. Brick elements are used to simulate all components of the CMU. The front face, which is exposed to the blast loads first, has three times finer mesh than other walls in the model. The model has no boundary conditions in order to simulate the freestanding condition used in the actual blast tests.

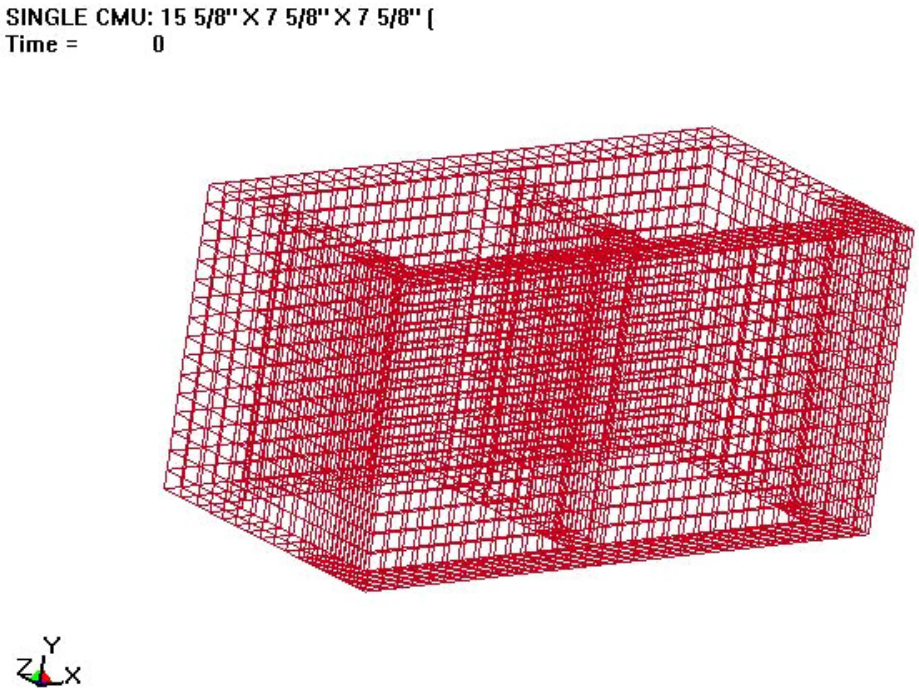

Figure 4.0-1 Isometric View of CMU Finite Element Model

The eight-node solid element in DYNA-3D was used to represent the basic elements of the model. This element has 24 degrees of freedom (three translations at each node), and computes three normal and three shear stresses (LS-DYNA Theoretical Manual 2001). The element formulation uses the lumped mass method, and the volume integration is carried out with one-point Gaussian quadrature. The greatest advantage to one-point integration is the substantial savings in computer time. On the other hand, a disadvantage to the one-point integration is the need to control zero energy modes that arise, called hourglassing modes. These modes tend to have much shorter periods than the periods of structural response, and are often observed to be oscillatory. MATSUM

and GLSTAT output files are tracked to make sure hourglass energy remains negligible, and the results are reported in Chapter 5.0.

4.1 CMU Material Properties

Material properties of common CMUs are presented in a paper titled "Evaluation of Anchorage Fabric Retrofits for Reducing Masonry Wall Debris Hazard" (Slawson et al 1999), and a paper from the US Army Corps of Engineers titled "Masonry Walls Subjected to Blast Loading – DYNA3D Analysis" (Dennis, 1999).

CMU
Weight = 32 lb
Volume = 367 in^3
Mass Density = 0.0002247 lb s^2/in^4
Ultimate Compressive Strength (f'c) = 2000 psi
E = 1000x f'c = 2,000,000 psi
Poison = 0.15 to 0.2
G = 833,333 psi
Ultimate Tensile Strength = 1/10 (f'c) = 200 - 250 psi
Ultimate Shear Strength = 100 psi

4.2 Structural Damping

Structural damping was considered for the single CMU based on recommendations from Biggs (1964) and Fintel (1974). The value of the structural damping is directly proportional to the value of critical damping calculated from (also see Appendix E):

$$c_{cr} = 2\, w\, M$$

Where:

c_{cr}: Critical Damping
w: Fundamental system frequency in terms of radians per seconds
M: Mass of system

To arrive at the fundamental system frequency of the CMU, an eigenvalue run was performed using the finite element model of the CMU. A total of 18 eigenvalues and their associated eigenvectors were calculated by DYNA-3D as shown in Appendix E. The first six eigenvalues were related to the six rigid body modes the system must experience due to its free-free boundary conditions. The 7^{th} and 8^{th} eigenvalues, at 2725 radians/sec and 2859 radians/sec respectively, are associated with torsional and bending modes of the CMU due to the flexibilities at its four corners as shown in Figures 4.2-1 and 4.2-2. The first true bending mode of the front and back walls is mode number 9 at 3425 radians/sec as shown in Figure 4.2-3. Critical damping was calculated for all three conditions and used to compute a damping value for the CMU. One of the parameters used for structural damping is the ratio of damping over critical damping, and is commonly referred to as the damping ratio (c/c_{cr}). Fintel recommends values of 2% to 20% for common structural problems. Tests as well as other sources recommend values from 1% to 3% for reinforced concrete structures with rigid connections. Ratios between 1% and 20% yielded damping values of 5 to 105 depending of the eigenvalue used for the

fundamental system frequency. For the purpose of this evaluation, an average damping value of 50 was chosen which results in damping ratios of around 11% for mode #7 and 8.8% for mode #9.

Biggs (1964) points out that the effect of structural damping is not significant if the load duration is short and only the maximum dynamic response is of interest, which was the case for the single CMU exposed to blast loading. The effect of damping is much more significant for continuing state of vibration where damping may help reduce the dynamic response. This point was investigated for the MAT_SOIL_AND_FOAM case with 500 lb ANFO at 10 ft. The first case looked at a damping value of 250, which is 5 times greater than that used in the analysis. The second case examined a damping value of 10, which is 5 times smaller than that used in the analysis. Examination of the results showed no significant impact on the stress and displacement levels within the CMU. The failure mode remained the same, and the maximum stress levels were unchanged.

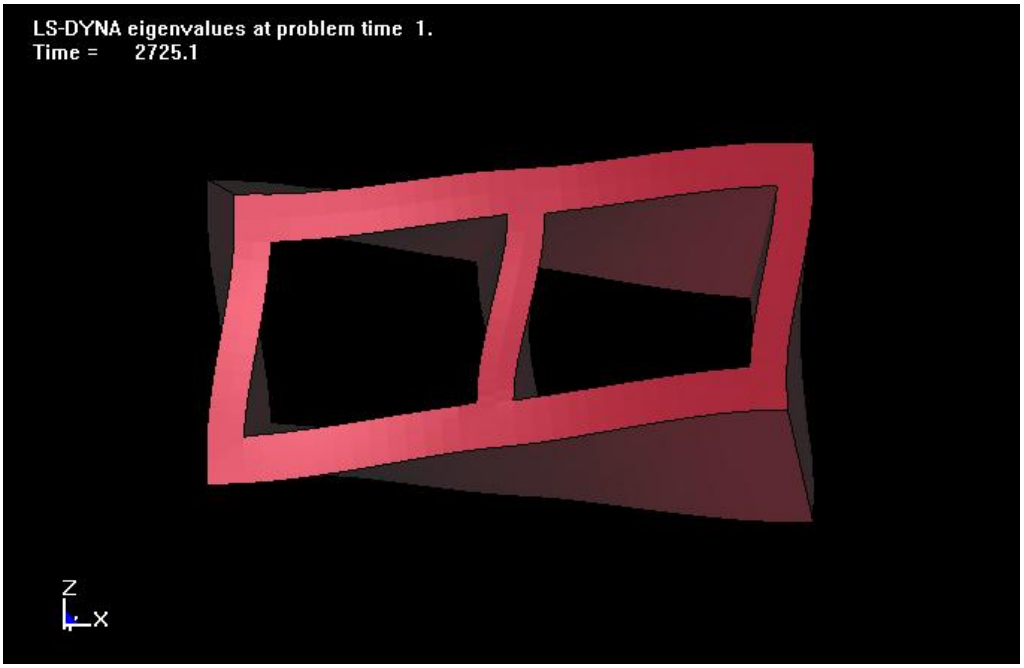

Figure 4.2-1 First System Mode at 2725 radians/sec

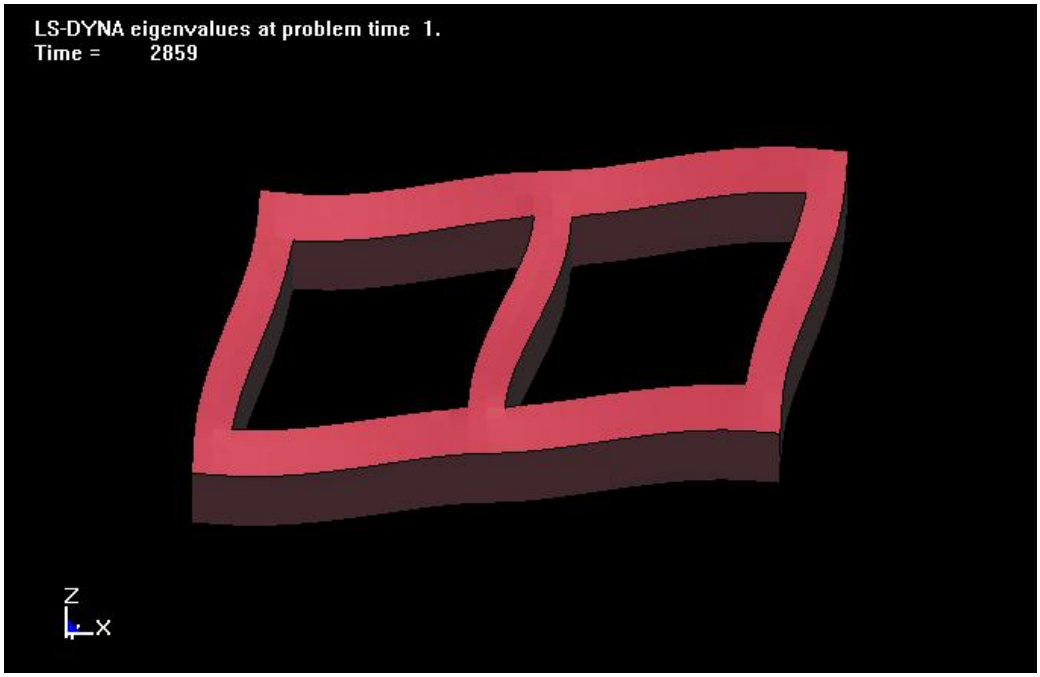

Figure 4.2-2 Second System Mode at 2859 radians/sec

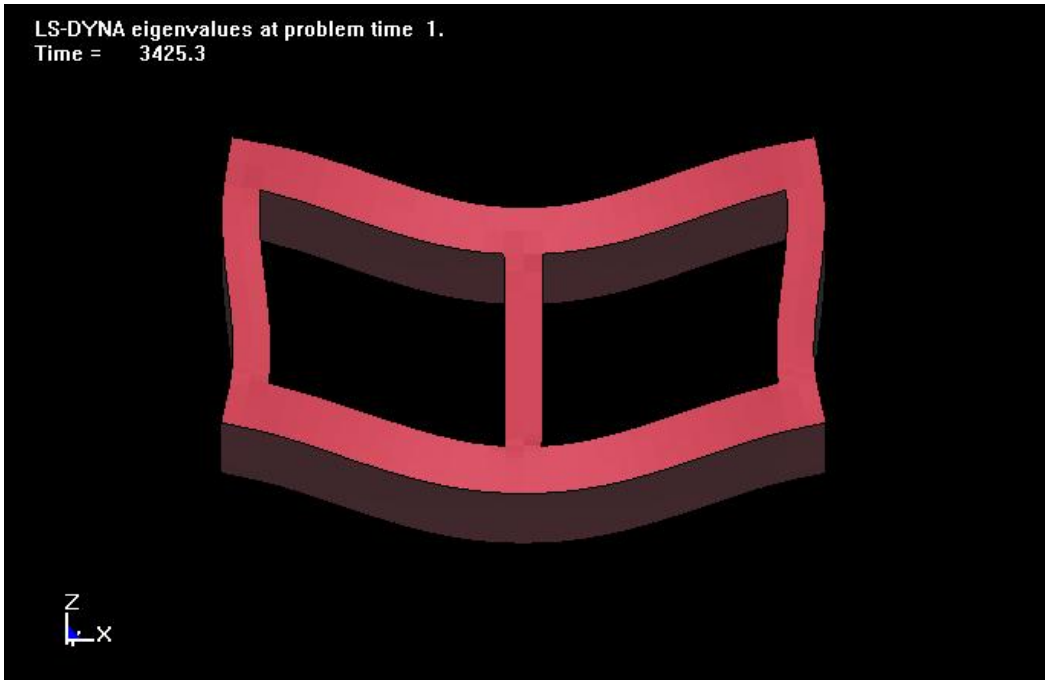

Figure 4.2-3 Third System Mode at 3425 radians/sec

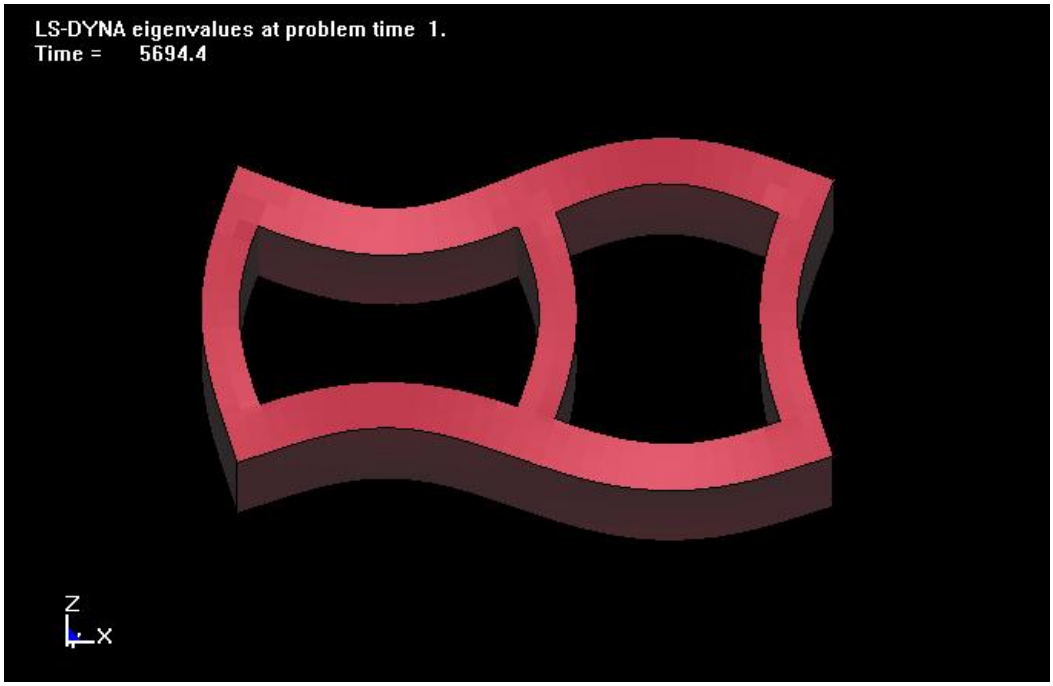

Figure 4.2-4 Fourth System Mode at 5694 radians/sec

4.3 DYNA-3D and Material Property Cards

DYNA-3D was developed at Lawrence Livermore National Laboratory in the mid-seventies. It is a general-purpose finite element code for analysis of large deformation dynamic response of structures including structures coupled with fluids. The main solution methodology is based on explicit time integration. For analysis of concrete structures, DYNA provides a variety of constitutive models (material cards) simulating numerous behavior patterns.

Before describing the constitutive models used in this investigation, a brief summary of the characterization of these models (Len Schwer 2001) would be helpful to the reader. Material characteristics of geomaterials such as concrete, soil, rock, and some foams require tests for calibrating the constitutive model's parameters. Three common laboratory tests are used to derive the characteristic parameters.

1. Hydrostatic compression
2. Triaxial compression/extension
3. Uniaxial strain

A typical laboratory test specimen is a right circular cylinder. A concrete standard (United States) specimen has a 6-inch diameter and 12-inch height, and is tested 28 days after the concrete is poured. The cylinder is tested by applying axial and lateral loads, and recording corresponding axial and lateral displacements (strains). The geometry of the cylinders, and applied loads, provides for an axisymmetric state of stress and strain.

In the hydrostatic compression case, the axial and lateral stresses are equal, and the specimen is compressed equally on all sides. The corresponding measured axial and lateral strain components provide the volume strain ε_{kk}. The corresponding pressure versus volume strain response describes the compaction behavior of the material as shown in Figure 4.3-1. A typical geomaterial compaction response has three phases:

1. $P_0 < P < P_1$ is the initial elastic response. The elastic bulk modulus is the slope of this segment.
2. $P_1 < P < P_2$ is when the pores (voids) in the material are compressed.
3. $P > P_2$ removal of the voids results in a fully compacted material

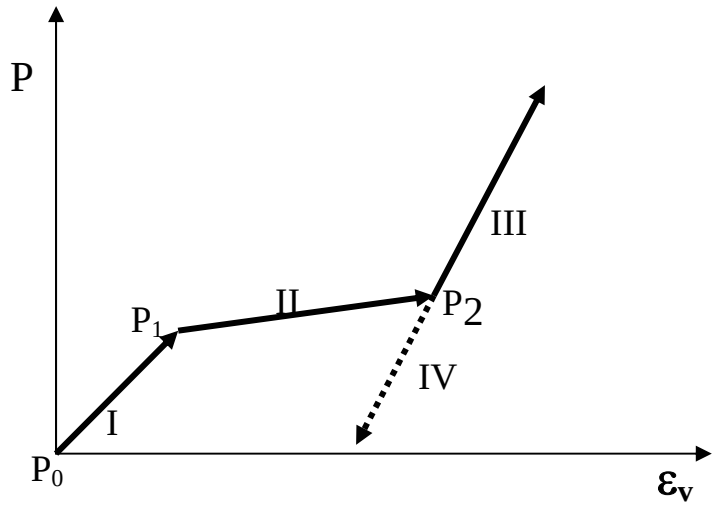

Figure 4.3-1 Schematic of Pressure Versus Volume Response for Geomaterials (Len Schwer 2001)

The indicated fourth phase is the unloading from the fully compacted state. The slope of this segment defines the bulk unloading modulus, which is a user input for the MAT_SOIL_AND_FOAM model. The bulk unloading modulus should always be greater than the elastic modulus to prevent fictitious generation of energy during loading-unloading cycles.

A special case of the triaxial compressive test is when the lateral (confining) stress is zero, which is referred to an unconfined compressive test. The corresponding value of the axial stress, when the specimen fails, is referred to as the unconfined compressive strength. The initial elastic stress-strain response of an unconfined compression test can be used to calibrate Young's modulus and Poisson's ratio by using Hook's Law for uniaxial state of stress:

$$\varepsilon_{axial} = \sigma_{axial} / E$$
$$\varepsilon_{lateral} = -\nu\sigma_{axial} / E$$

An examination of the available LS-DYNA constitutive models showed eight possible candidates for this research.

1. **MAT_SOIL_AND_FOAM –** Material type 5 in LS-DYNA
2. **MAT_SOIL_AND_FOAM_FAILURE –** Material type 14 in LS-DYNA
3. **MAT_BRITTLE_DAMAGE -** Material type 96 in LS-DYNA
4. **MAT_PSEUDO_TENSOR -** Material type 16 in LS-DYNA
5. **MAT_WINFRITH_CONCRETE -** Material type 84 in LS-DYNA
6. **MAT_CONCRETE_DAMAGE -** Material type 72 in LS-DYNA
7. **MAT_SOIL_CONCRETE -** Material type 78 in LS-DYNA
8. **MAT_DRUCKER_PRAGER -** Material type 193 in LS-DYNA

The list was narrowed down to four when limitations in available material property, or in applicability of the material card proved obvious for the other four. MAT_SOIL_AND_FOAM_FAILURE was not investigated because it was developed for soil or foam that is confined within a structure. MAT_DRUCKER_PRAGER was not investigated because it was developed solely for soil. MAT_CONCRETE_DAMAGE was eliminated from the list because it was developed for buried steel reinforced concrete structures. MAT_SOIL_CONCRETE requires several load curves defining strain, yield, and fracture versus pressure. Since these load curves were not readily available for CMUs, MAT_SOIL_CONCRETE was not considered in this investigation.

For the remaining four constitutive models, LS-DYNA's description indicates reasonable accuracy between analysis and test. A brief description of each material card is provided herein based on the LS-DYNA user's manuals. The material model parameters for MAT_SOIL_AND_FOAM, MAT_PSEUDO_TENSOR, and MAT_WINFRITH_CONCRETE can be calibrated to the parameters derived from the tests described above.

The MAT_SOIL_AND_FOAM is the most basic of the geomaterial models available in LS-DYNA (Len Schwer 2001). It is also the oldest and therefore has had a considerable amount of user experience, and feedback, and is quite robust. The model requires minimum amount of input data, and hence material characterization. These facts make it the recommended model for preliminary analyses involving geomaterials. The model simulates crushing through the volumetric deformations (LS-DYNA 1999). A pressure-dependent flow rule governs the deviatoric behavior with three user specified constants. Volumetric yielding is determined by a tabulated curve of pressure versus volumetric strain. Elastic unloading from this curve is assumed to a tensile cutoff. One history variable, the maximum volumetric strain in compression, is stored. If the new compressive volumetric strain exceeds the stored value, loading is indicated. When the yield condition is violated, the updated trail stresses are scaled back using a simple radial return algorithm. If the hydrostatic tension exceeds the cutoff value, the pressure is set to the cutoff value and the deviatoric tensor is zeroed.

The material card used in the analysis for MAT_SOIL_AND_FOAM is listed below with corresponding tabulated values. Values that could be readily calculated using available data in the literature are shown accordingly. Values for the bulk unloading modulus, pressure cutoff for tensile fracture, volumetric strain values, and their corresponding pressures are test dependent, and therefore estimated for this exercise.

```
*MAT_SOIL_AND_FOAM
$      mid        ro         g      bulk        a0        a1        a2        pc
         1 2.22470-4 7.88000+5 6.00000+6   13333.3       0.0       0.0 -200.0000
$      vcr       ref
 0.0000000 0.0000000
$     eps1      eps2      eps3      eps4      eps5      eps6      eps7      eps8
 0.0000000-0.0200000-0.0377000-0.0418000-0.0513000-0.1000000-0.5000000 0.0000000
$     eps9     eps10
 0.0000000 0.0000000
$       p1        p2        p3        p4        p5        p6        p7        p8
 0.0000000 21000.000 34800.000 45000.000 58000.000 1.25000+5 9.44500+5 0.0000000
$       p9       p10
 0.0000000 0.0000000
```

Where:

mid: Material identification number
ro: Mass density
g: Shear modulus
bulk: Unloading bulk modulus (from test), must be greater than elastic modulus
a0: Yield function constant = 1/3 σ_y^2
a1, a2: Yield function constant equal to zero to eliminate pressure dependence on the yield/tensile strength
pc: Pressure cutoff for tensile fracture (from test)
vcr: Volumetric crushing option = 0.0 means on
ref: User reference geometry to initialize the pressure = 0.0 means off
eps1,..: Volumetric strain values; ln (v/v_o) from test
p1, p2,…: Pressure corresponding to volumetric strain values (from test)

The MAT_BRITTLE_DAMAGE model is anisotropic designed primarily for concrete and steel reinforced concrete, though it can be applied to a wide variety of brittle materials (LS-DYNA 1999). It admits progressive degradation of tensile and shear strengths across smeared cracks that are initiated under tensile loadings. Compressive failure is governed by J2 flow correction that can be disabled if not desired. For concrete, an initial tensile strength is specified by the user. Once this stress is reached at a point in the body a smeared crack is initiated there with a normal that is co-linear with the first principal direction. As the loading progresses the allowed tensile traction normal to the crack plane is progressively degraded to a small machine dependent constant. The degradation is implemented by reducing the material's modulus normal to the smeared crack plane according to a maximum dissipation law that incorporates exponential softening. The crack field intensity is output in the equivalent plastic strain field in a normalized fashion. When normalized value reaches unity, it means that the material's strength has reached 2% of its original value in the normal and parallel directions to the smeared crack. The initial shear traction may be transmitted across a smeared plane. The shear degradation is coupled to the tensile degradation through the internal variable, which measures the intensity of the crack field. The shear degradation is accounted for by reducing the material's shear stiffness parallel to the smeared crack plane.

The material card used in the analysis for MAT_BRITTLE_DAMAGE is listed below with corresponding tabulated values. Values that could be readily calculated using available data in the literature are shown accordingly. Values for the fracture toughness, shear retention, and viscosity were estimated using recommendations provided in the LS-DYNA user's manuals.

```
*MAT_BRITTLE_DAMAGE
$      mid        ro         e        pr    tlimit    slimit    ftough    sreten
         1 0.00022247 2000000.0      0.15     200.0     100.0      0.80     0.030
$     visc    fra_rf      e_rf     ys_rf     kh_rf     fs_rf      sigy
     104.0       0.0       0.0       0.0       0.0       0.0         0
```

Where:

mid: Material identification number
ro: Mass density
e: Elastic modulus

pr: Poisson's ratio
tlimit: Tensile strength
slimit: Shear strength
ftough: Fracture toughness
sreten: Shear retention
visc: Viscosity
fra_rf….sigy: Values related to reinforcement not applicable to this exercise

The MAT_PSEUDO_TENSOR model has been used to analyze buried steel reinforced concrete structures subjected to impulsive loadings (LS-DYNA 1999). For the purpose of this project, the MAT_PSEUDO_TENSOR model is used in its simple tabular pressure-dependent yield surface mode. This model is well suited for implementing standard geological models like the Mohr-Coulomb yield surface with a Tresca limit. This material card has been used very successfully to model ground shocks and soil-structure interactions at pressures up to 1.5 million psi. The tabulated values of pressure are specified with corresponding values of yield stress. The parameters relating to reinforcement properties are set to zero. LS-DYNA internally defines a failed material curve of slope 3*p* based on the specified pressure. The yield strength is taken from the tabulated yield vs. pressure curve until the maximum principal stress in the element exceeds the tensile cut-off. Scaling back of the yield strength is performed for several time steps until the yield strength is defined by the failed curve. For the purpose of this exercise, response mode II is utilized with the concrete model option where the only required material characterization data is limited to the unconfined compressive strength f'_c.

The material card used in the analysis for MAT_PSEUDO_TENSOR is listed below with corresponding tabulated values. Values that could be readily calculated using available data in the literature are shown accordingly.

```
*MAT_PSEUDO_TENSOR
$      mid        ro         g        pr
         1 0.0002247  833333.0      0.20
$     sigf        a0        a1        a2       a0f       a1f        b1       per
    2000.0        -1
$       er       prr      sigy      etan       lcp       lcr

$       x1        x2        x3        x4        x5        x6        x7        x8

$       x9       x10       x11       x12       x13       x14       x15       x16

$      ys1       ys2       ys3       ys4       ys5       ys6       ys7       ys8

$      ys9      ys10      ys11      ys12      ys13      ys14      ys15      ys16
```

Where:
mid: Material identification number
ro: Mass density
g: Shear modulus
pr: Poisson's ratio

sigf: Tensile cutoff (maximum principal stress for failure); when **ao** is negative, **sigf** is assumed to be the unconfined concrete compressive strength f'_c
a0: Cohesion = -1
a1 - alf: Calculated by DYNA internally when a0 = -1
b1: Damage scaling factor
per - ys : N/A

The MAT_WINFRITH_CONCRETE is a smeared crack model implemented in the 8-node single integration point continuum element (LS-DYNA 1999). This model was developed by Broadhouse and Neilson (LS-DYNA 1999), and has been validated against experiments. Steel reinforcement properties are set to zero (even if they are specified on the material card).

The material card used in the analysis for MAT_WINFRITH_CONCRETE is listed below with corresponding tabulated values. Values that could be readily calculated using available data in the literature are shown accordingly. Values for the crack size, aggregate radius, volumetric strains, and corresponding pressures were estimated for this exercise.

```
*MAT_WINFRITH_CONCRETE
$      mid        ro        tm        pr       ucs       uts        fe     asize
         1 2.22470-4 3000000.0      0.20    2000.0     200.0       .15    0.0625
$        e        ys        eh    uelong      rate      conm      conl      cont
     30.+6   60000.0      4.+7     0.003       1.0        -1
$     eps1      eps2      eps3      eps4      eps5      eps6      eps7      eps8
$ 0.0000000-0.0200000-0.0377000-0.0418000-0.0513000-0.1000000-0.5000000 0.0000000

$       p1        p2        p3        p4        p5        p6        p7        p8
$ 0.0000000 21000.000 34800.000 45000.000 58000.000 1.25000+5 9.44500+5 0.0000000
```

Where:

mid: Material identification number
ro: Mass density
tm: Tangent modulus for concrete
pr: Poisson's ratio
ucs: Uniaxial compressive strength
uts: Uniaxial tensile strength
fe: Crack width at which normal tensile stress goes to zero
asize: Aggregate radius
e - uelong: Reinforcement properties
rate: Strain rate effect = 1.0, turned off
conm : mass units = -1 (lb, in, seconds)
esp1, p1,…: Same as Soil_Foam

4.4 Blast Loads

The LOAD_BLAST option of LS-DYNA was used to simulate blast. This load simulates the hemispherical pressure distributions for blast at ground level. Analyses were performed for a maximum of 25 m-seconds using the CONWEP (LS-DYNA 1999) blast loads for different charges. The first charge was made of 500 lb of a mixture of Ammonium Nitrate and Fuel Oil (ANFO), and second charge is made of 1000 lb ANFO. During the actual blast tests at AFRL, the CMUs were placed at distances of 20 ft, 25 ft, 30 ft, 32 ft, 35 ft, 40 ft, 45 ft, and 50 ft respectively. Blast pressure was calculated using CONWEP for each distance, and applied to the front face of the CMU. The simulated blast pressures agreed with loads calculated from other sources. The results were compared to pressure gage data provided by AFRL for the distances indicated herein.

4.5 Dynamic Analysis

Direct transient analysis was performed for each model using LS-DYNA. The basic loading conditions in the tests for the 500 lb ANFO are as follows. Similar distances were used in the tests for the 1000 lb ANFO. Analyses were performed for all loading conditions for each of the MAT cards described in section 4.3.

- ANFO = 500 lb at 10 ft
- ANFO = 500 lb at 20 ft
- ANFO = 500 lb at 25 ft
- ANFO = 500 lb at 30 ft
- ANFO = 500 lb at 32 ft
- ANFO = 500 lb at 35 ft
- ANFO = 500 lb at 40 ft
- ANFO = 1000 lb at 20 ft
- ANFO = 1000 lb at 35 ft
- ANFO = 1000 lb at 40 ft
- ANFO = 1000 lb at 50 ft

The analyses closely followed these conditions to simulate the tests and compare results. Where results did not closely match, small variation of distances was used for investigation. The results of the analyses are documented in Chapter 5.

4.6 Time Steps

CONTROL_TIMESTEP was used in LS-DYNA to define time step parameters. Default values were used for the initial time step size and the scale factor as recommended by LS-DYNA for blast loading. The accuracy of results was examined by analyzing a few of the cases with significantly smaller time steps. The results of the runs with significantly smaller time steps agreed closely with those using LS-DYNA's default time steps. It was therefore concluded that the default option of LS-DYNA produces reasonable results for this research and was adopted for the analyses performed herein.

CHAPTER 5

RESULTS OF ANALYSIS

Stress, displacement, and energy results were studied for each load level to examine failure modes of the CMU. These results are discussed in four sub-sections, namely 5.1, 5.2, 5.3, and 5.4, dedicated to the constitutive models used in this investigation. Each sub-section starts with a discussion of stress distribution, displacement plots during failure, failure modes, and various energy checks associated with each analysis. The discussions are followed by stress and displacement fringe plots, displacement history plots, as well as energy plots associated with the particular constitutive model. To ensure clarity, sub-sections 5.2, 5.3, and 5.4 start on a new page and will not follow the convention of this report.

5.1 MAT_SOIL_AND_FOAM

The stress fringe levels indicate that the exposed wall of the CMU reaches its ultimate strength within the first three m-seconds depending on the distance from the source. Stresses remain at this level as the elements of the exposed wall (front face of the CMU) experience large displacements in the following m-seconds of the blast. This is clearly demonstrated in the stress and displacement fringe plots for the 500 lb ANFO at distances of 10, 20, 30, and 32 ft. However, at greater distances the CMU experiences more of a rigid body movement as indicated by the displacement fringe plots at 35 and 40 ft. In these cases, the stress level may reach the ultimate strength but fracture does not occur. Additional data is provided for the 500 lbs ANFO load cases in the form of displacement time histories for three nodal points. The failure of the front wall of the CMU is demonstrated by plotting the displacement time history of a node at mid-point of the right front wall versus the displacement in safer areas of the CMU such as the rear right corner, or the middle of the center rib. Figure 7.1-3 shows a cross section of the CMU with three nodes highlighted. Node number 5430 is at the center of the front right wall, which is exposed to blast pressure. Node 8961 is close to the rear right corner of the CMU, and node number 4949 is at the center of the middle rib of the CMU. In order to save space, Figure 7.1-3 is shown only in this section but will be referred to in the remaining sections of this chapter. The first case to examine is 500 lb ANFO at 10 ft. Displacement time histories are plotted in Figure 7.1-4 in order to show clearly that the front wall displaces more and at earlier time steps than the other two locations. It is also observed that the other two nodes move exactly the same distance and at the same time step indicating a rigid body movement of the rest of the block. In this case, the mid-point of the right front wall displaces 0.2 in at time step 1.5 m-sec whereas the other two points of interest move slightly above zero. At time step 4.5 m-sec, the mid-point of the right wall displaces 1.2 in and the other two points of interest displace around 0.4 in. Energy plots are shown in Figure 7.1-5 for kinetic energy, internal (strain) energy, total energy, hourglass energy, as well as the energy ratio. For the 500 lb ANFO at 10 ft, significant kinetic and internal energy are present, and the hourglass energy and energy ratio are

negligible. Stress and displacement fringes, as well as displacement time histories and energy plots are provided for most cases of 500 lb ANFO subsequent to the case at 10 ft.

Similar results are noted for the 1000 lb ANFO where fracture is noticed at 40 ft or less, but rigid body movement in noticed at 45 ft or more.

The complete results of the MAT_SOIL_AND_FOAM complement are included in the following list.

500lb10ft	Failure	1000lb40ft	Failure
500lb20ft	Failure	1000lb45ft	No Failure
500lb30ft	Failure	1000lb50ft	No Failure
500lb32ft	Failure		
500lb35ft	No Failure		
500lb40ft	No Failure		

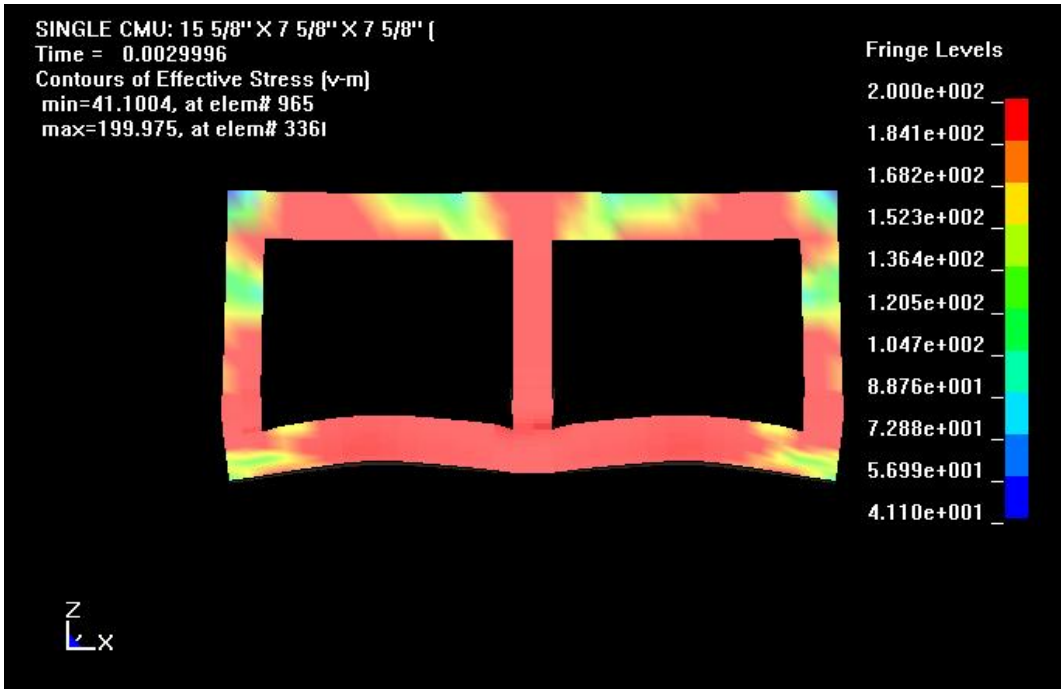

Figure 5.1-1 MAT_SOIL_AND_FOAM Stress Fringes for 500 lb ANFO at 10 ft

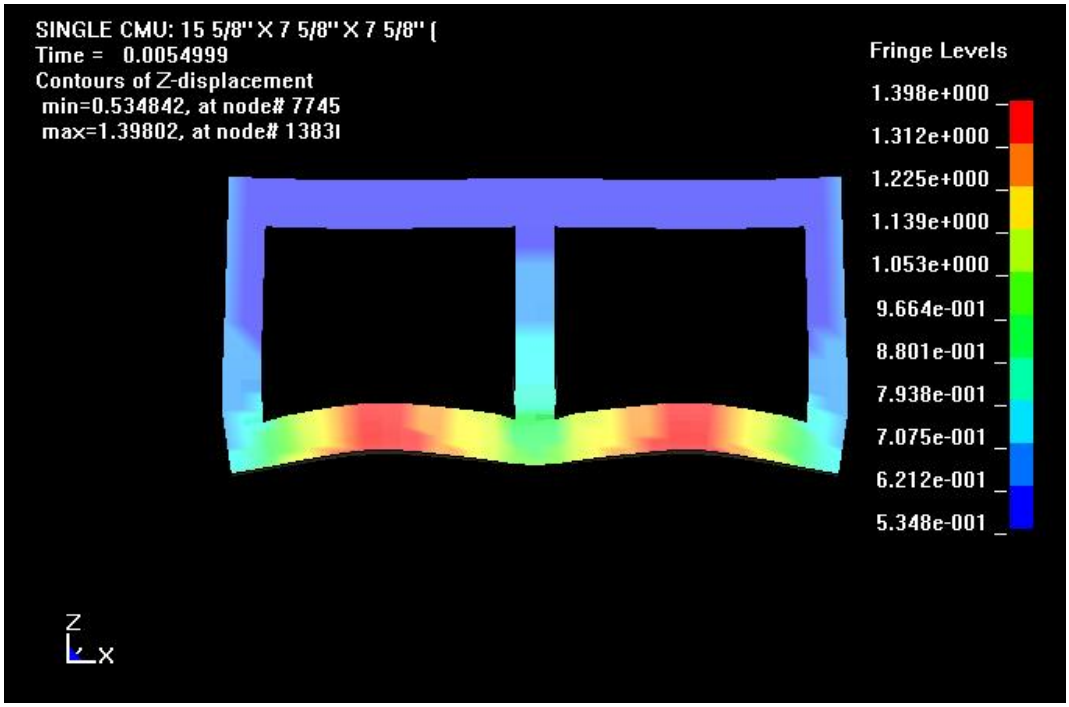

Figure 5.1-2 MAT_SOIL_AND_FOAM Displacement Fringes for 500 lb ANFO at 10 ft

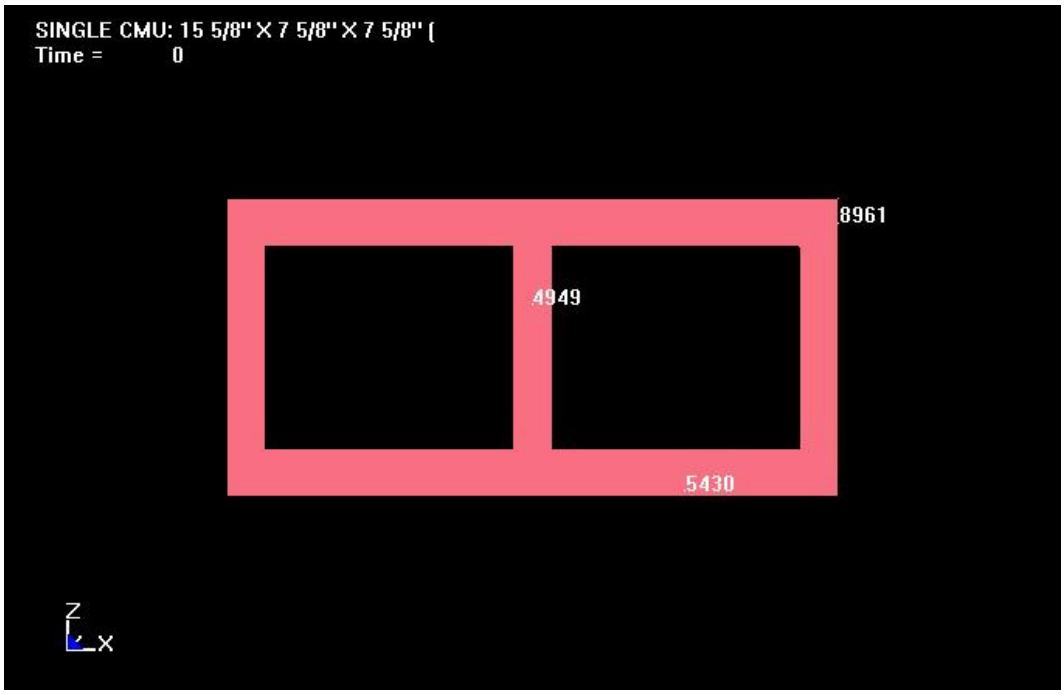

Figure 5.1-3 Reference Node Numbers for Displacement History Plots

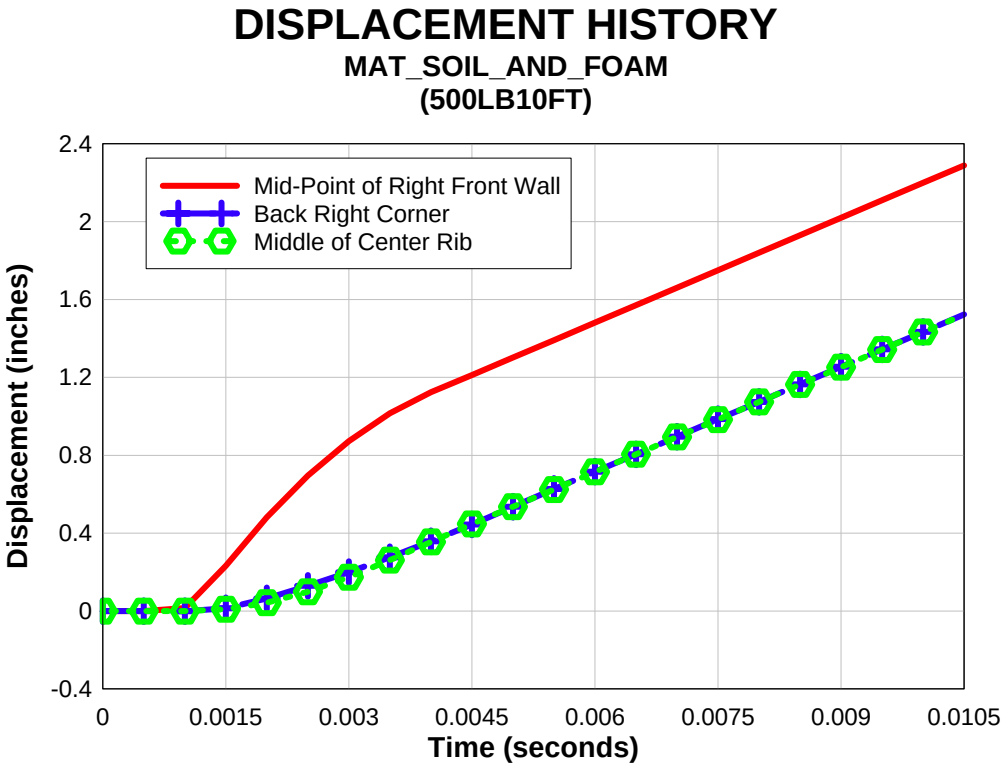

Figure 5.1-4 Displacement History Plots

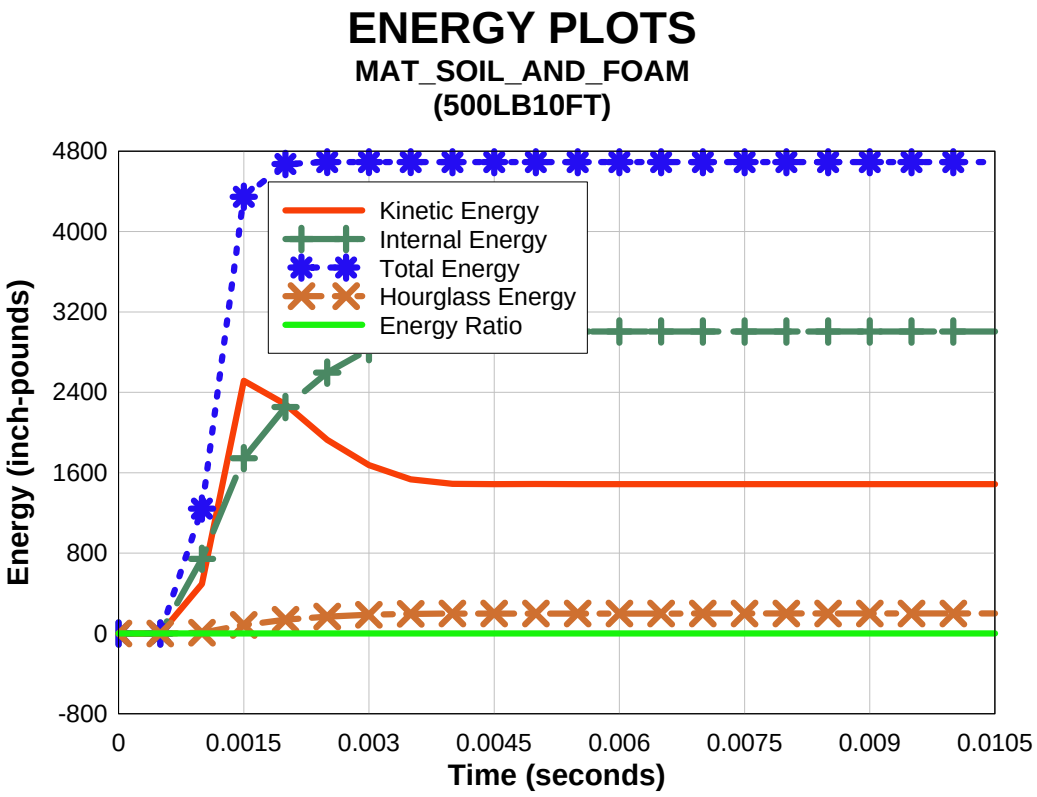

Figure 5.1-5 Energy Plots

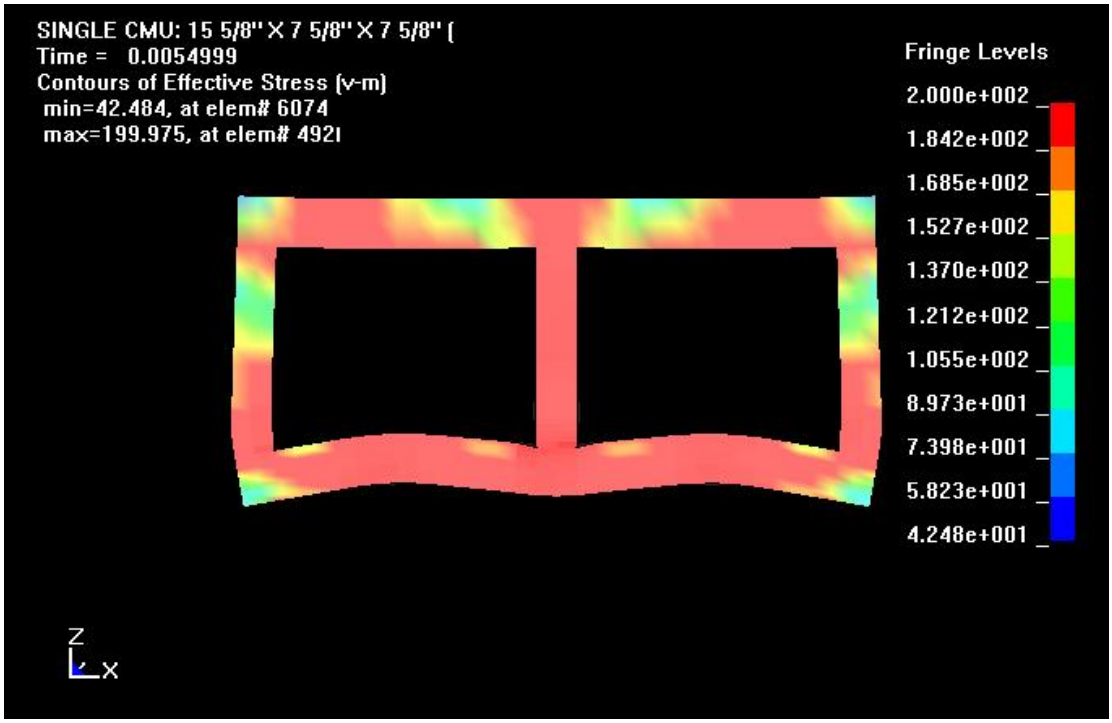

Figure 5.1-6 MAT_SOIL_AND_FOAM Stress Fringes for 500 lb ANFO at 20 ft

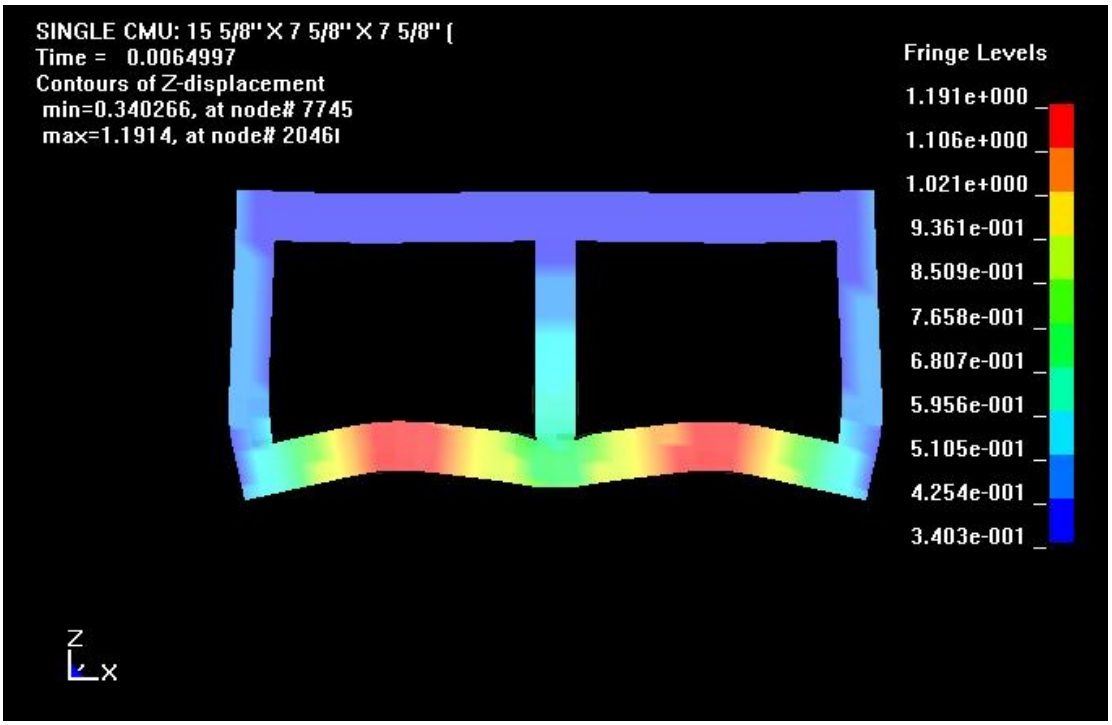

Figure 5.1-7 MAT_SOIL_AND_FOAM Displacement Fringes for 500 lb ANFO at 20 ft

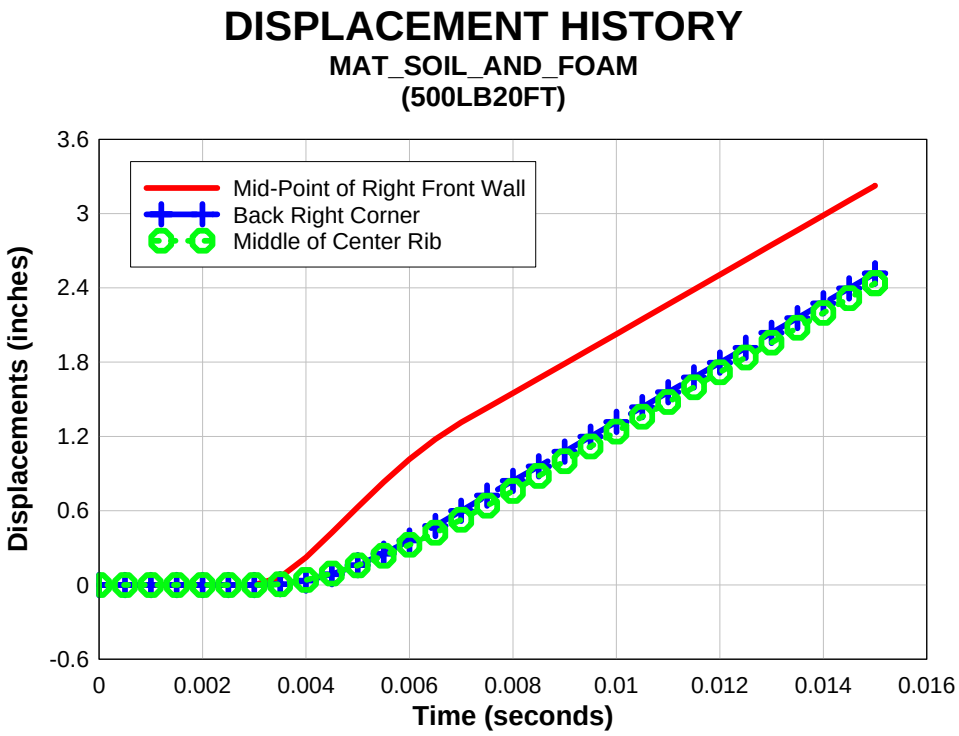

Figure 5.1-8 Displacement History Plots

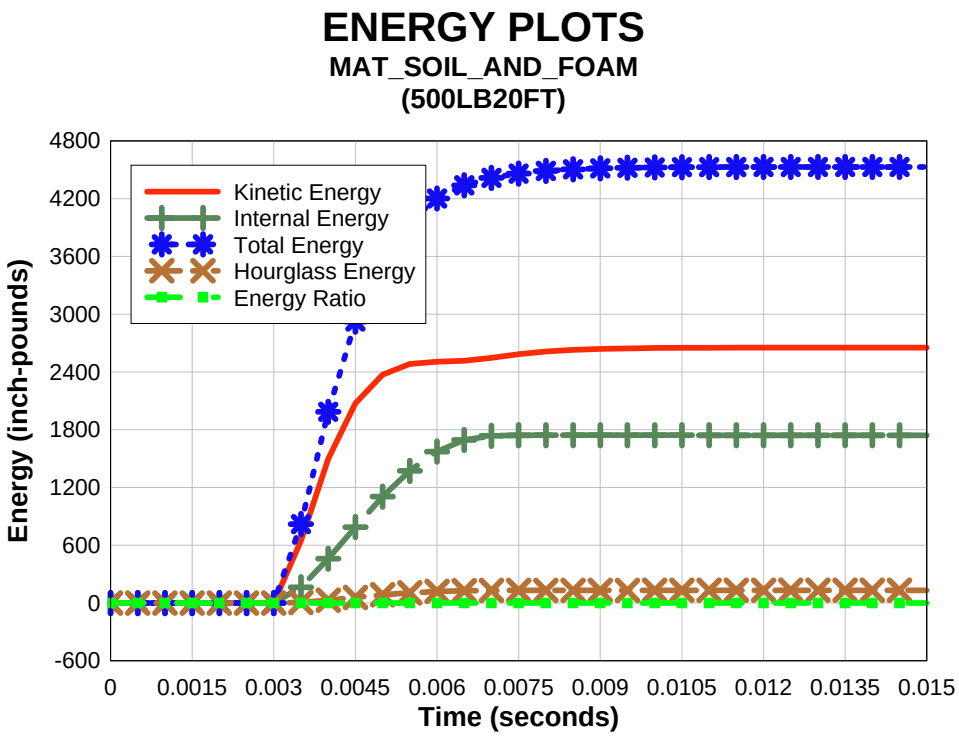

Figure 5.1-9 Energy Plots

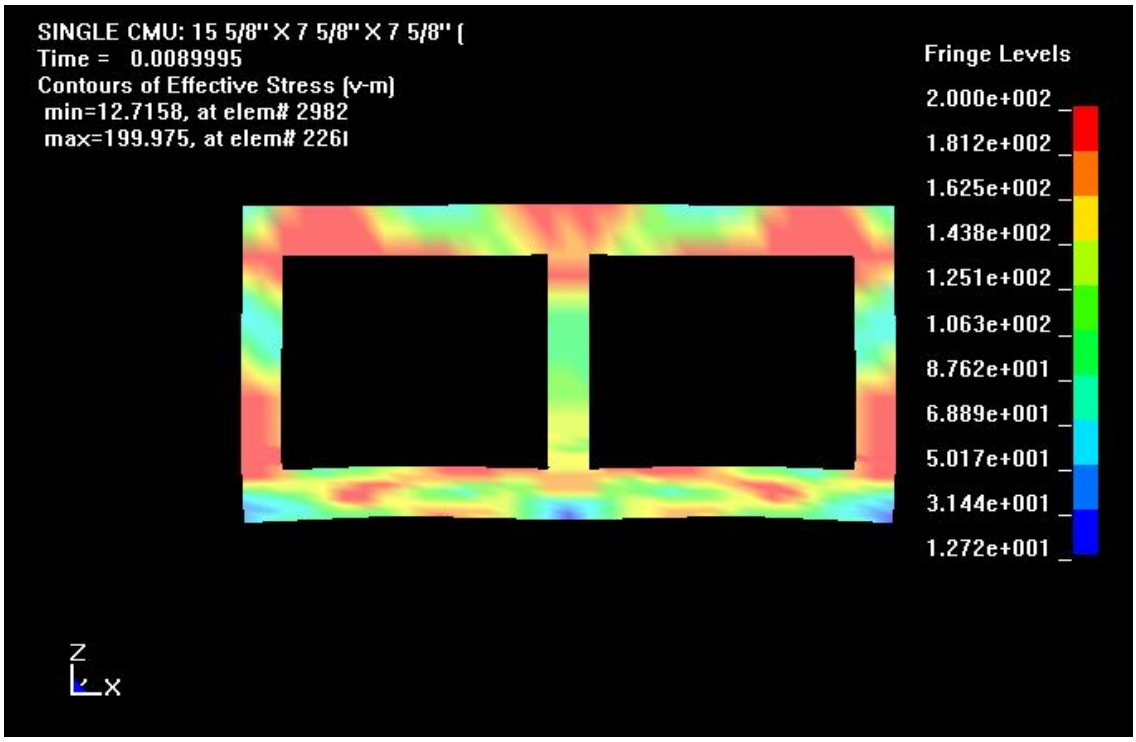

Figure 5.1-10 MAT_SOIL_AND_FOAM Stress Fringes for 500 lb ANFO at 30 ft

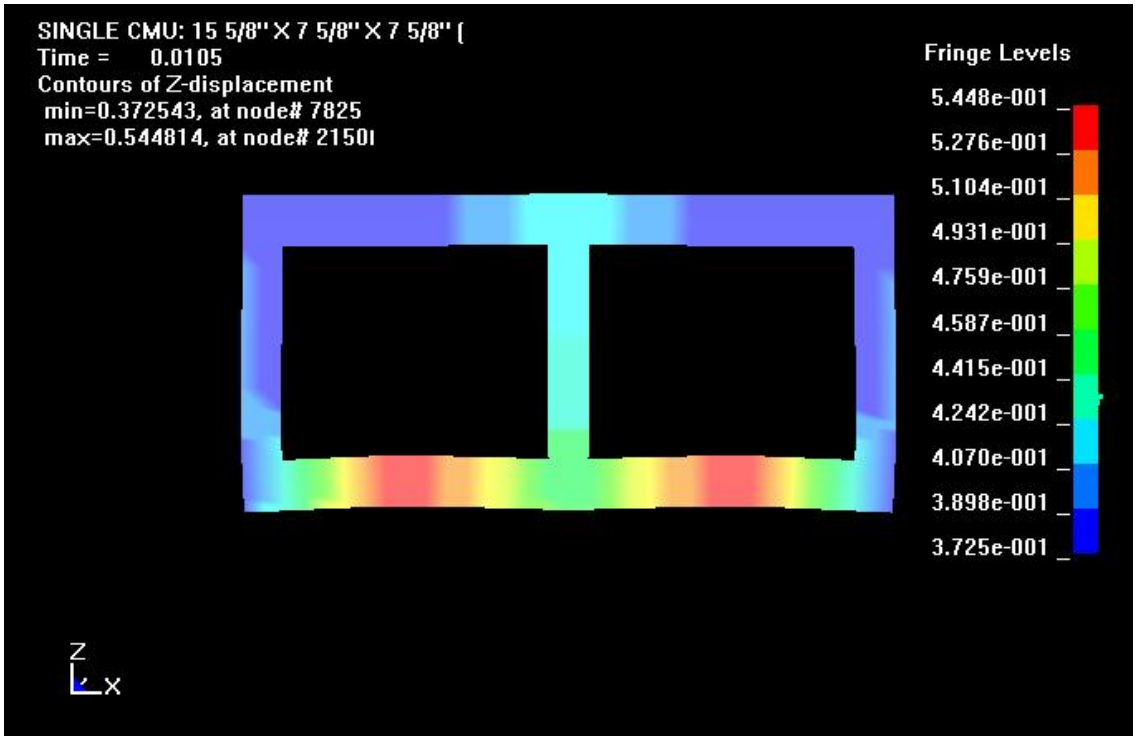

Figure 5.1-11 MAT_SOIL_AND_FOAM Displacement Fringes for 500 lb ANFO at 30 ft

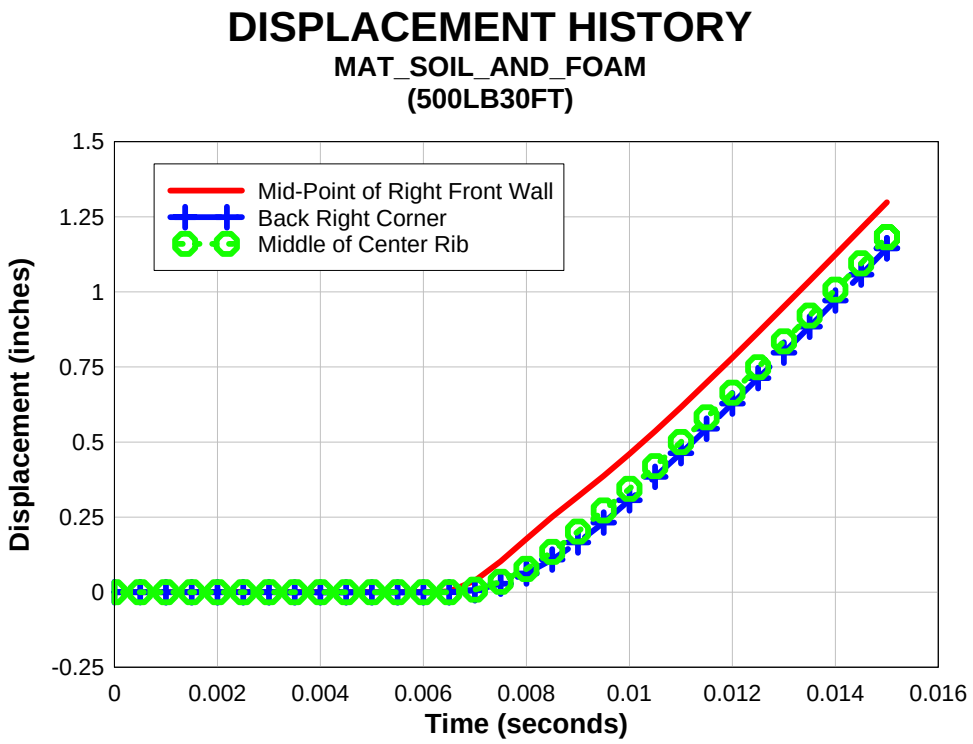

Figure 5.1-12 Displacement History Plots

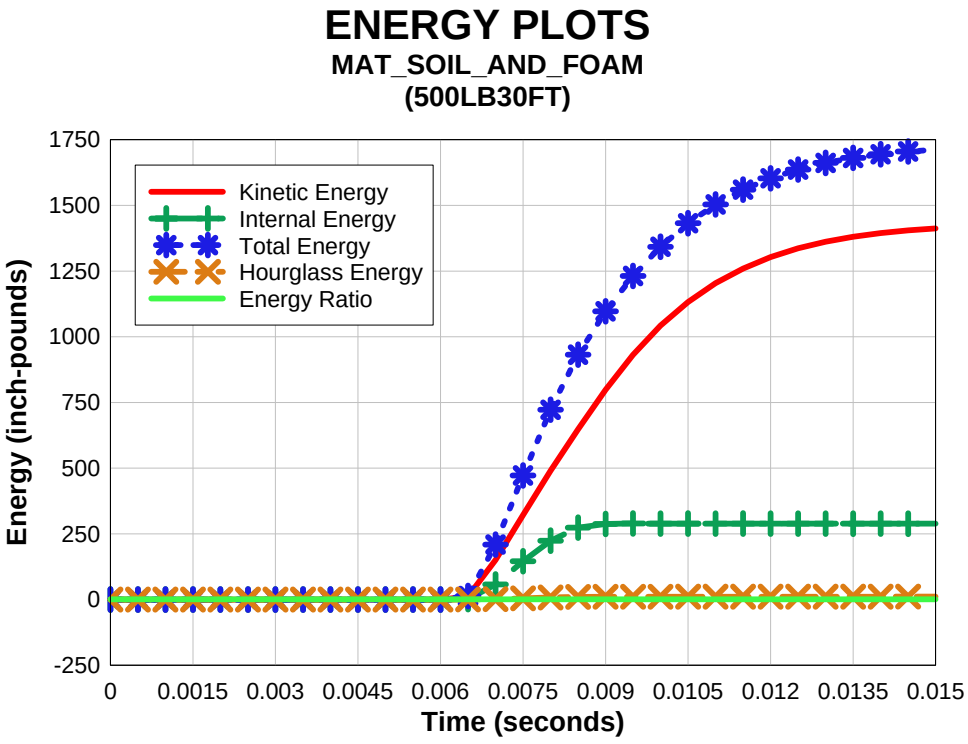

Figure 5.1-13 Energy Plots

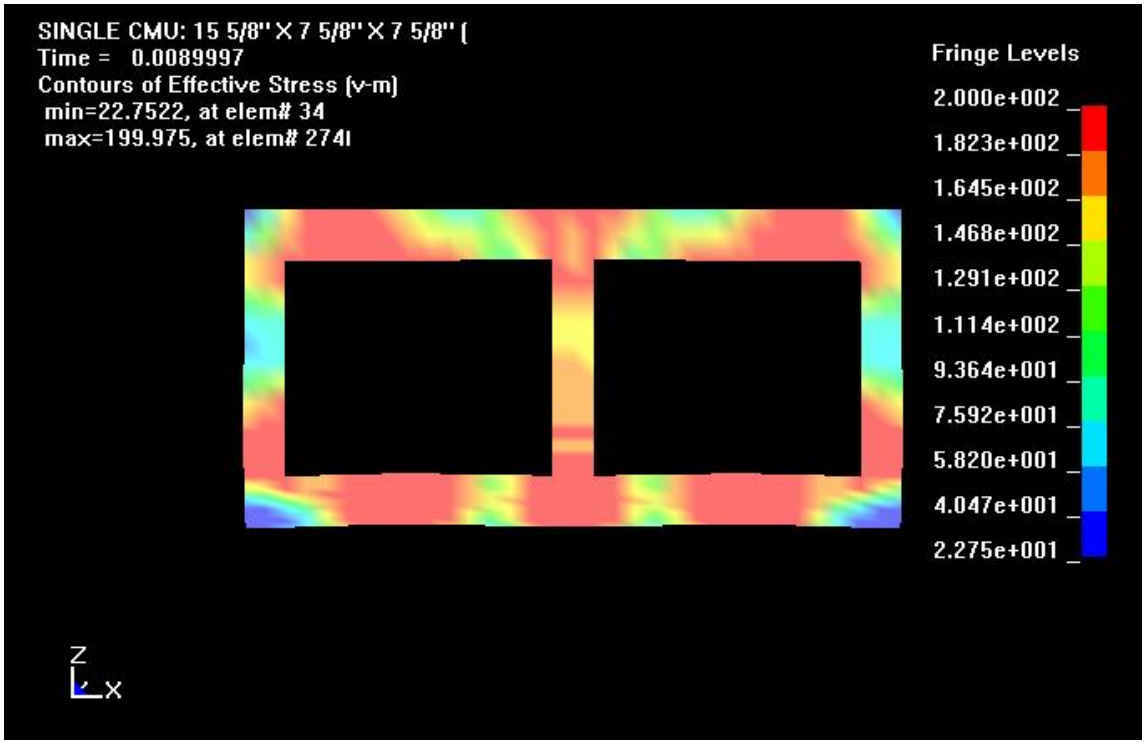

Figure 5.1-14 MAT_SOIL_AND_FOAM Stress Fringes for 500 lb ANFO at 32 ft

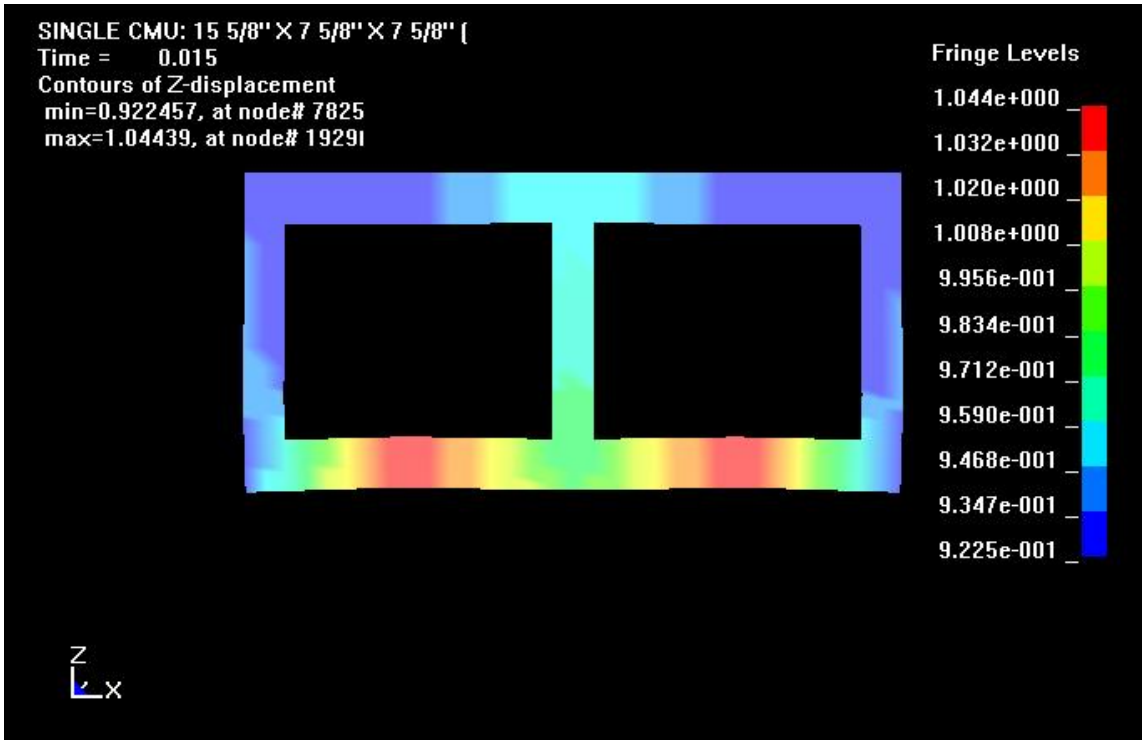

Figure 5.1-15 MAT_SOIL_AND_FOAM Displacement Fringes for 500 lb ANFO at 32 ft

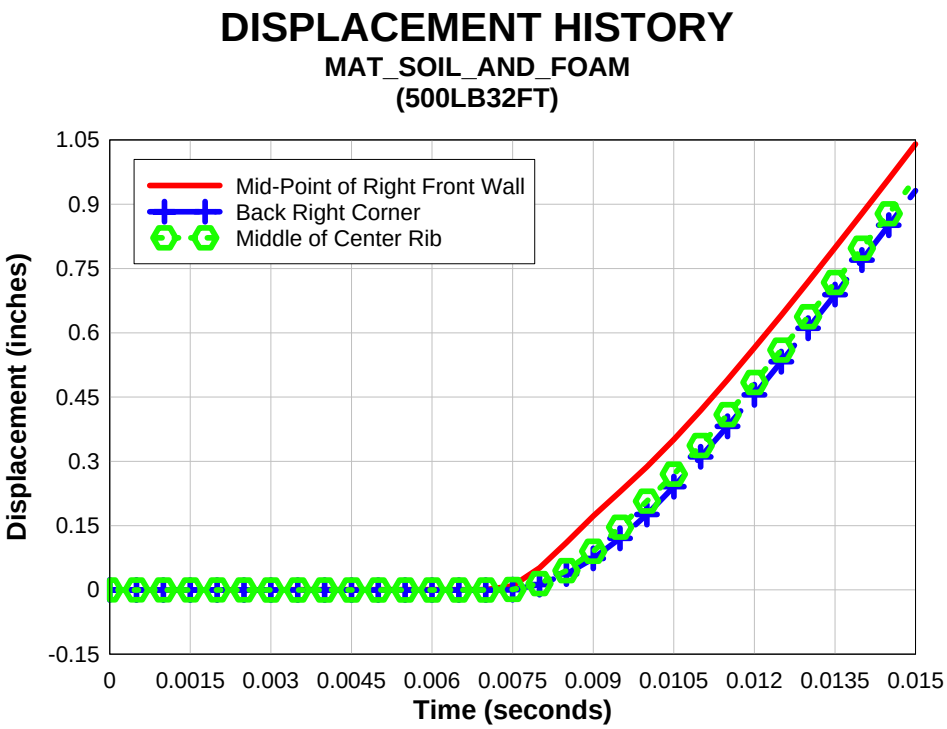

Figure 5.1-16 Displacement History Plots

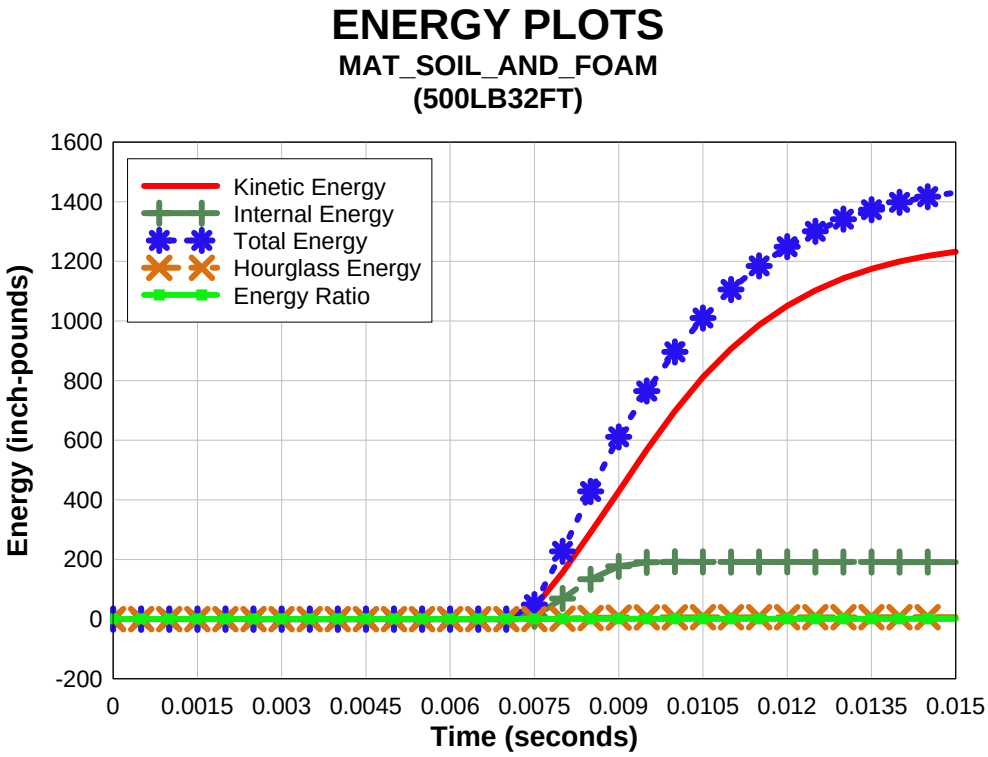

Figure 5.1-17 Energy Plots

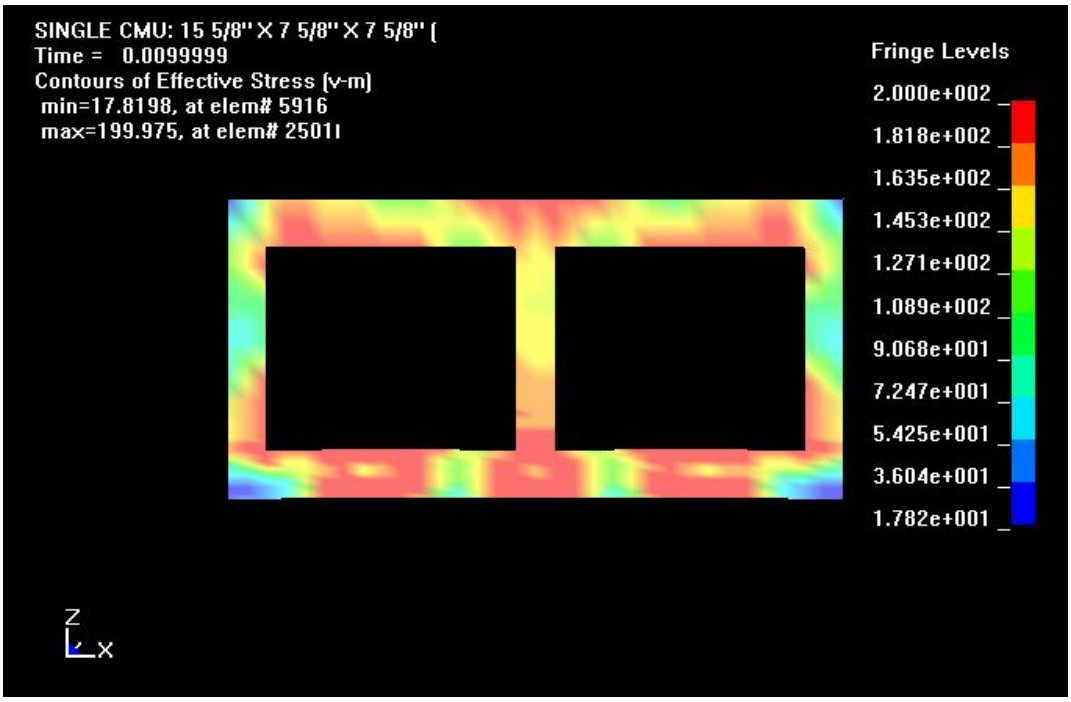

Figure 5.1-18 MAT_SOIL_AND_FOAM Stress Fringes for 500 lb ANFO at 35 ft

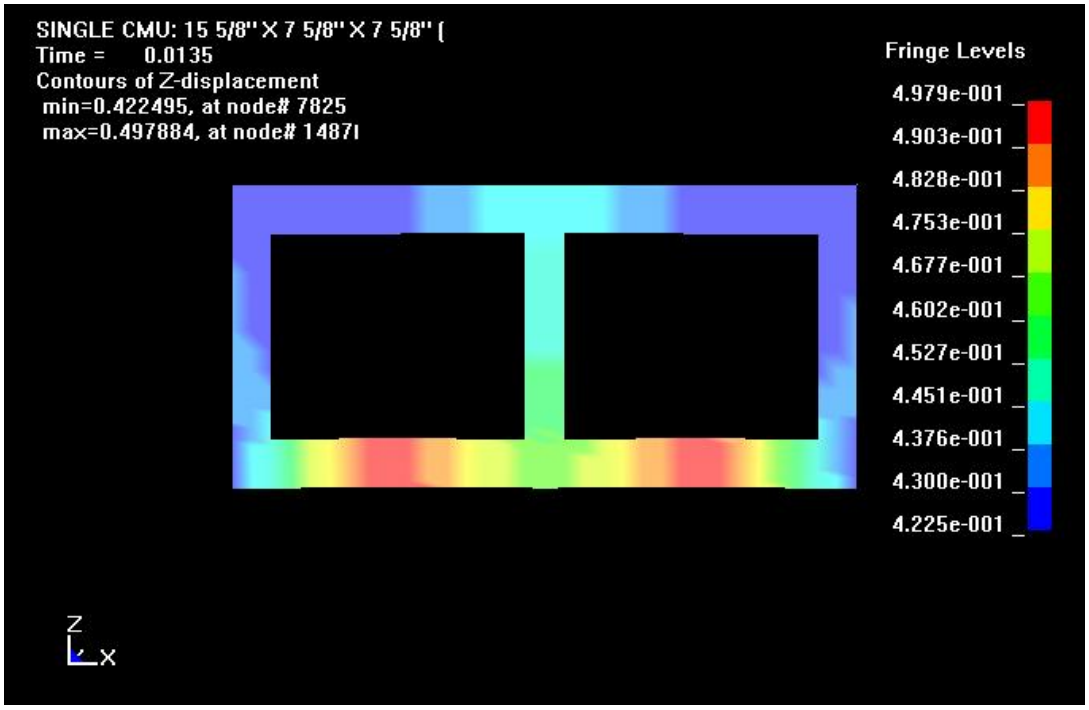

Figure 5.1-19 MAT_SOIL_AND_FOAM Displacement Fringes for 500 lb ANFO at 35 ft

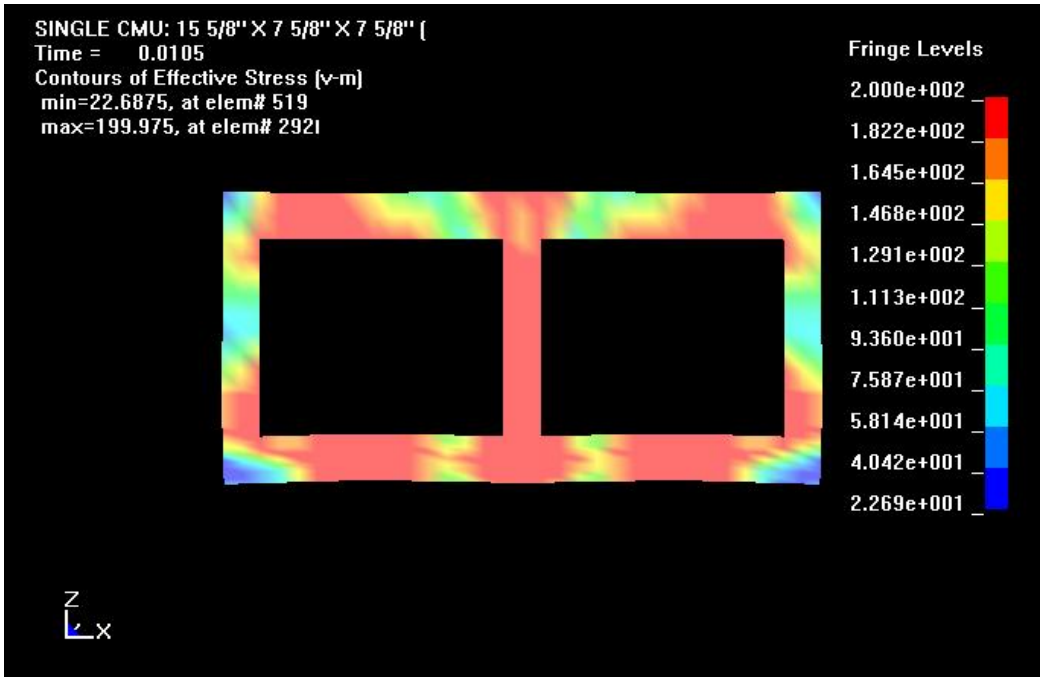

Figure 5.1-20 MAT_SOIL_AND_FOAM Stress Fringes for 1000 lb ANFO at 40 ft

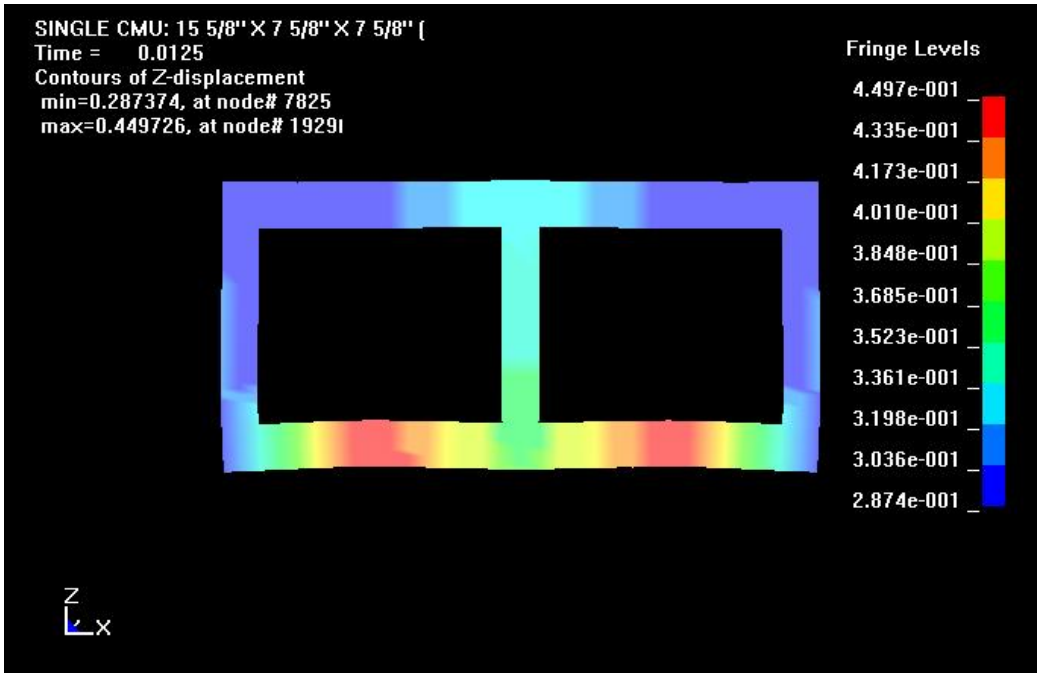

Figure 5.1-21 MAT_SOIL_AND_FOAM Displacement Fringes for 1000 lb ANFO at 40 ft

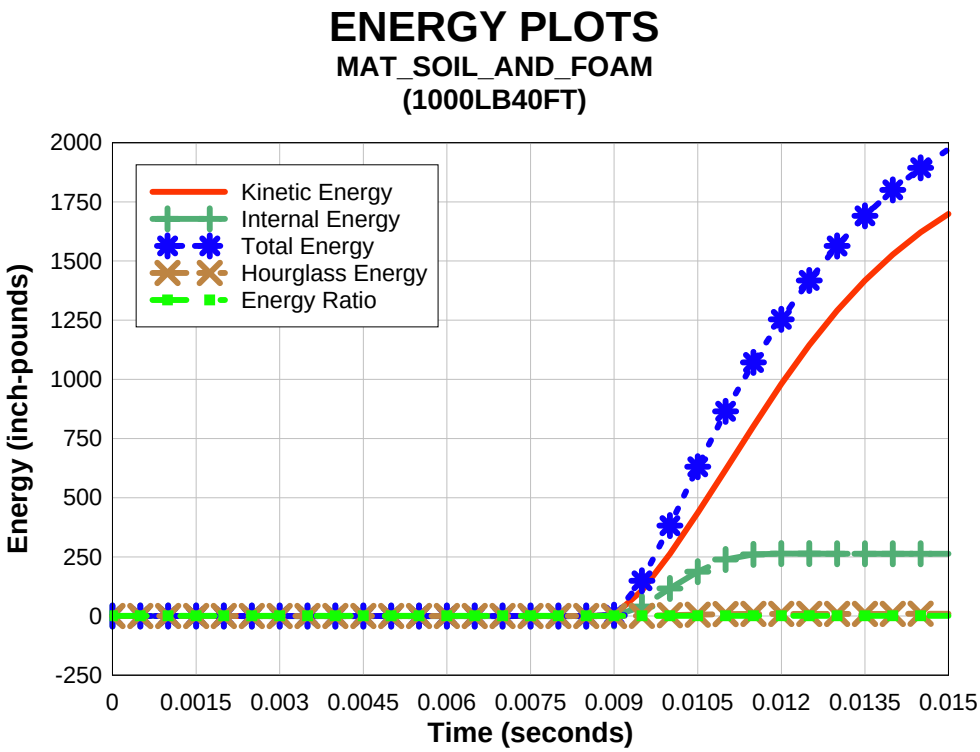

Figure 5.1-22 Energy Plots

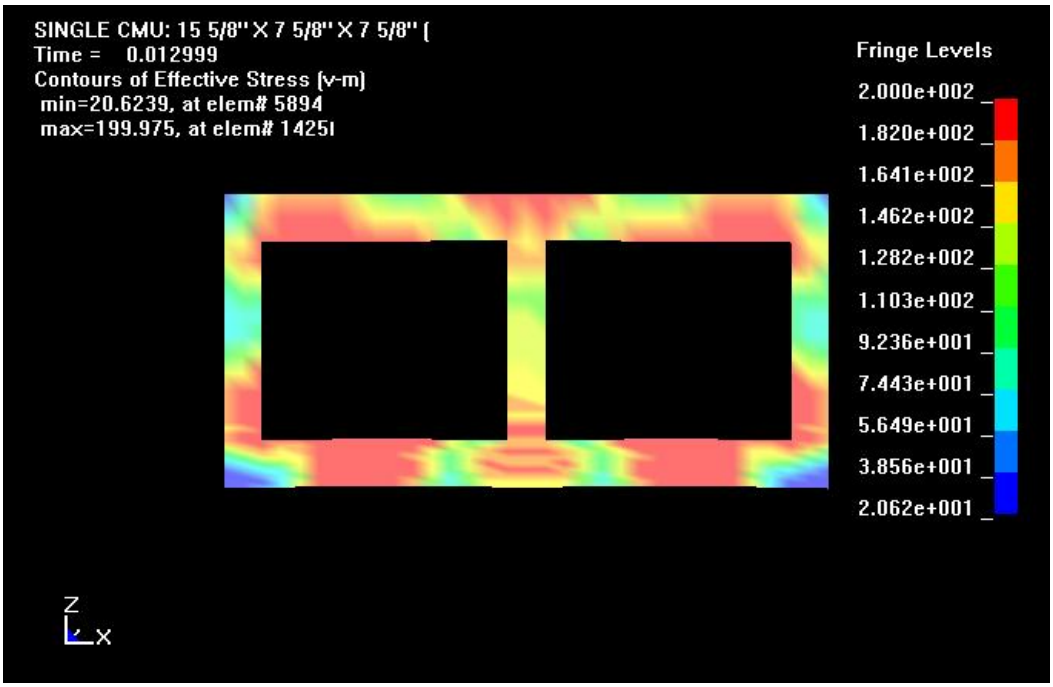

Figure 5.1-23 MAT_SOIL_AND_FOAM Stress Fringes for 1000 lb ANFO at 45 ft

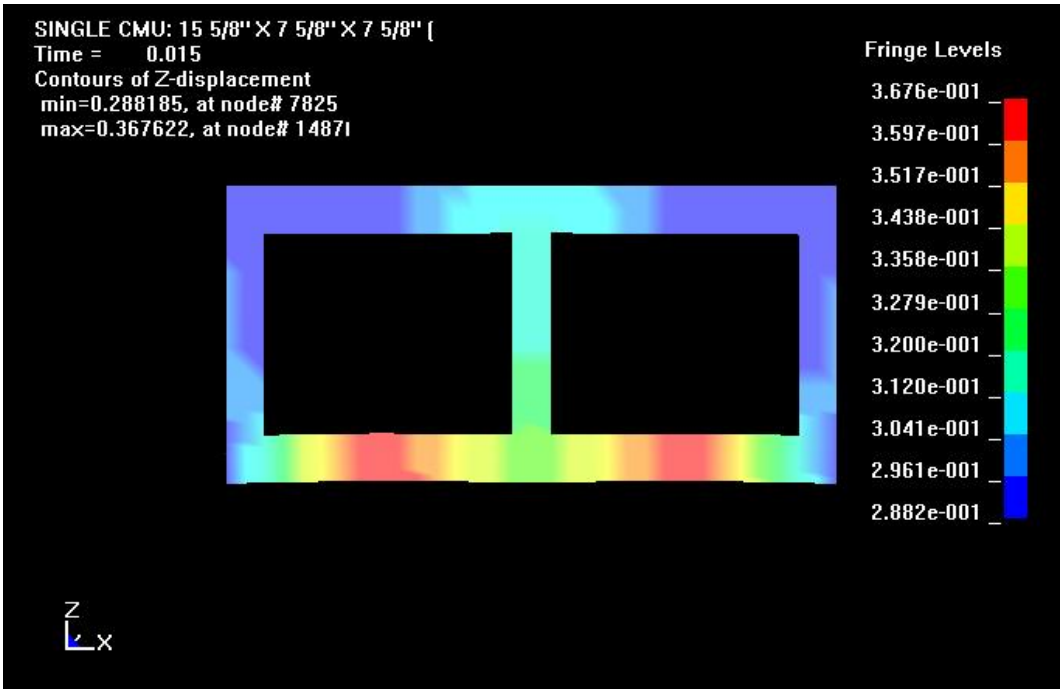

Figure 5.1-24 MAT_SOIL_AND_FOAM Displacement Fringes for 1000 lb ANFO at 45 ft

5.2 MAT_BRITTLE_DAMAGE

Just as in the previous case, the stress fringe levels for the MAT_ BRITTLE_DAMAGE constitutive model indicate that most sections of the CMU reach their ultimate strength within the first few m-seconds. However, examination of the displacement fringes and time histories show that most points on the CMU move at the same level and at the same time. For the 500 lb ANFO at 10 ft, the middle of the center rib displaces larger than the mid-point of the right front wall. At time step 1.5 m-sec, the maximum displacement is 0.08 in for the front wall and center rib of the CMU. This is 250% less than the MAT_SOIL_AND_FOAM case for the same loading condition. The energy plots exhibits significantly lower strain energy for all loading conditions except for the 500 lb ANFO at 10 ft. The kinetic energy is by far the dominant factor in the MAT_BRITTLE_DAMAGE constitutive model, and the hourglass energy and energy ratio appear to be at negligible levels. Similar results are noted for the 1000 lb ANFO where fracture is noticed at 20 ft, but rigid body movement in noticed at 40 ft or more. The complete results of the MAT_BRITTLE_DAMAGE complement are included in the following list.

500lb20ft	Failure	1000lb20ft	Failure
500lb30ft	Failure	1000lb40ft	No Failure
500lb35ft	No Failure	1000lb45ft	No Failure
500lb36ft	No Failure	1000lb46ft	No Failure
500lb37ft	No Failure		

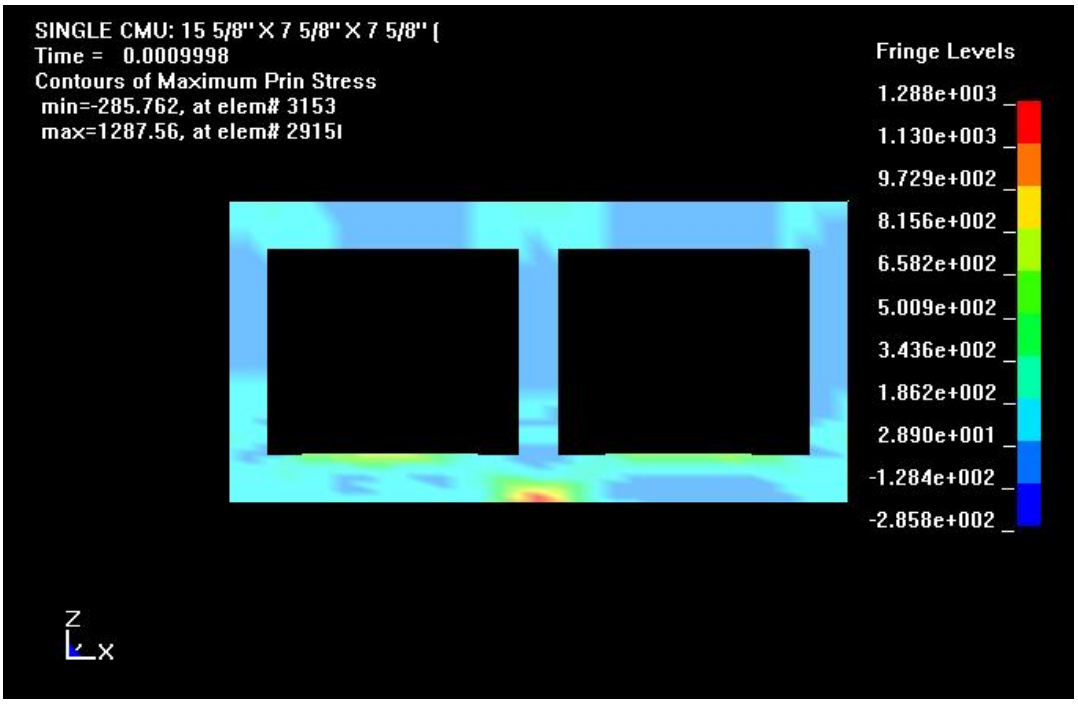

Figure 5.2-1 MAT_BRITTLE_DAMAGE Stress Fringes for 500 lb ANFO at 10 ft

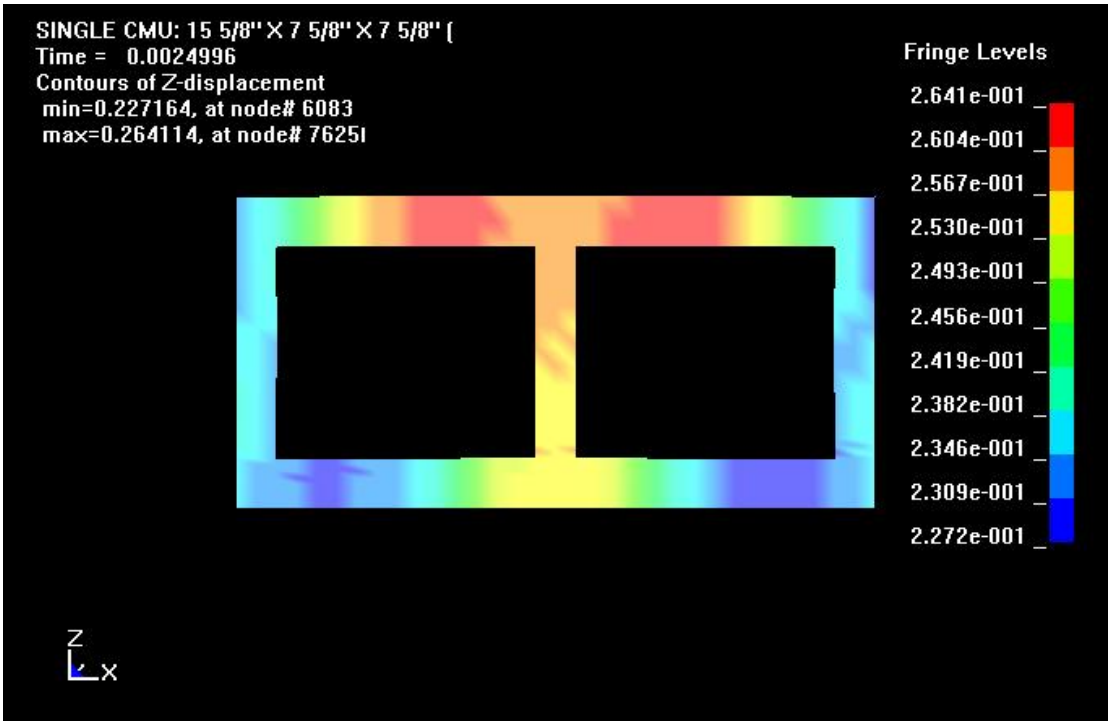

Figure 5.2-2 MAT_BRITTLE_DAMAGE Displacement Fringes for 500 lb ANFO at 10 ft

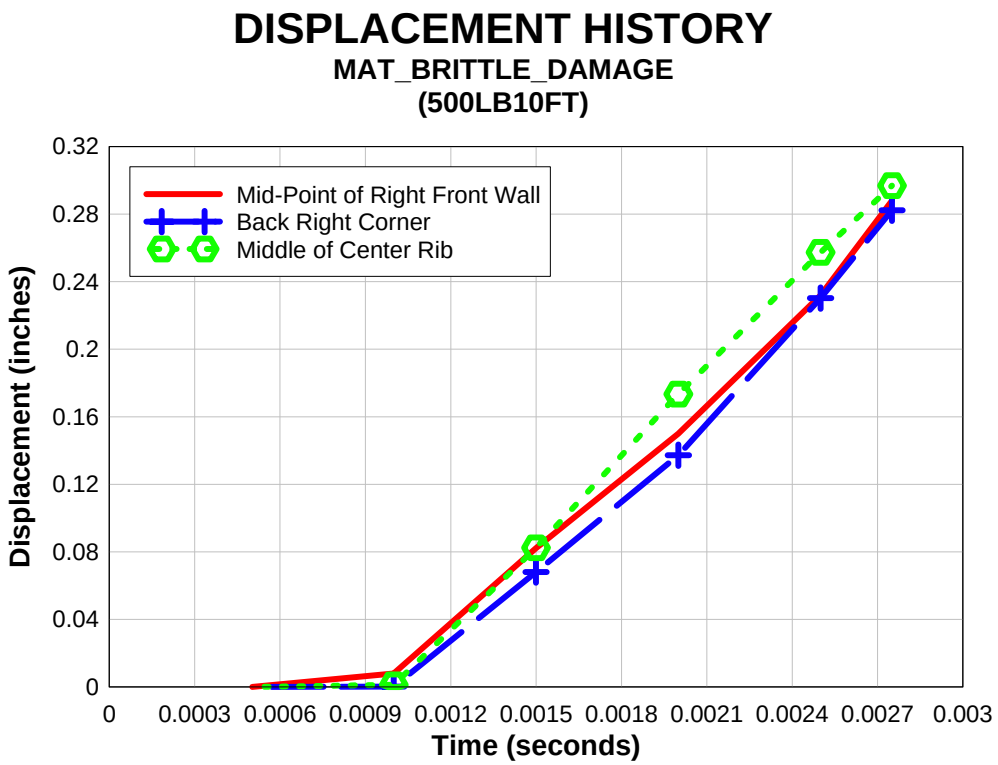

Figure 5.2-3 Displacement History Plots

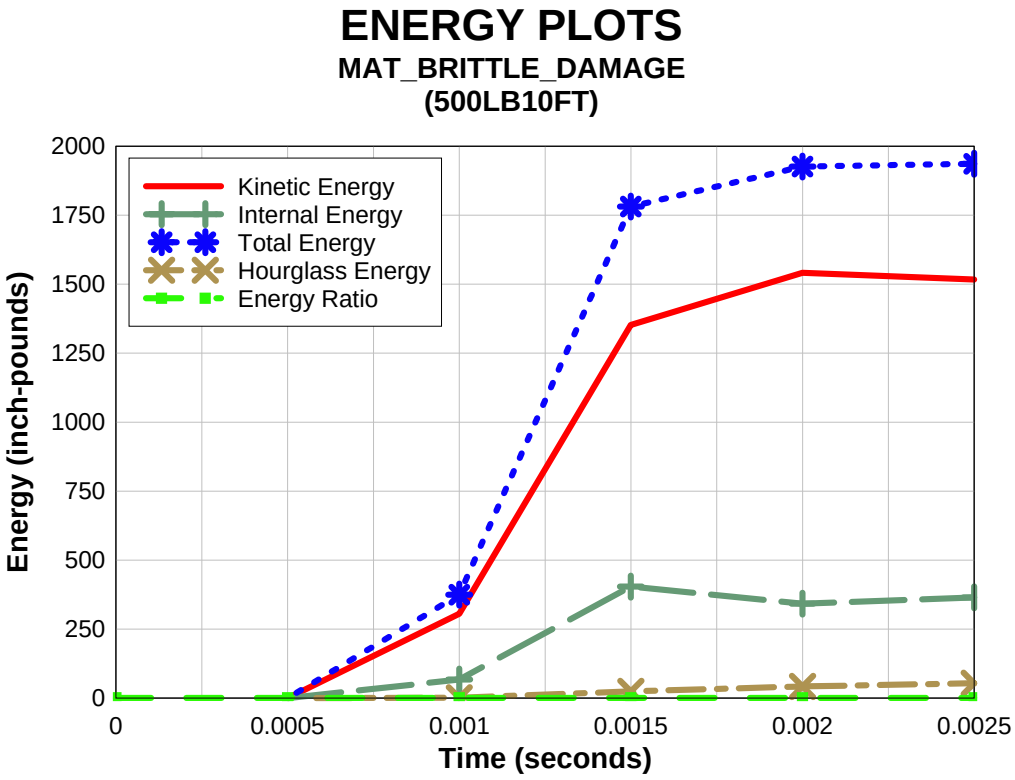

Figure 5.2-4 Energy Plots

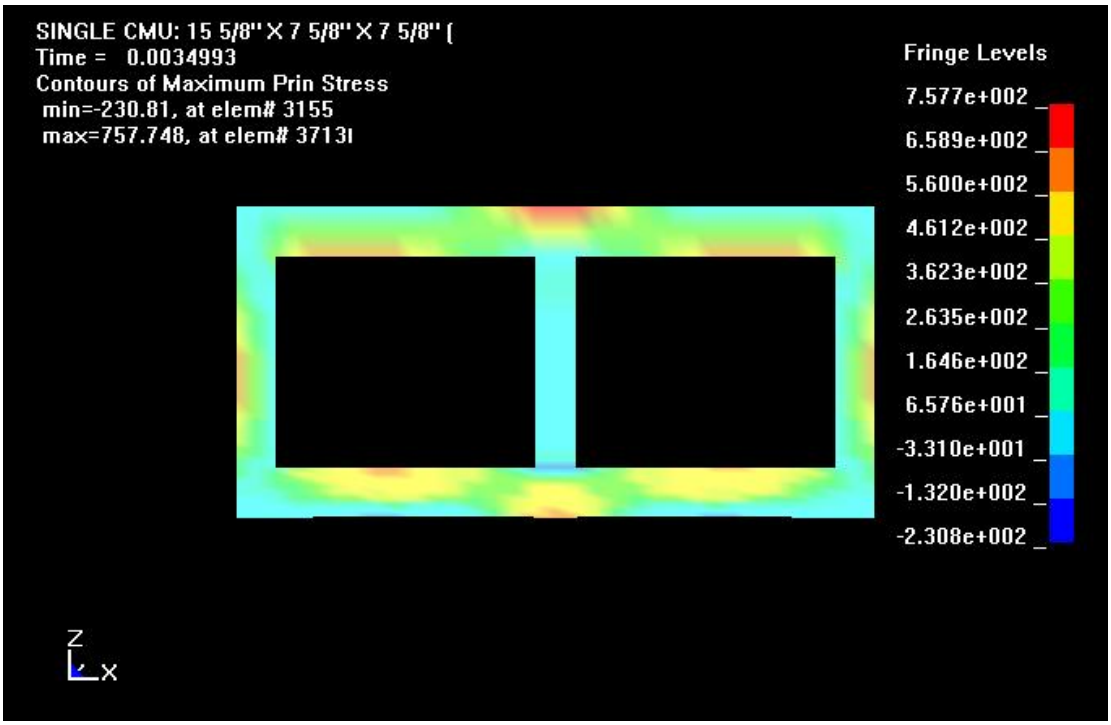

Figure 5.2-5 MAT_BRITTLE_DAMAGE Stress Fringes for 500 lb ANFO at 20 ft

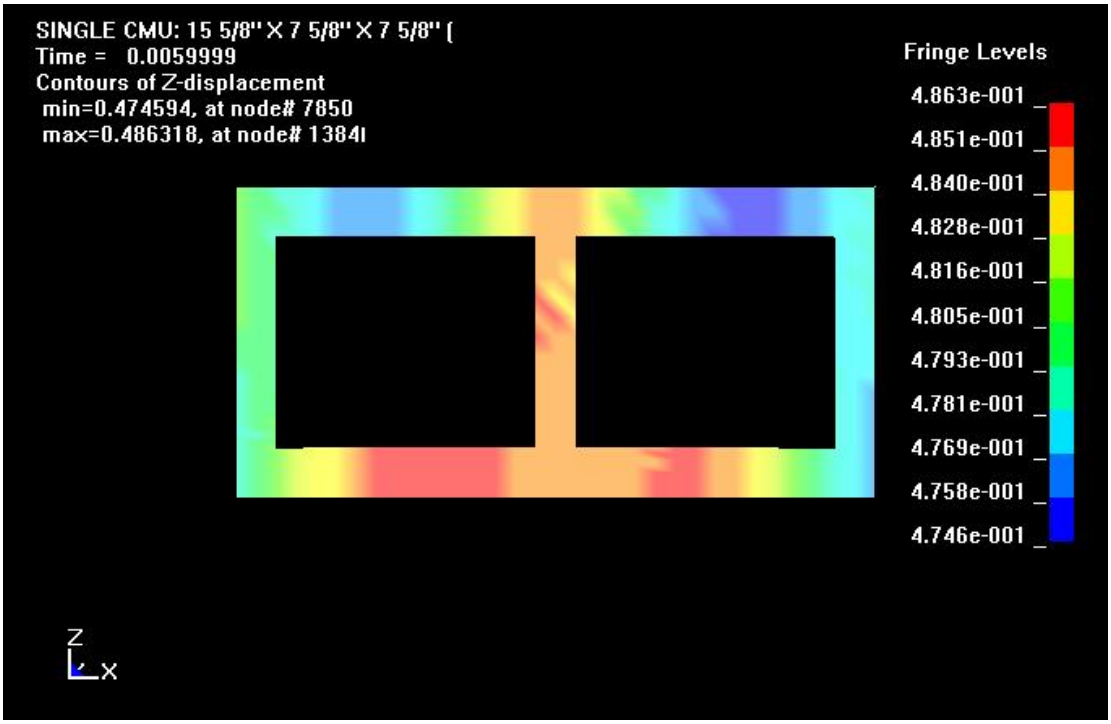

Figure 5.2-6 MAT_BRITTLE_DAMAGE Displacement Fringes for 500 lb ANFO at 20 ft

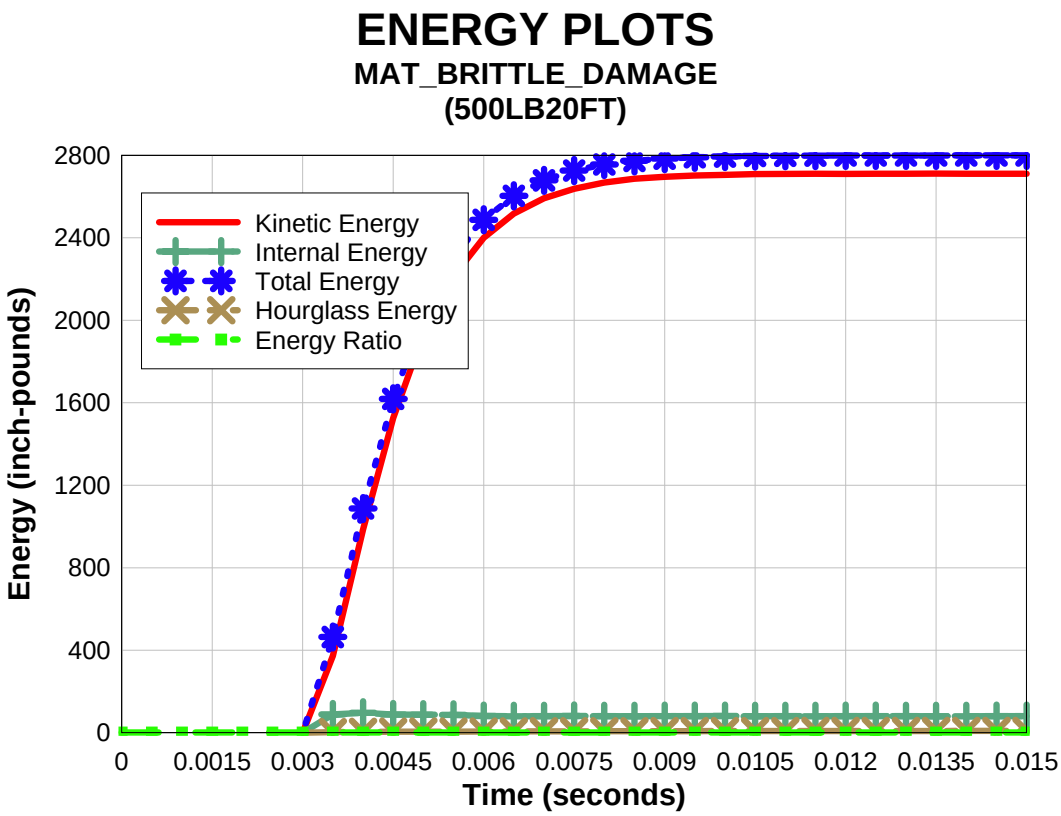

Figure 5.2-7 Energy Plots

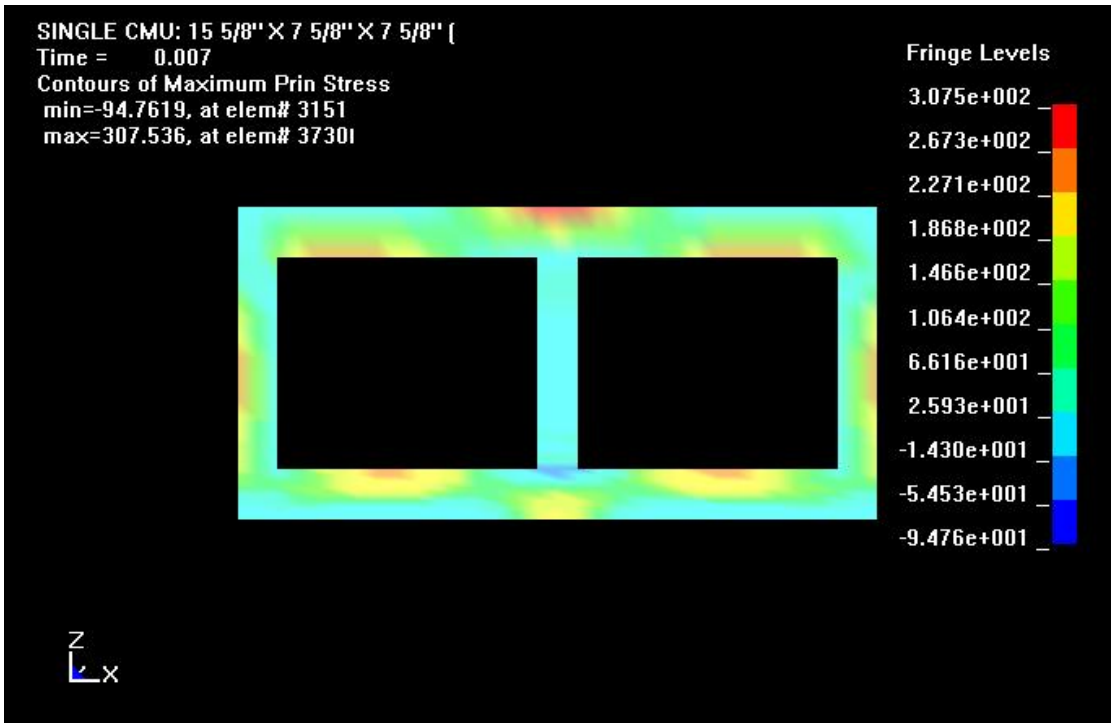

Figure 5.2-8 MAT_BRITTLE_DAMAGE Stress Fringes for 500 lb ANFO at 30 ft

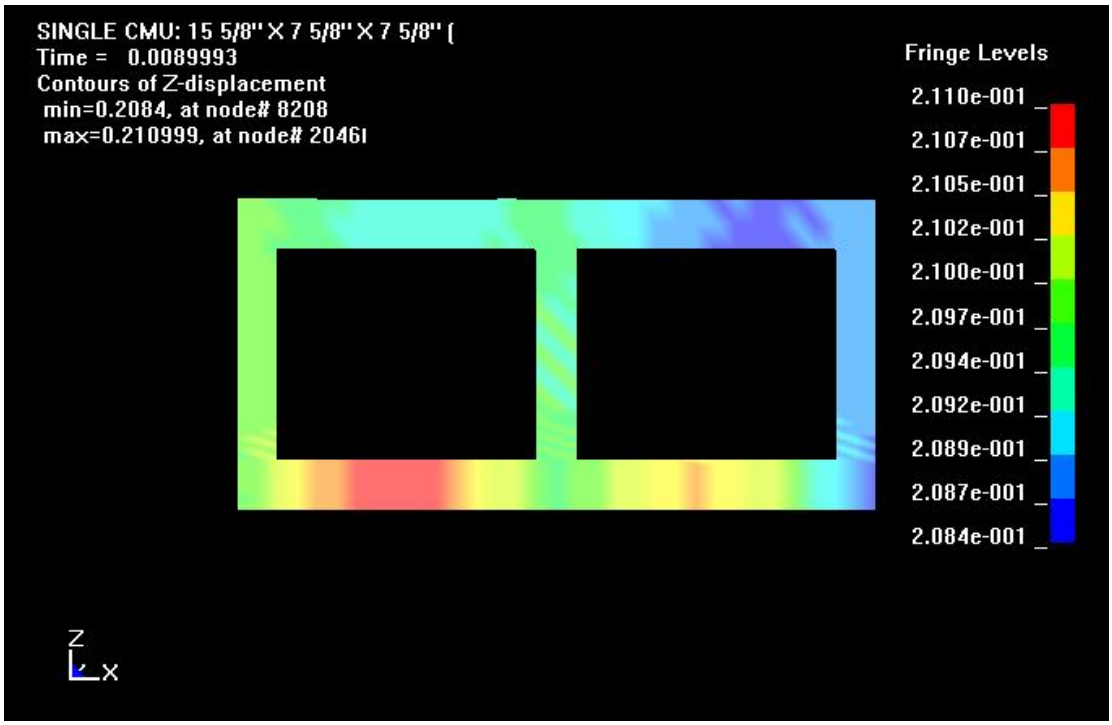

Figure 5.2-9 MAT_BRITTLE_DAMAGE Displacement Fringes for 500 lb ANFO at 30 ft

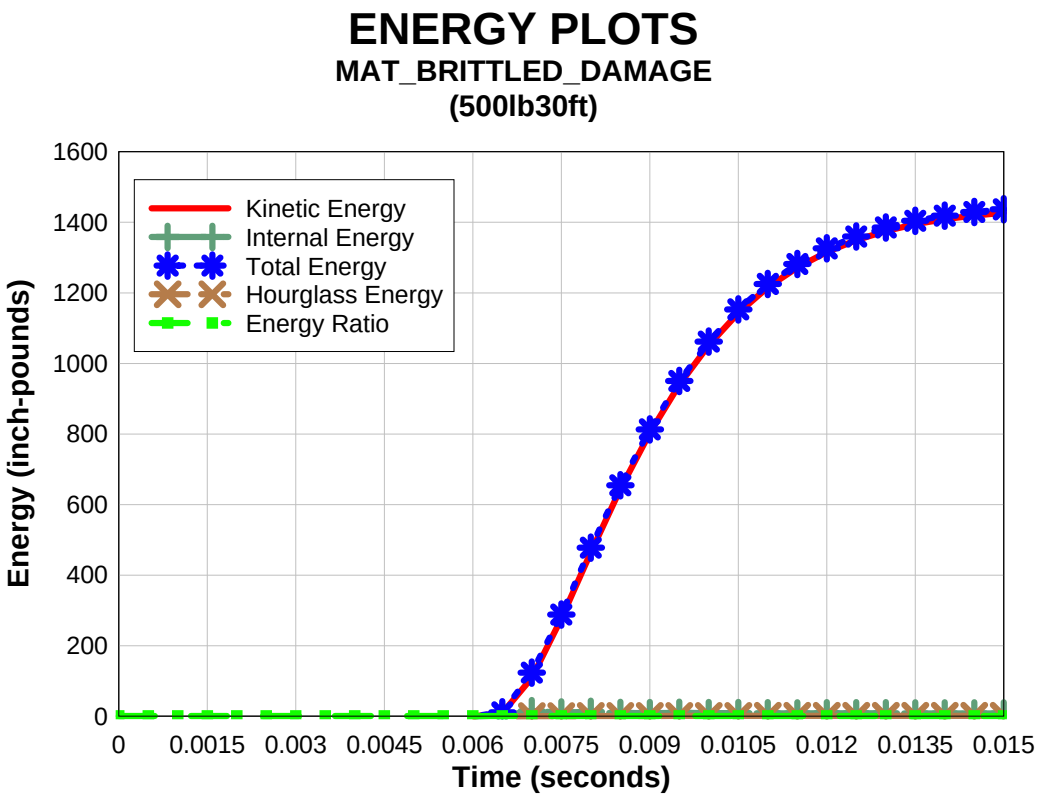

Figure 5.2-10 Energy Plots

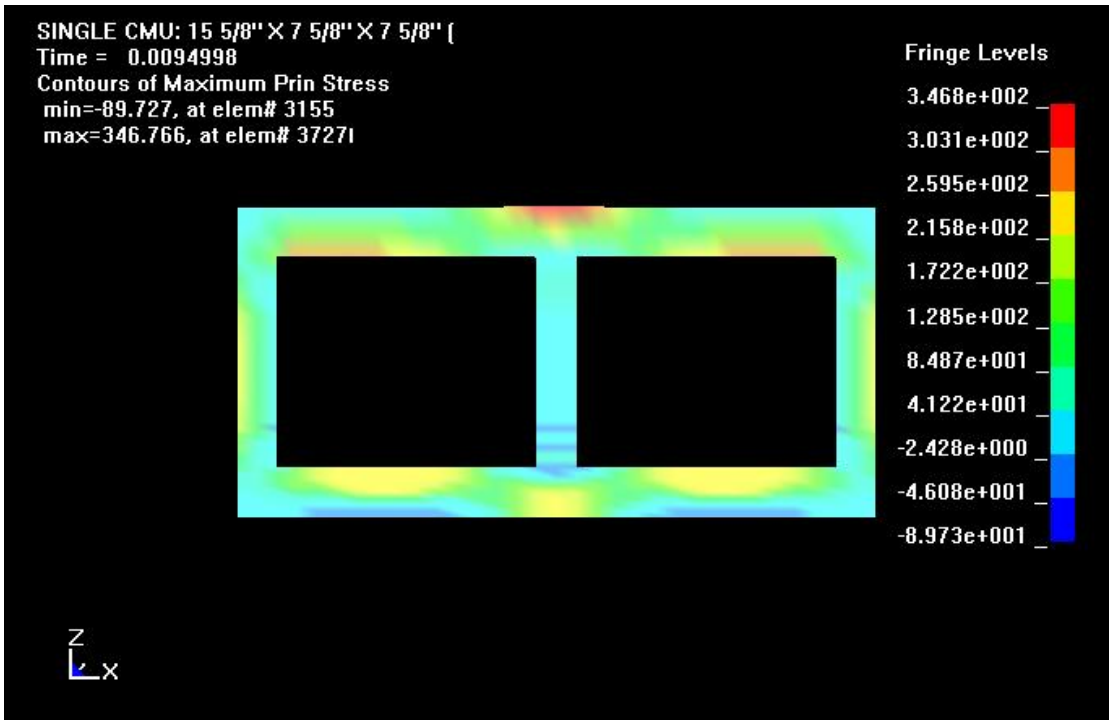

Figure 5.2-11 MAT_BRITTLE_DAMAGE Stress Fringes for 1000 lb ANFO at 40 ft

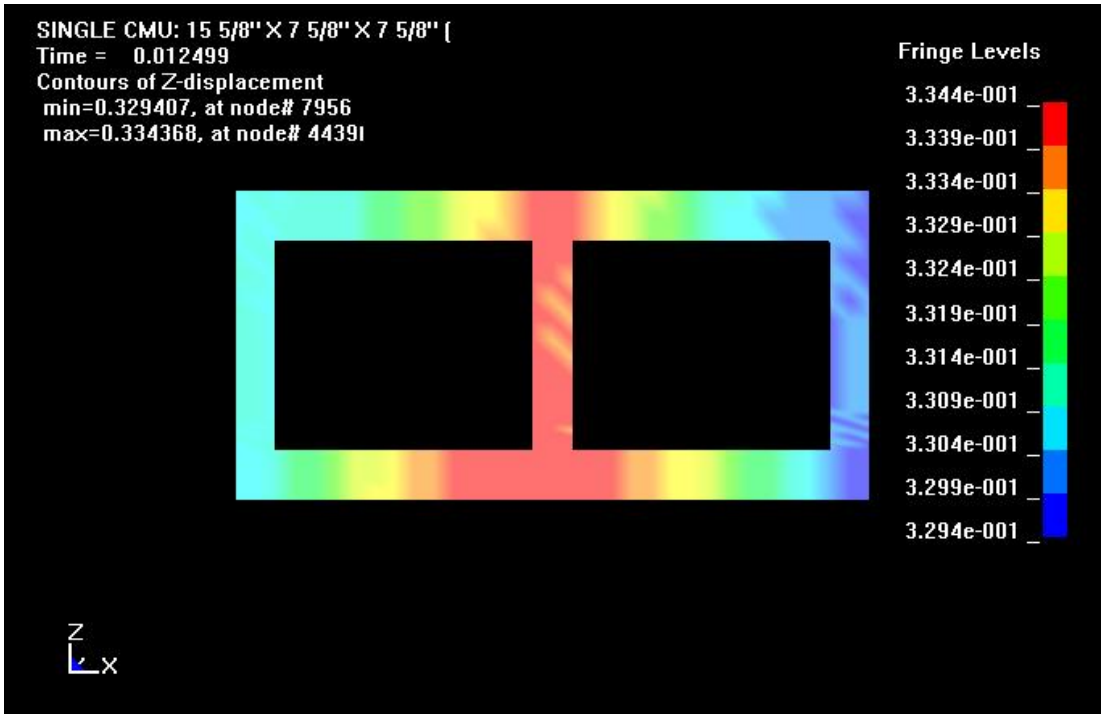

Figure 5.2-12 MAT_BRITTLE_DAMAGE Displacement Fringes for 1000 lb ANFO at 40 ft

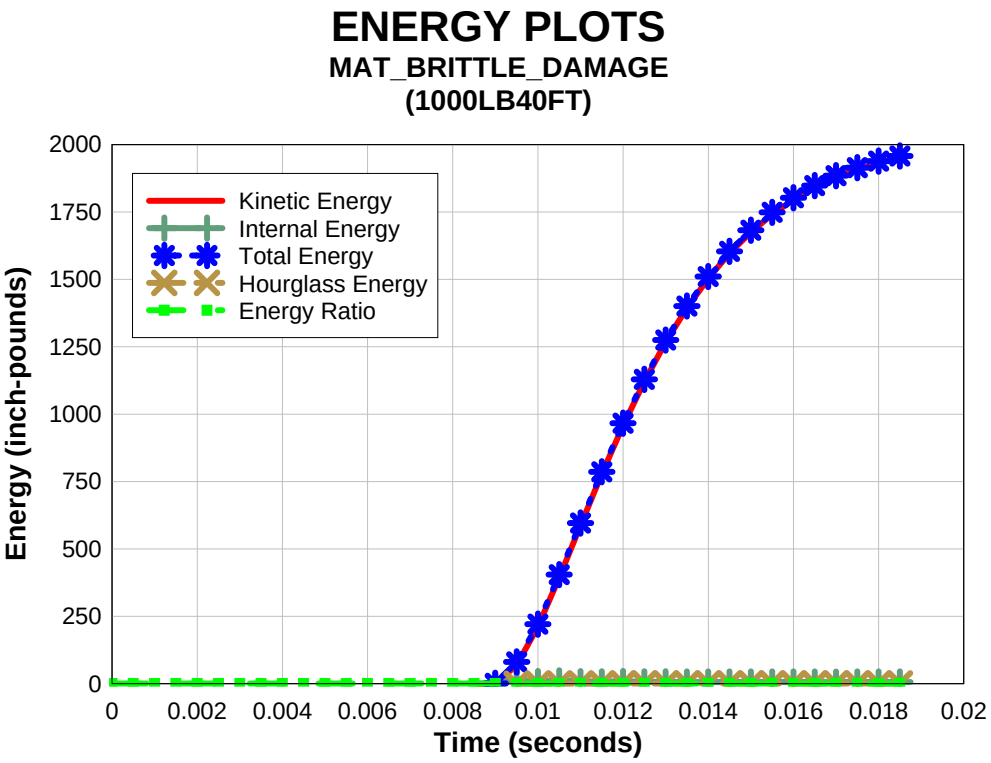

Figure 5.2-13 Energy Plots

5.3 MAT_PSEUDO_TENSOR

The stress fringe levels indicate that the exposed front wall of the CMU reaches its ultimate strength within the first few m-seconds. Stress levels tend to remain at this level as the elements of the exposed wall experience large displacements in the following m-seconds of the blast. Examination of the displacement fringes and time histories show that the mid-point of the right (or left) front wall of the CMU moves at significantly greater levels than the rear corner or a point on the middle rib of the CMU. In the case of 500 lb ANFO at 10 ft, the mid-point of the right wall displaces 0.2 in at 1.5 m-sec whereas the other two points of interest displace slightly above zero. This is in agreement with the MAT_SOIL_AND_FOAM results of the same loading condition. Examination of the energy plots show that the CMU exhibits significantly low strain energy for all loading conditions, and the kinetic energy is the dominant factor in this case. The hourglass energy seems to be significantly higher than the MAT_SOIL_AND_FOAM and MAT_BRITTLE_DAMAGE results. Overall, the CMU experiences fracture for 500 lb ANFO at 28 ft or less. However, at 29 ft or more the CMU experiences more of a rigid body movement where the stress level reaches the ultimate strength but fracture does not occur. Similar results are noted for the 1000 lb ANFO where fracture is noticed at 37 ft or less, but rigid body movement in noticed at 38 ft or more. The conclusion drawn is that although the MAT_PSEUDO_TENSOR constitutive model predicts stress fracture fairly accurately, it has difficulties with hourglass energy for this application. The complete results of the MAT_PSEUDO_TENSOR complement are included in the following list.

500lb10ft	Failure	1000lb20ft	Failure
500lb20ft	Failure	1000lb35ft	Failure
500lb25ft	Failure	1000lb36ft	Failure
500lb28ft	Failure	1000lb37ft	Failure
500lb29ft	No Failure	1000lb38ft	No Failure
500lb30ft	No Failure	1000lb40ft	No Failure
500lb35ft	No Failure		

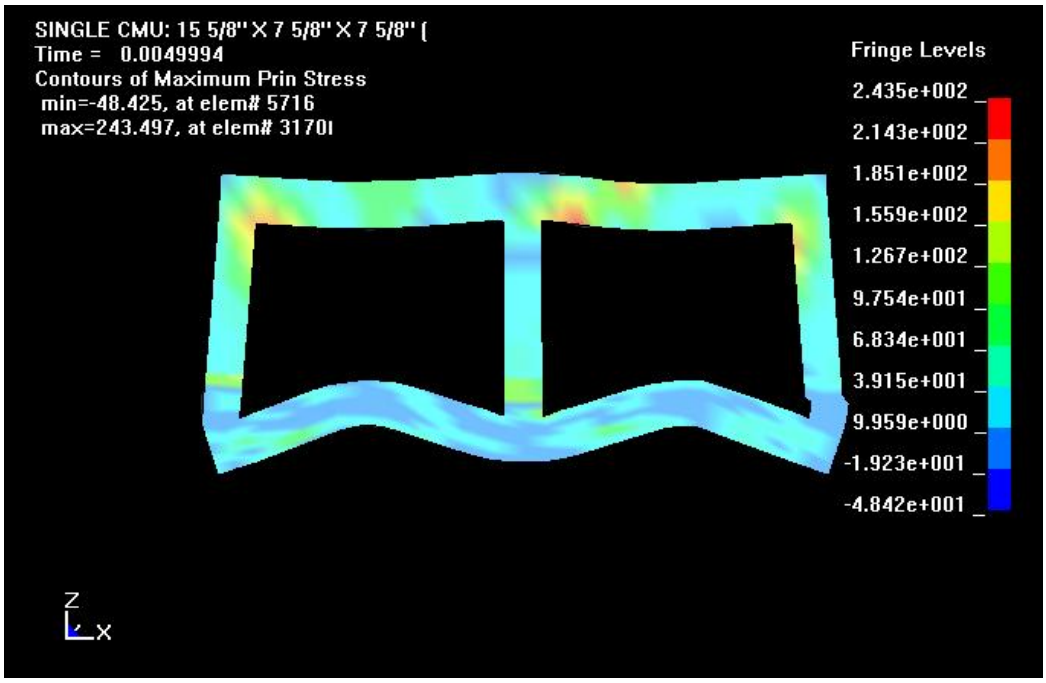

Figure 5.3-1 MAT_PSEUDO_TENSOR Stress Fringes for 500 lb ANFO at 10 ft

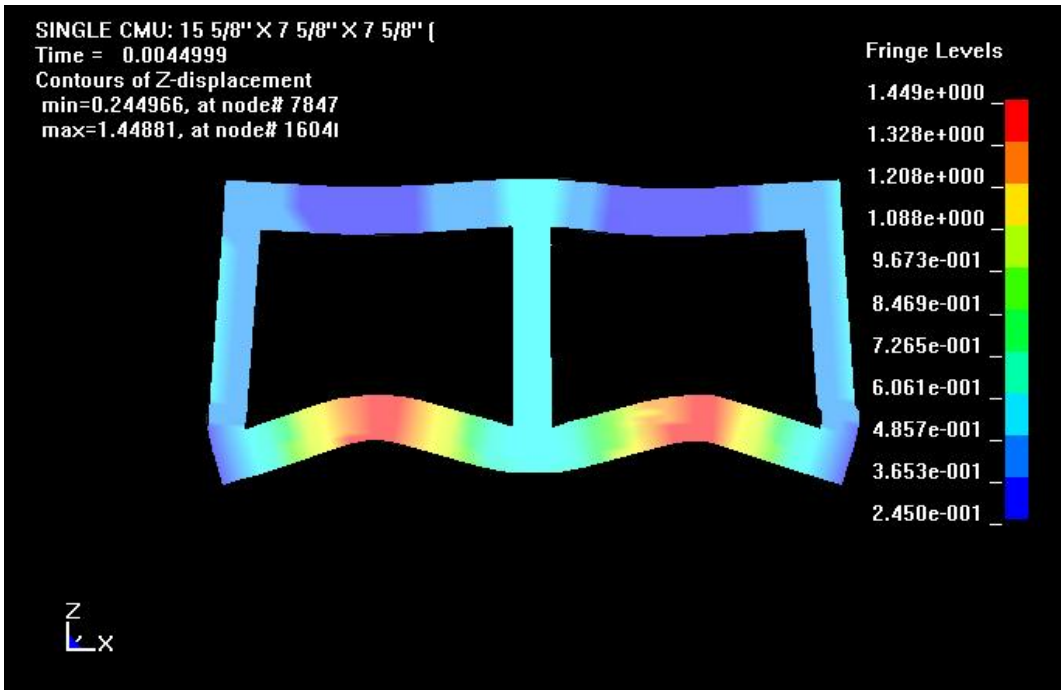

Figure 5.3-2 MAT_PSEUDO_TENSOR Displacement Fringes for 500 lb ANFO at 10 ft

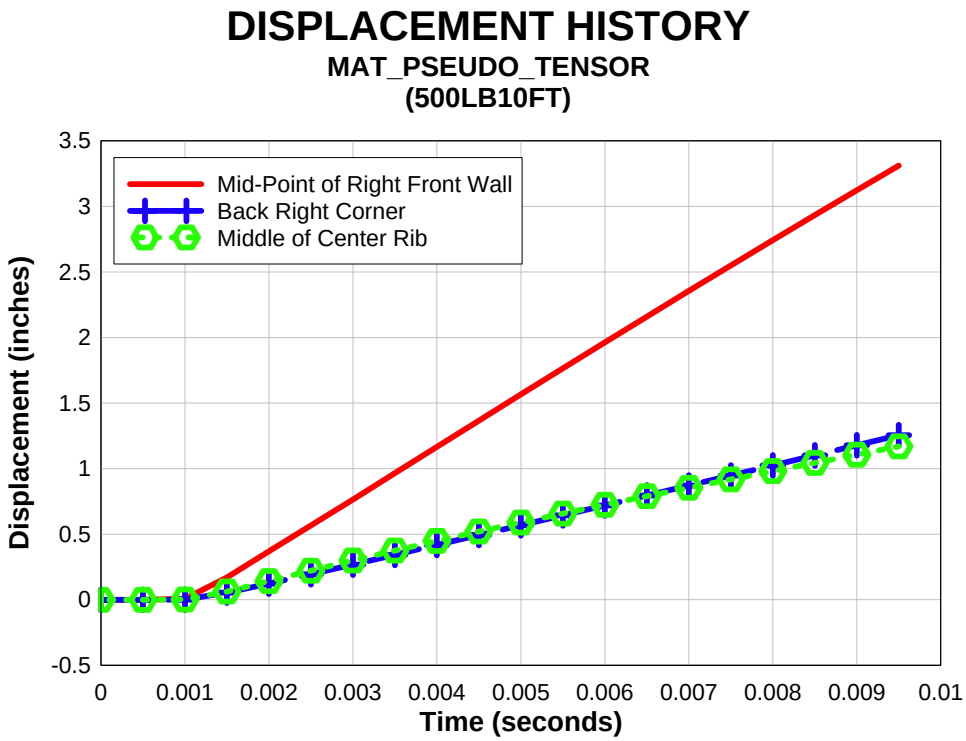

Figure 5.3-3 Displacement History Plots

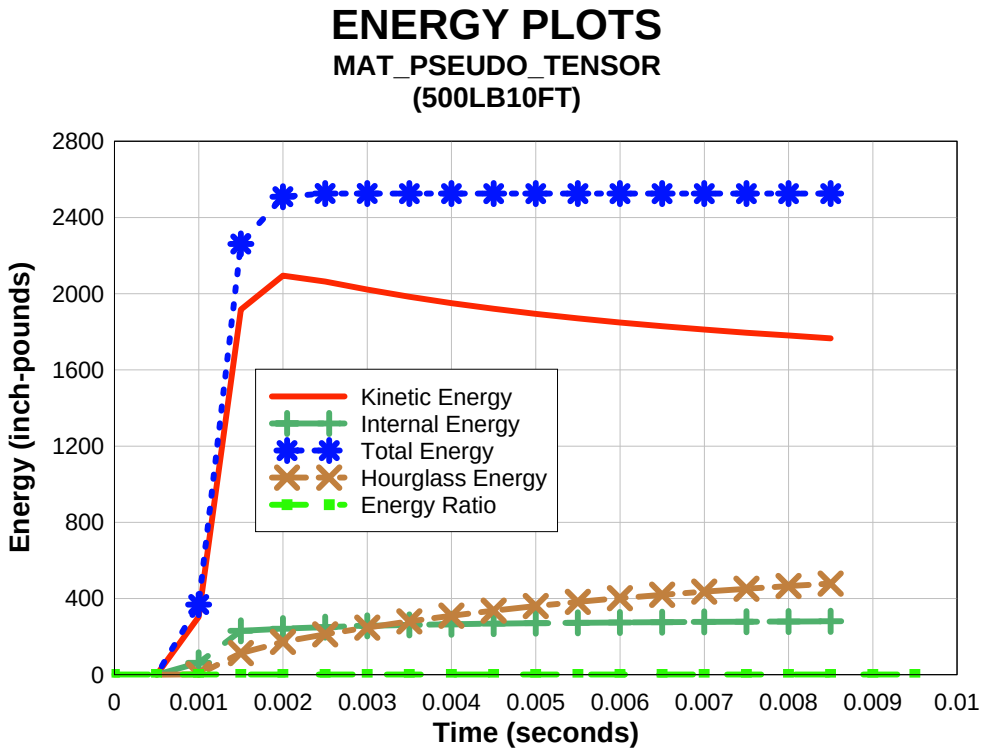

Figure 5.3-4 Energy Plots

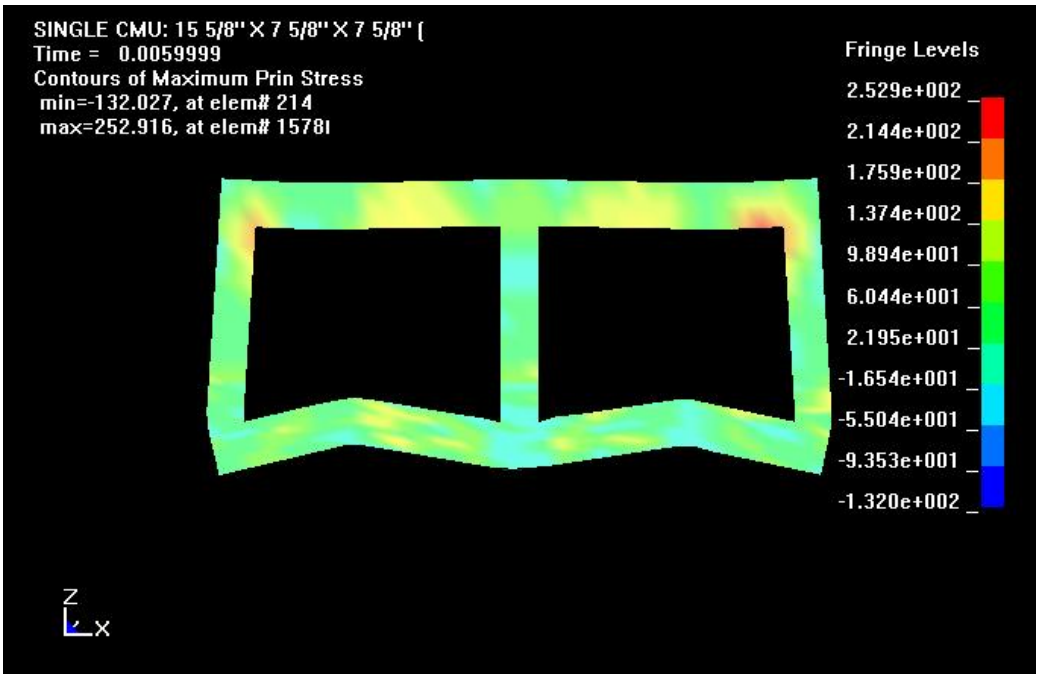

Figure 5.3-5 MAT_PSEUDO_TENSOR Stress Fringes for 500 lb ANFO at 20 ft

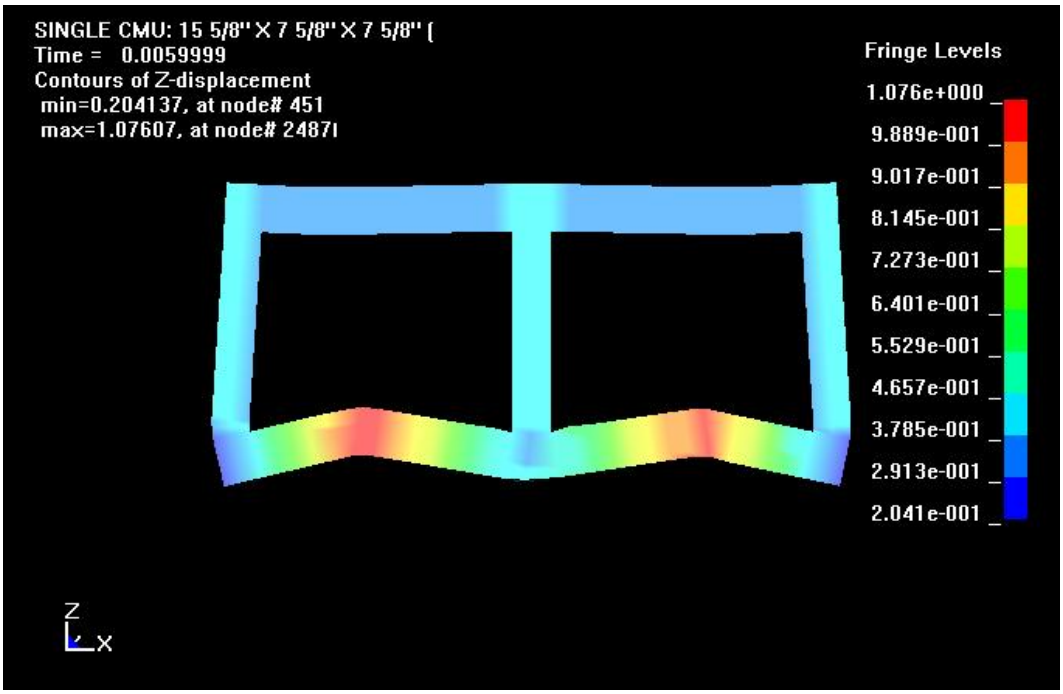

Figure 5.3-6 MAT_PSEUDO_TENSOR Displacement Fringes for 500 lb ANFO at 20 ft

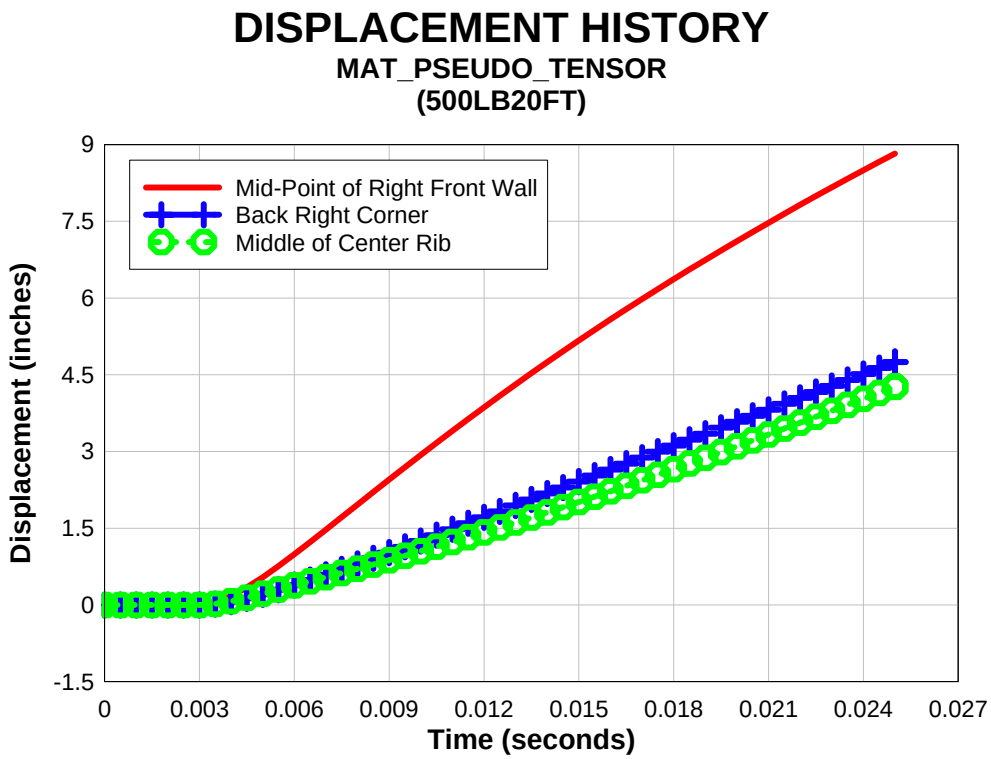

Figure 5.3-7 Displacement History Plots

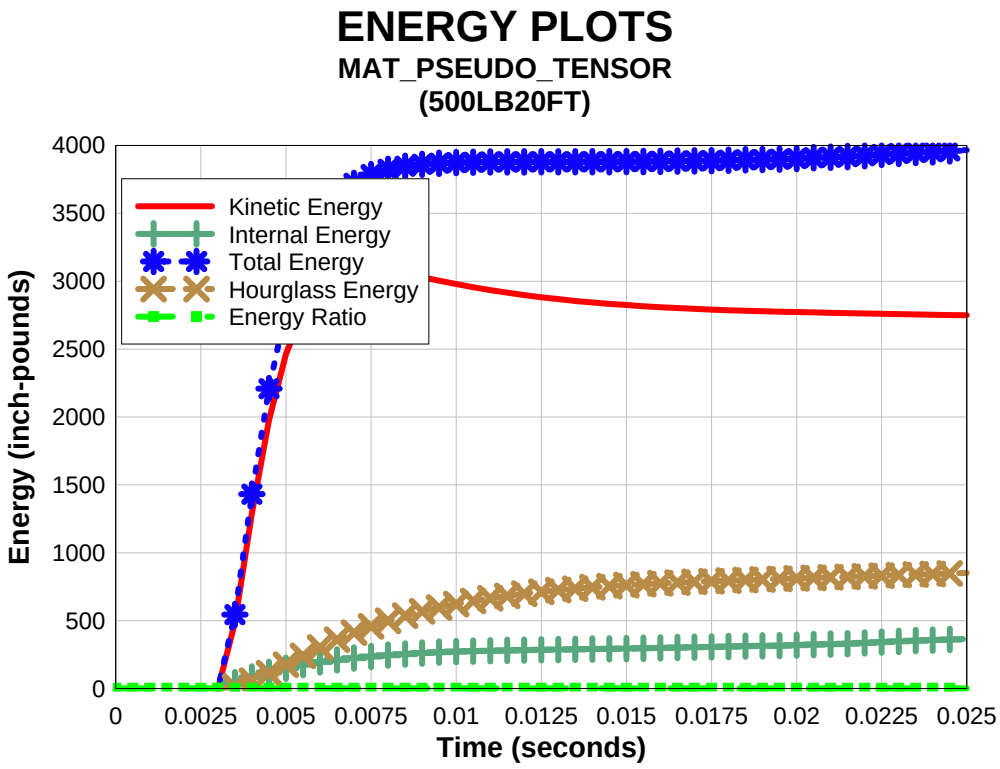

Figure 5.3-8 Energy Plots

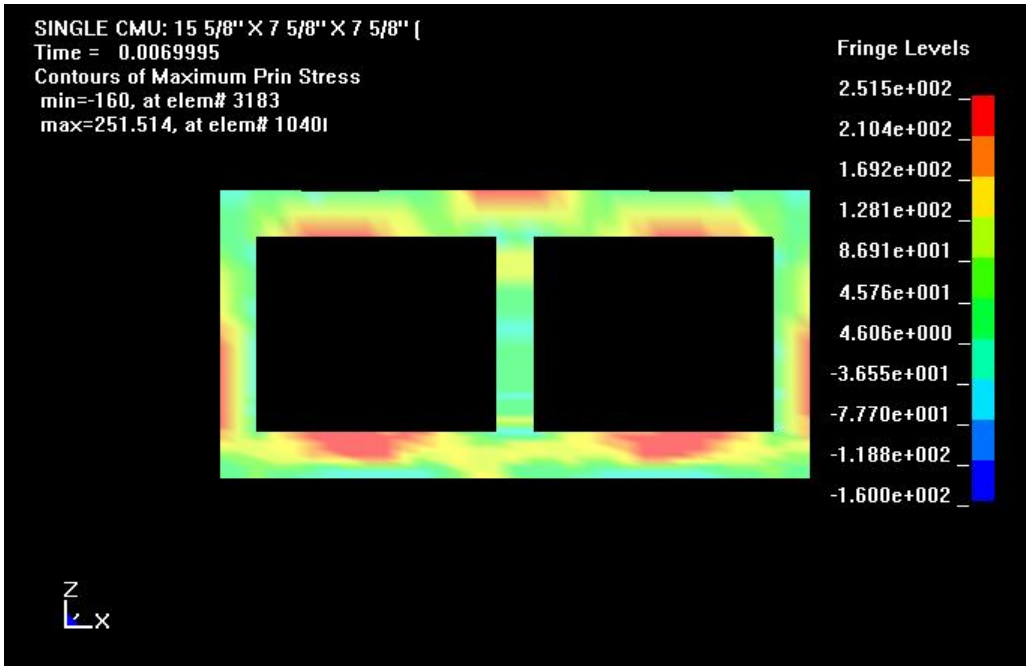

Figure 5.3-9 MAT_PSEUDO_TENSOR Stress Fringes for 500 lb ANFO at 30 ft

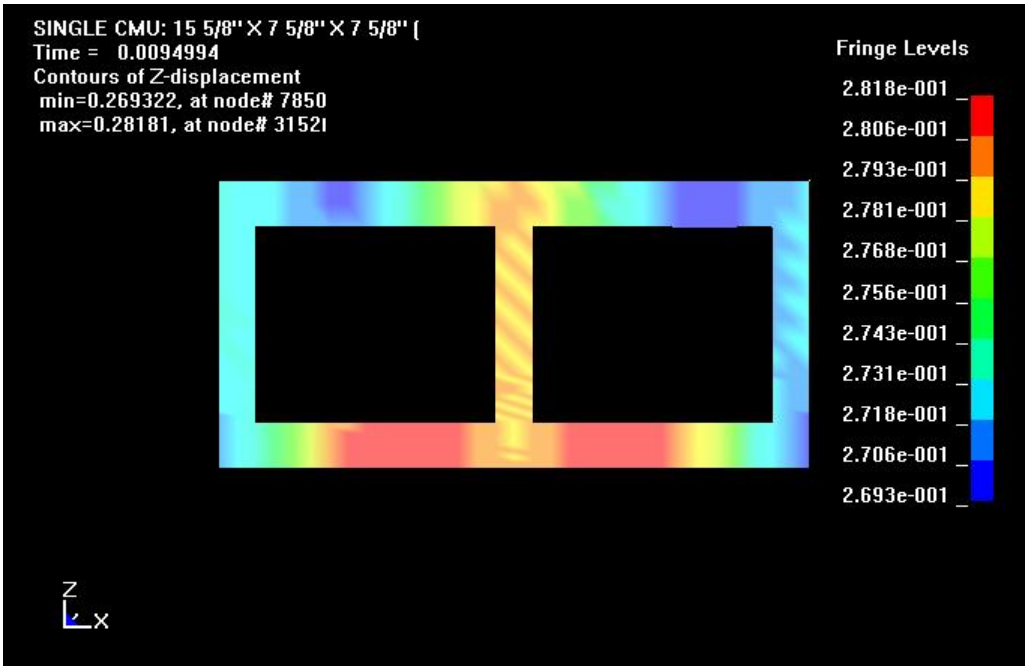

Figure 5.3-10 MAT_PSEUDO_TENSOR Displacement Fringes for 500 lb ANFO at 30 ft

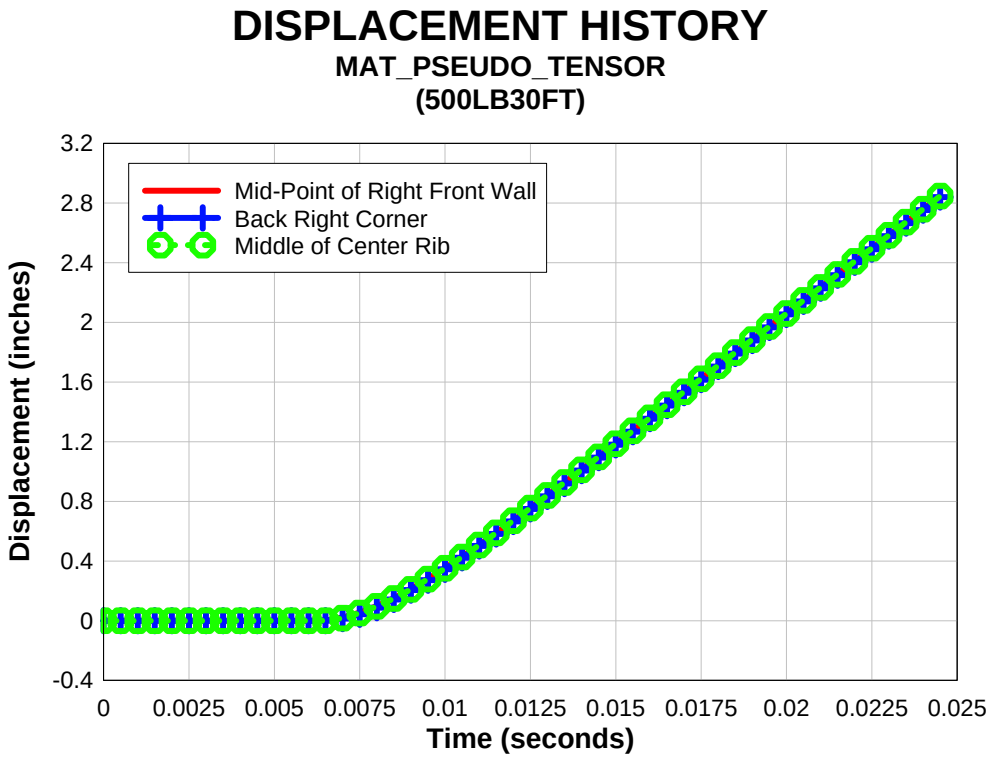

Figure 5.3-11 Displacement History Plots

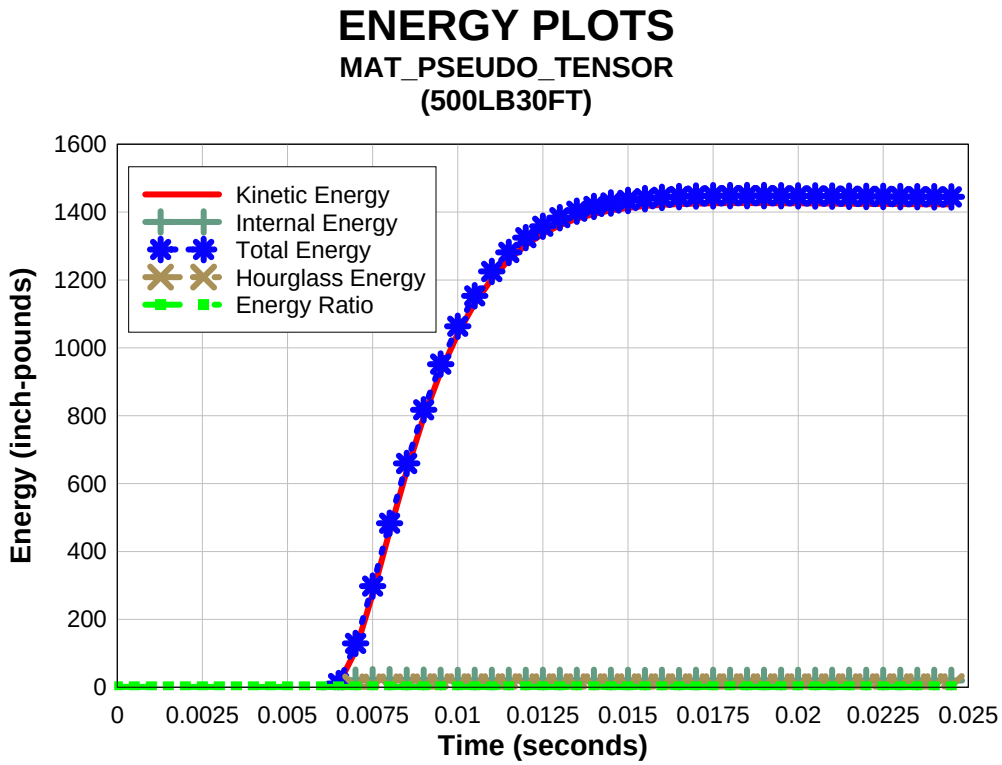

Figure 5.3-12 Energy Plots

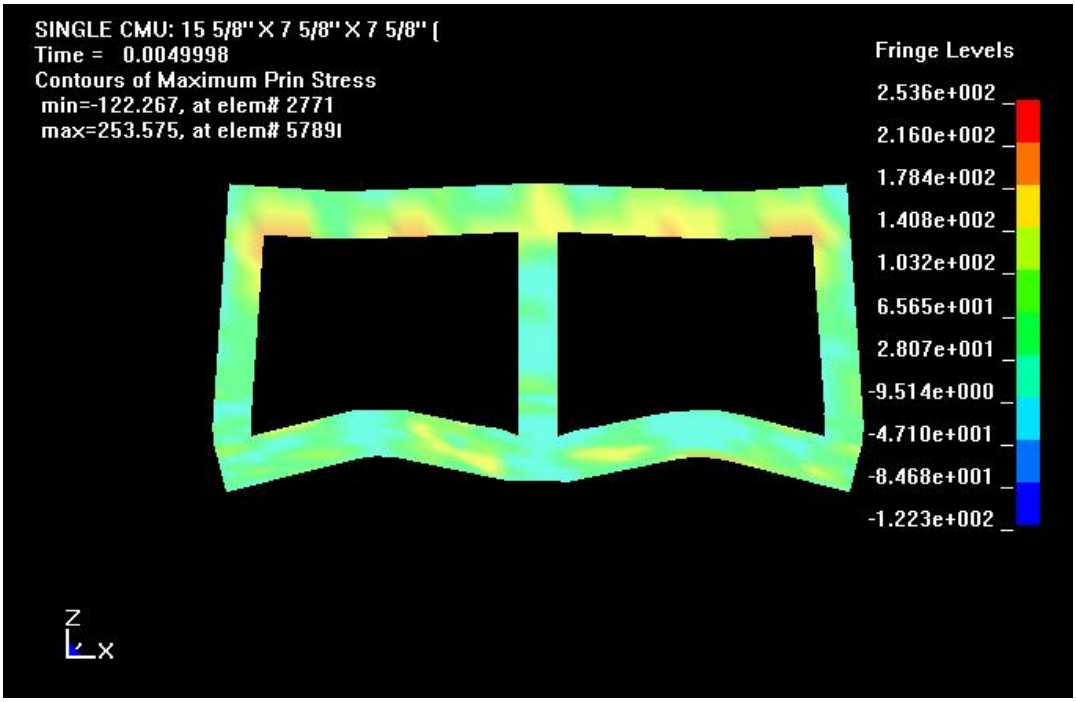

Figure 5.3-13 MAT_PSEUDO_TENSOR Stress Fringes for 1000 lb ANFO at 20 ft

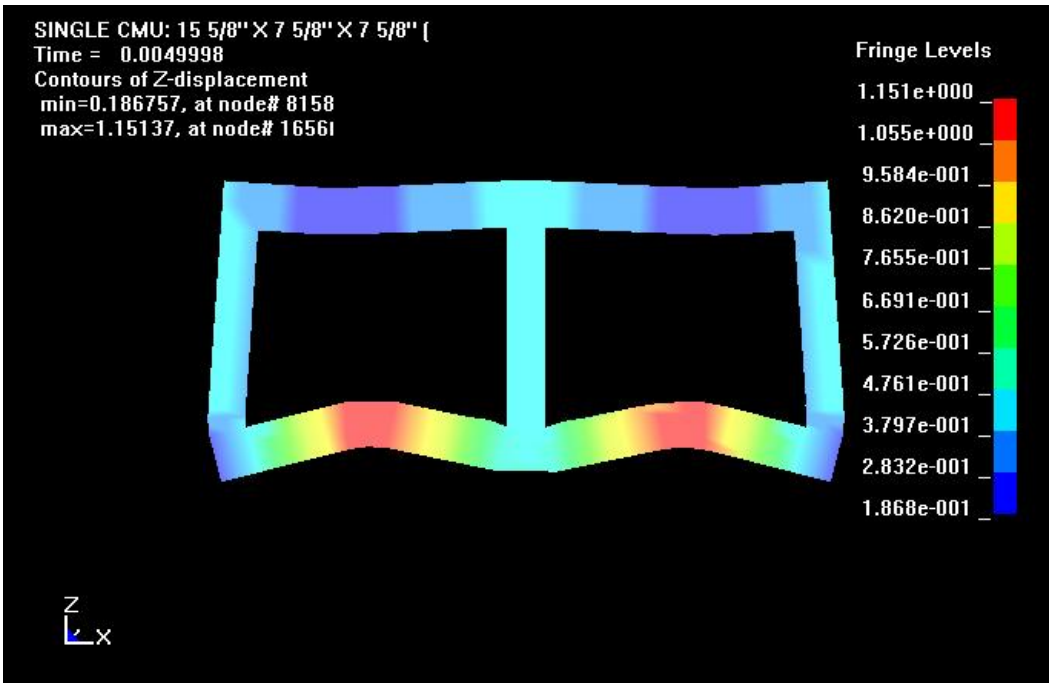

Figure 5.3-14 MAT_PSEUDO_TENSOR Displacement Fringes for 1000 lb ANFO at 20 ft

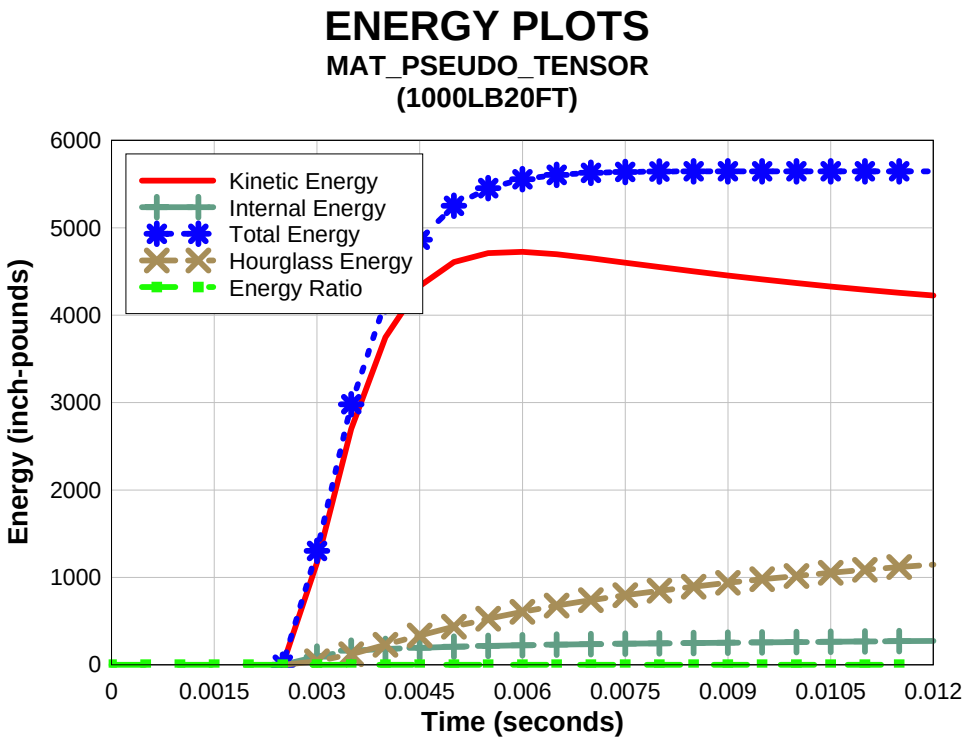

Figure 5.3-15 Energy Plots

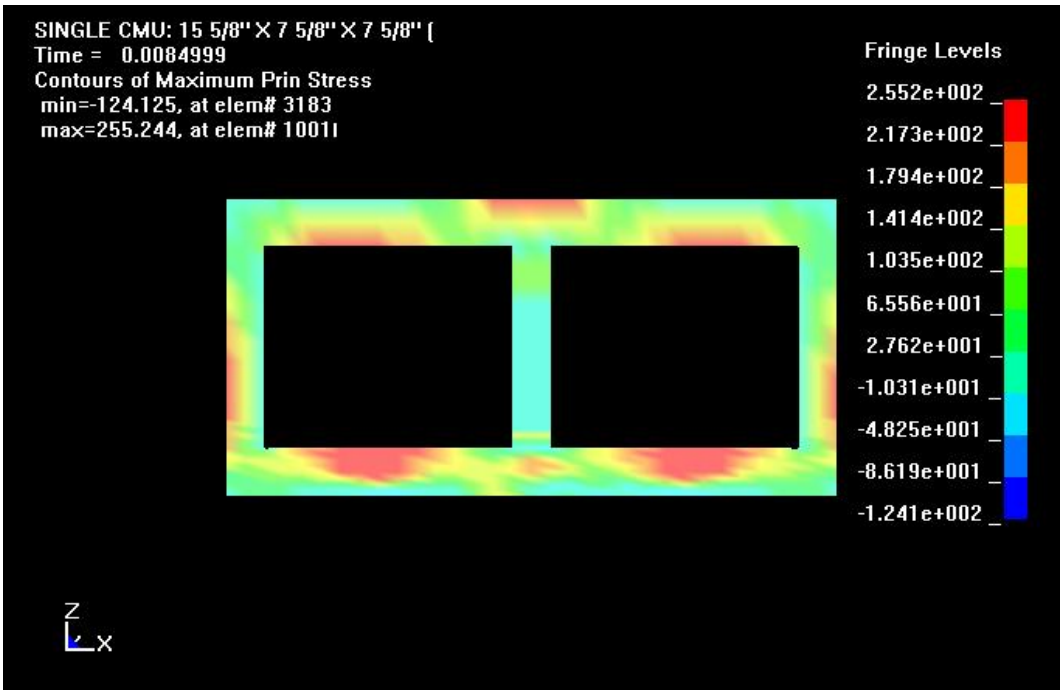

Figure 5.3-16 MAT_PSEUDO_TENSOR Stress Fringes for 1000 lb ANFO at 38 ft

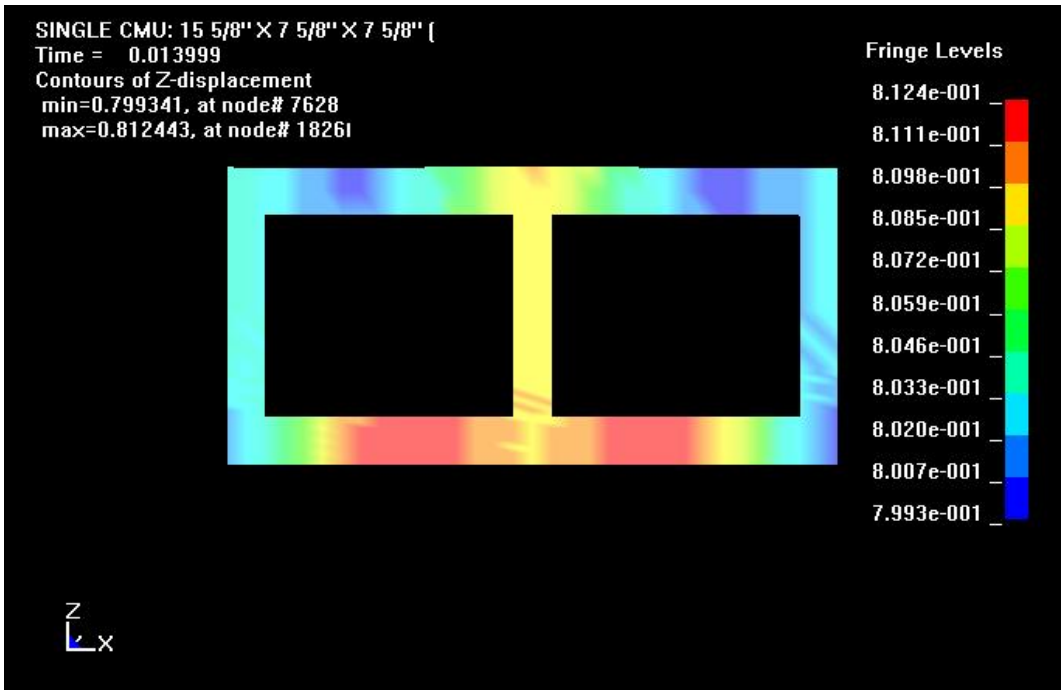

Figure 5.3-17 MAT_PSEUDO_TENSOR Displacement Fringes for 1000 lb ANFO at 38 ft

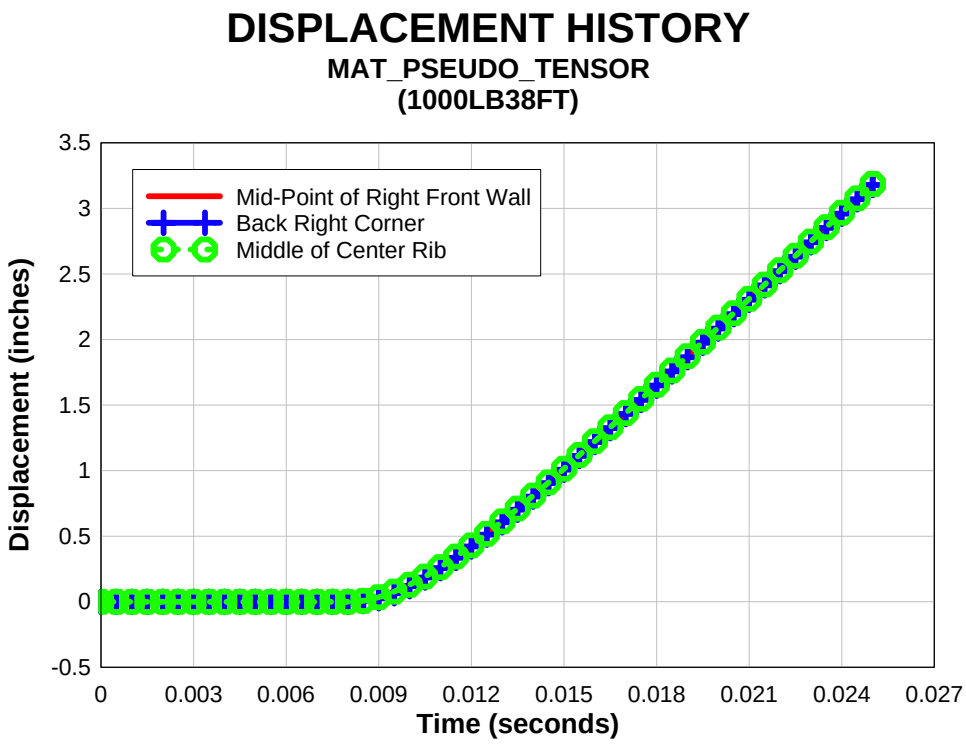

Figure 5.3-18 Displacement History Plots

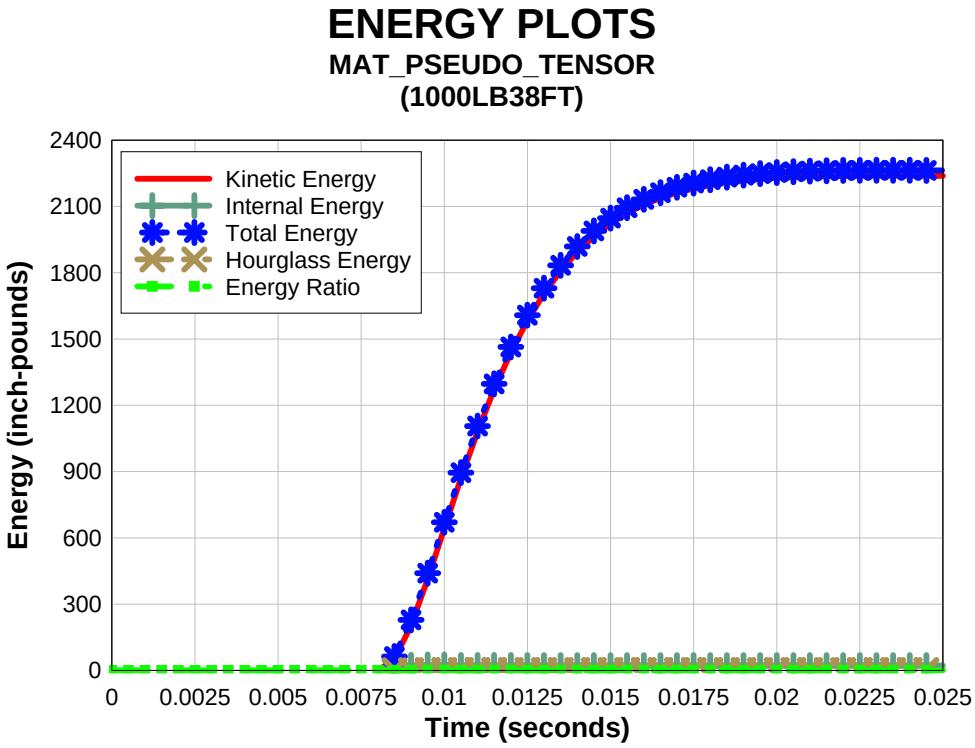

Figure 5.3-19 Energy Plots

5.4 MAT_WINFRITH_CONCRETE

The stress fringe levels indicate that the exposed front wall of the CMU reaches its ultimate strength within the first few m-seconds. Stress levels tend to remain at this level as the elements of the exposed wall experience large displacements in the following m-seconds of the blast. Examination of the displacement fringes and time histories show that the mid-point of the right (or left) front wall of the CMU displaces more than the other two points of interest. For the 500 lb ANFO at 10 ft, the mid-point of the right wall displaces 0.2 in at 1.5 m-sec whereas the other two points of interest displace less than half as much. Examination of the energy plots show that, for the exception of 500 lb ANFO at 10 ft, the CMU exhibits significantly low strain energy for all loading conditions, and the kinetic energy is the dominant factor in this case. The hourglass energy and energy ratio seem to be negligible for this constitutive model. Overall, the CMU experiences fracture for 500 lb ANFO at 30 ft or less. However, at larger distances the CMU seems to experience more of a rigid body movement. In these cases, the stress level may reach the ultimate strength but fracture does not occur. No analysis is performed for the 1000 lb ANFO, but similar results are expected. It was observed that changing of the initial crack size made little difference in the results of the analysis for this material card. Another observation is the three nodes of interest move more in unison as the distance from the blast source increases from 10 ft to 30 ft. This is most visible in Figure 5.4-11 where the displacement history is plotted for 500 lb ANFO at 30 ft. The conclusion drawn is that, although the MAT_WINFRITH_CONCRETE constitutive model predicts stress fracture fairly accurately, it has difficulties predicting displacements. The results of the MAT_WINFIRTH_CONCRETE complement are included in the following list.

500lb10ft	Failure
500lb20ft	Failure
500lb30ft	Failure
500lb35ft	No Failure
500lb40ft	No. Failure

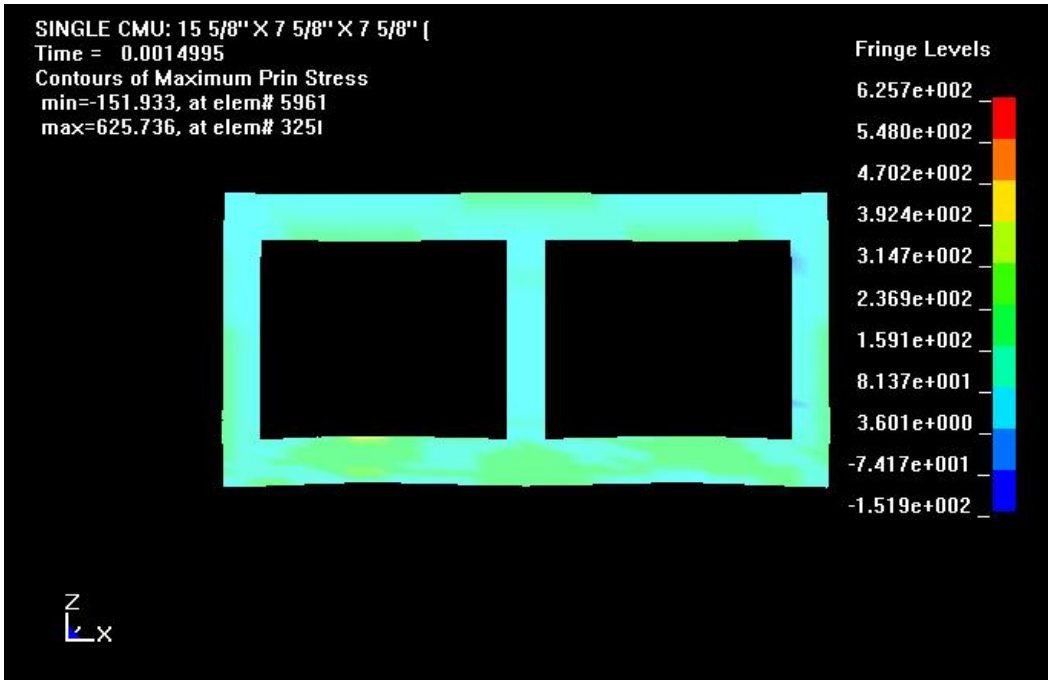

Figure 5.4-1 MAT_WINFRITH_CONCRETE Stress Fringes for 500 lb ANFO at 10 ft

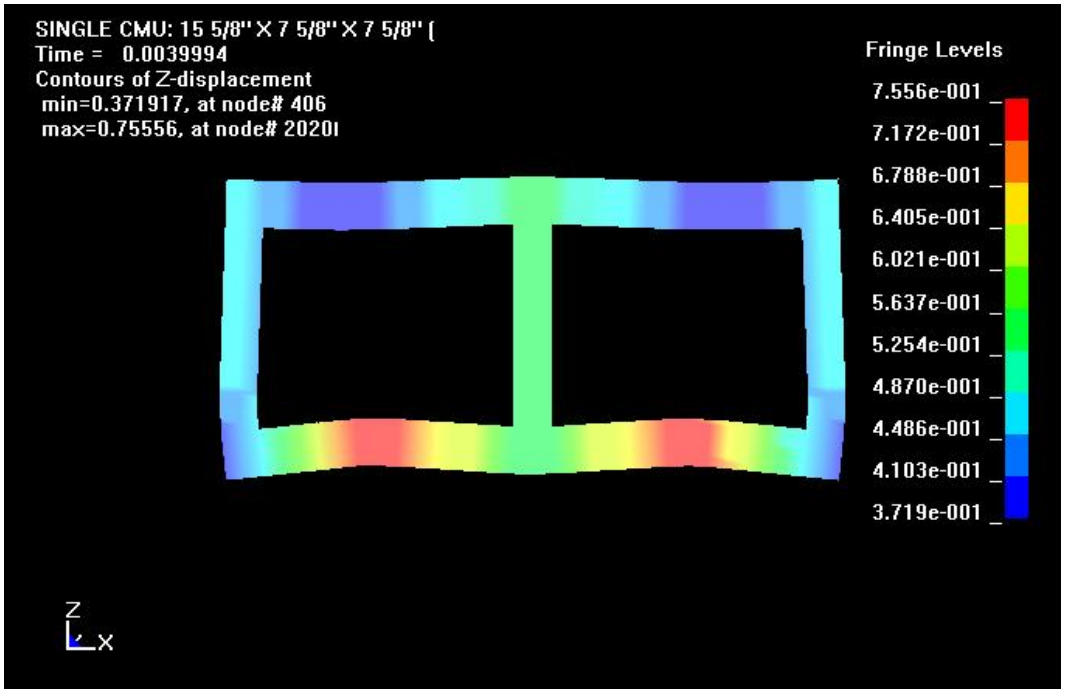

Figure 5.4-2 MAT_WINFRITH_CONCRETE Displacement Fringes for 500 lb ANFO at 10 ft

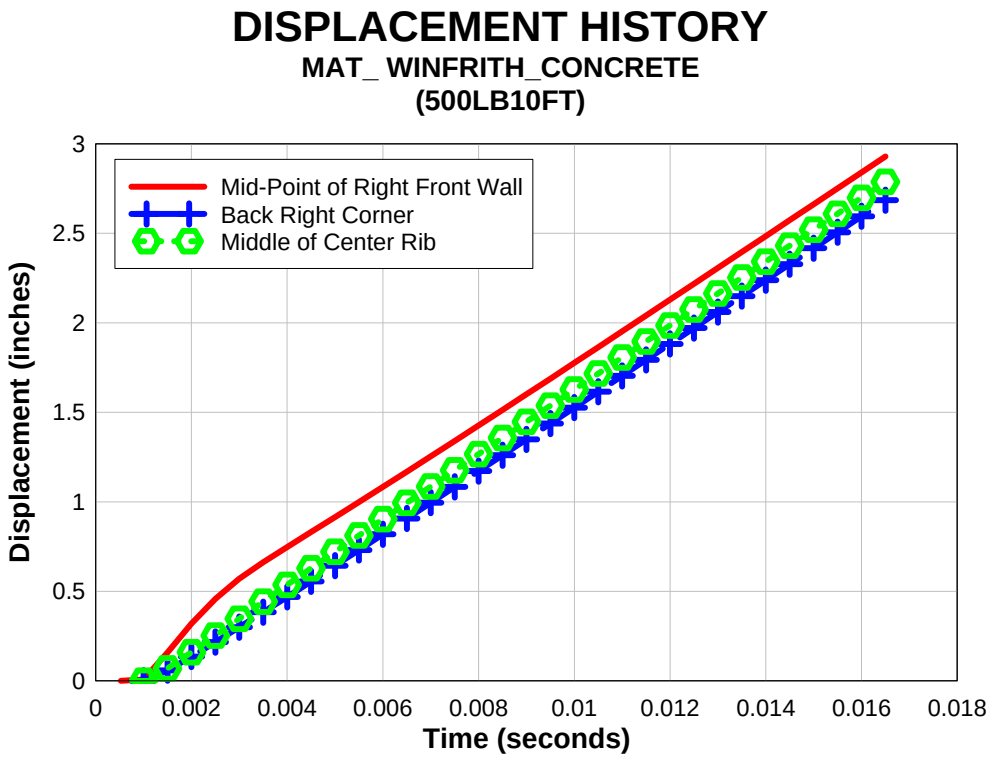

Figure 5.4-3 Displacement History Plots

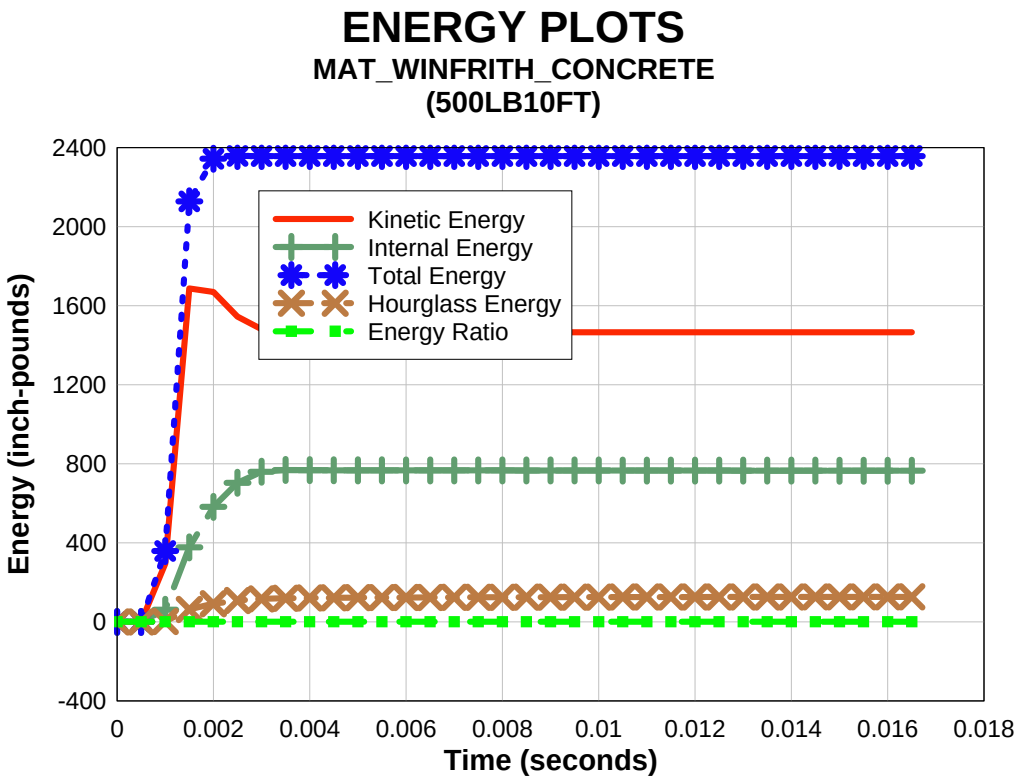

Figure 5.4-4 Energy Plots

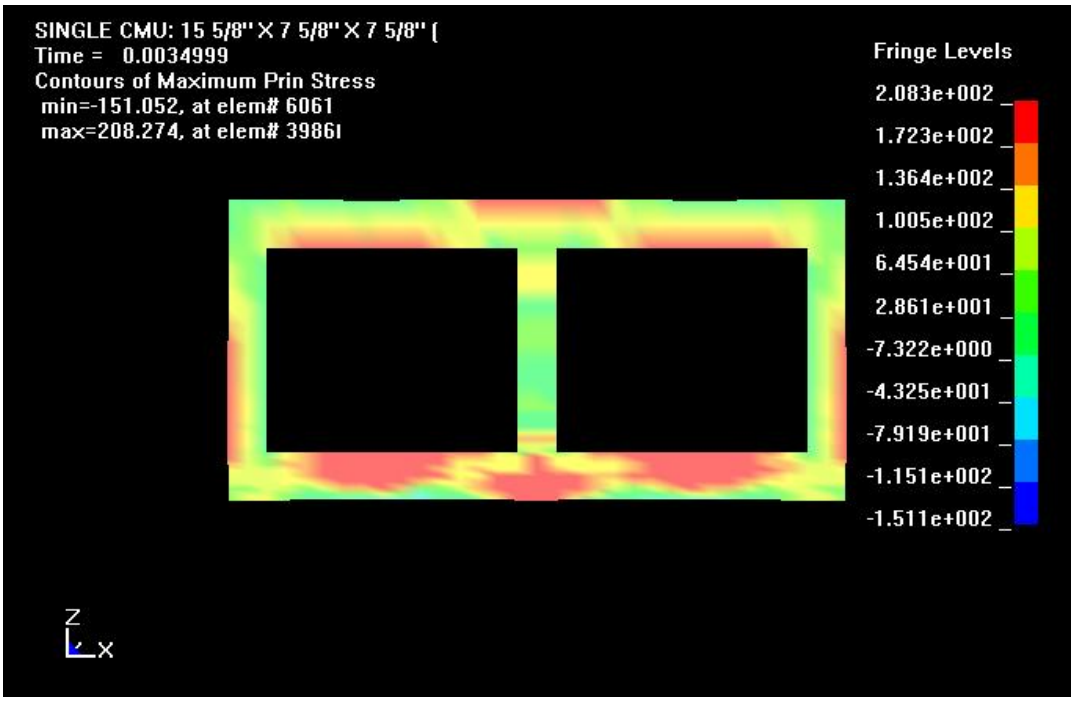

Figure 5.4-5 MAT_WINFRITH_CONCRETE Stress Fringes for 500 lb ANFO at 20 ft

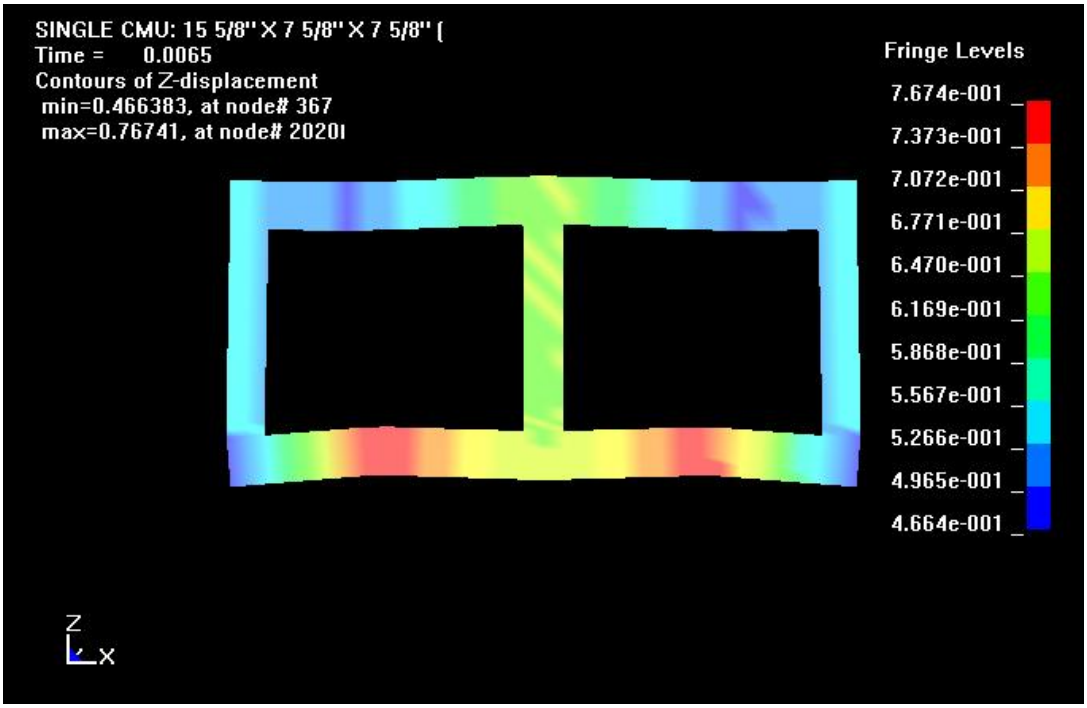

Figure 5.4-6 MAT_WINFRITH_CONCRETE Displacement Fringes for 500 lb ANFO at 20 ft

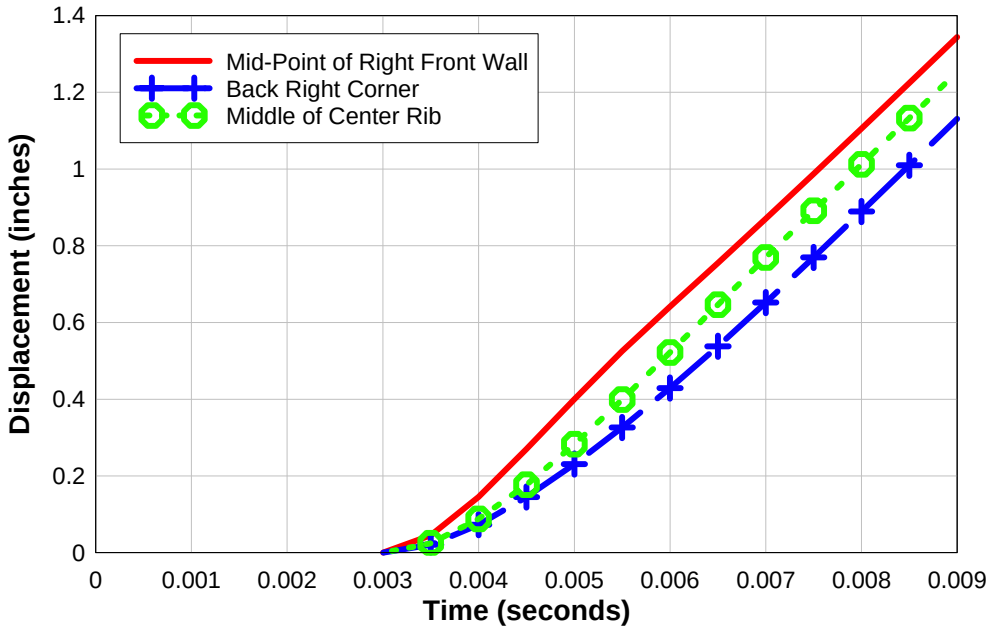

Figure 5.4-7 Displacement History Plots

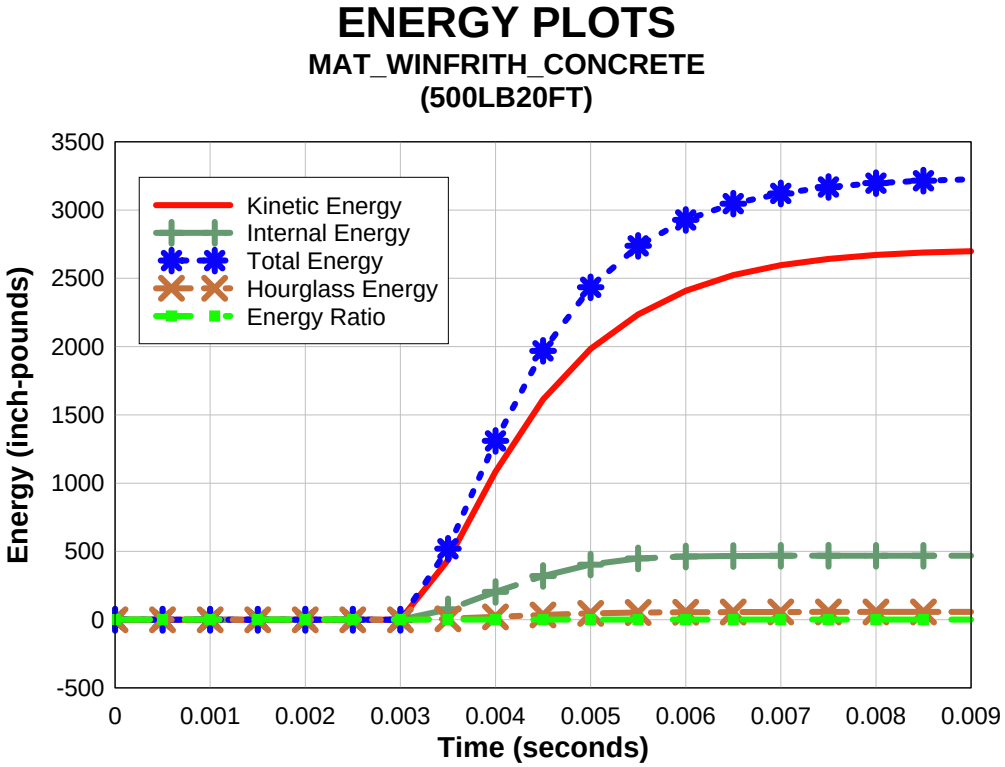

Figure 5.4-8 Energy Plots

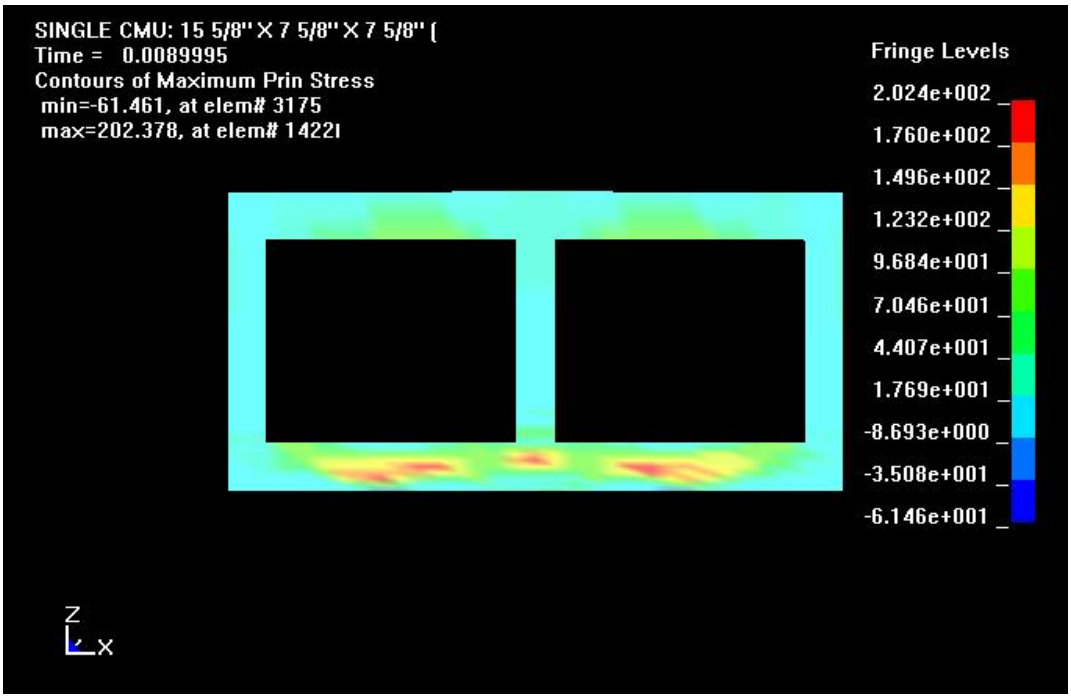

Figure 5.4-9 MAT_WINFRITH_CONCRETE Stress Fringes for 500 lb ANFO at 30 ft

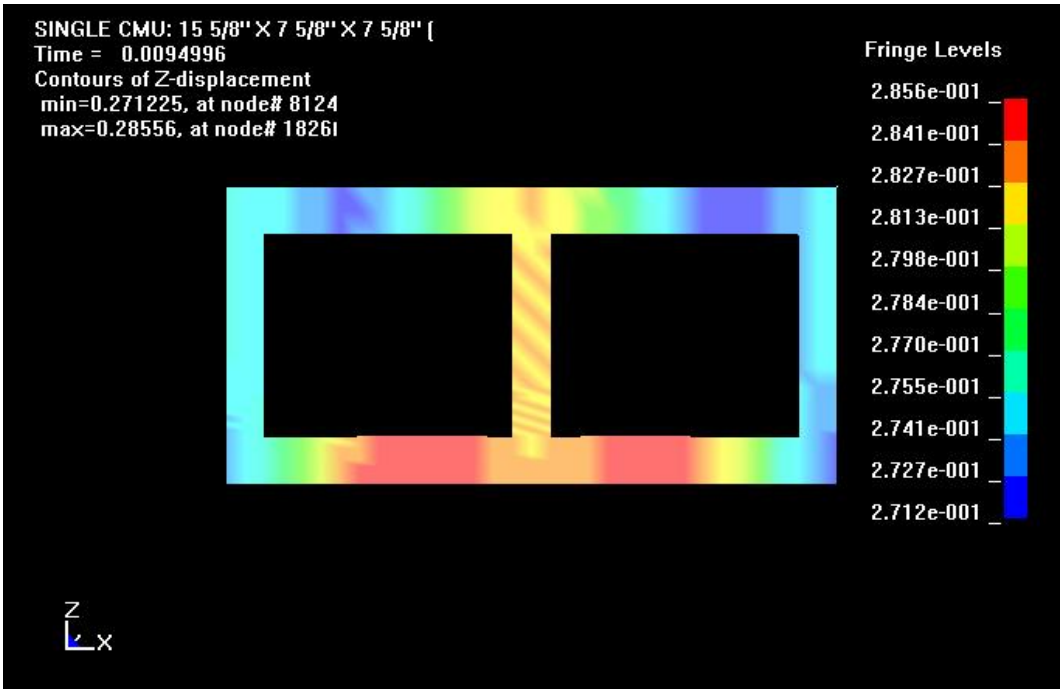

Figure 5.4-10 MAT_WINFRITH_CONCRETE Displacement Fringes for 500 lb ANFO at 30 ft

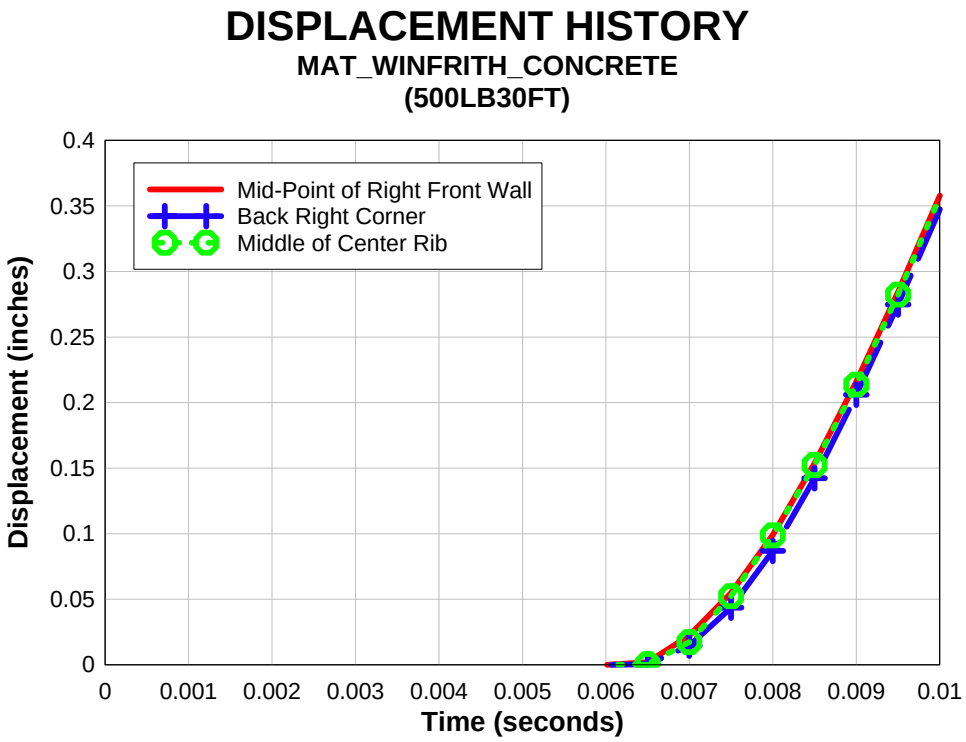

Figure 5.4-11 Displacement History Plots

5.5 Erode Element Option

An option is available in LS-DYNA for 2D and 3D solid elements, with one point integration, to remove elements when failure is reached. This option is described under MAT_ADD_EROSION in the LS-DYNA User's Manual, Volume II. The option finds the finite elements that reach the user input failure point, and eliminates them from the calculations. This elimination is also manifested graphically in stress or displacement plots, and can assist in the understanding of failure mechanisms. However, the option alters the global mass and stiffness matrices and response of the structure in the test runs performed for this research. Furthermore, accurate implementation depends on a highly refined mesh. Therefore, the option is recommended as a graphical tool only to better demonstrate fracture failure in structural analysis, and not recommended to be included in the data deck until after all analyses conclude failure. This is demonstrated in the following figures 5.5-1 and 5.5-2 where stress fringes are shown for the single block model for the 500 lbs of ANFO at 10 feet load case. Figure 5.5-1 is for the case without the erode option in contrast with Figure 5.5-2 for the case with the erode option. Note the difference in stress distribution across the cross section of the block for the two cases.

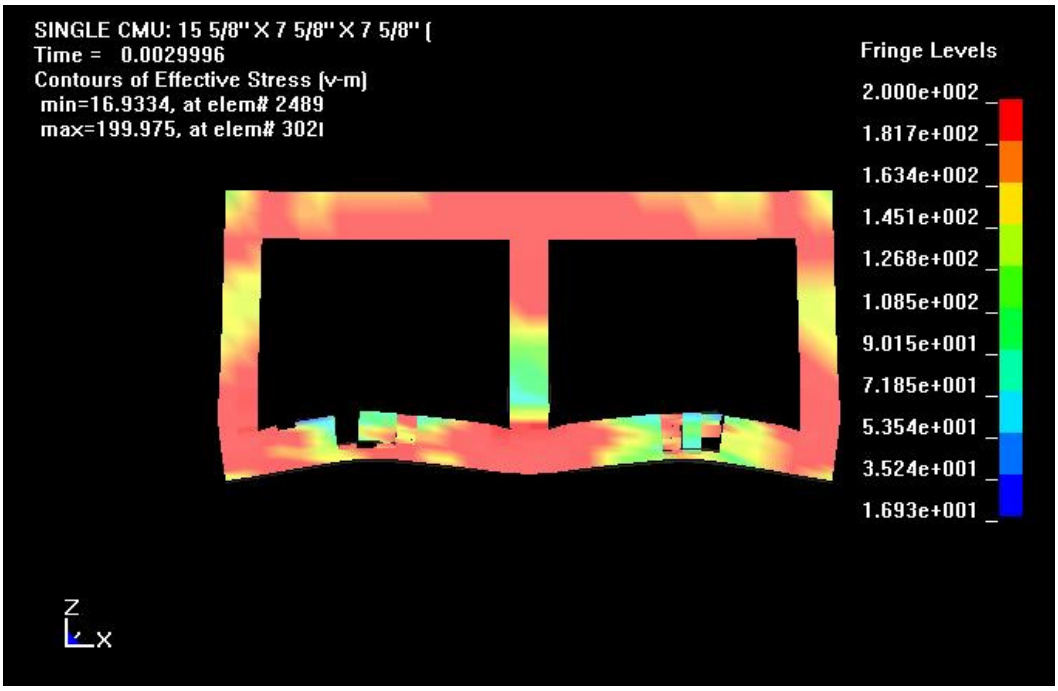

Figure 5.5-1 MAT_SOIL_AND_FOAM Stress Fringes for 500 lb ANFO at 10 ft

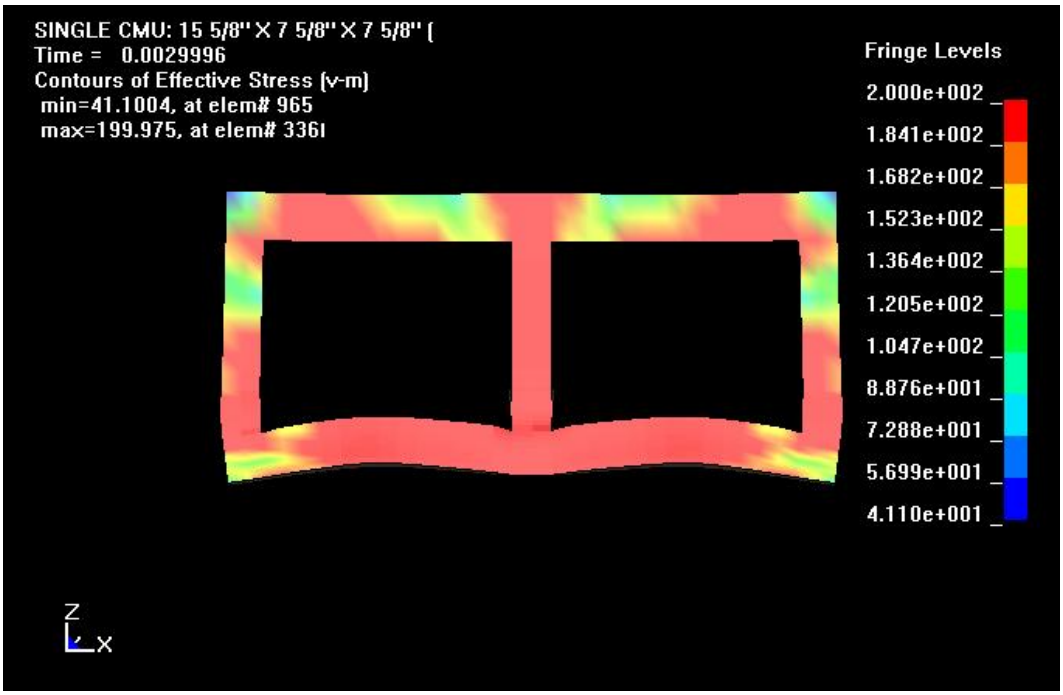

Figure 5.5-2 MAT_SOIL_AND_FOAM Stress Fringes for 500 lb ANFO at 10 ft with Erode Option

5.6 Higher Integration Elements

The analyses reported herein utilized a single point integration technique for computations regarding volume integration. According to the LS-DYNA Theoretical Manual, a major advantage of single point integration is the substantial savings in computer time. An anti-symmetry property of the strain matrix reduces the amount of effort required to compute this matrix by more than 25 times over an 8-point integration. Further cost savings are attained during calculations for element nodal forces. The biggest disadvantage to single point integration is the need to control zero energy modes called hourglassing modes. Undesirable hourglass modes tend to have periods that are typically much shorter than the periods of the structural responses, and they are often observed to be oscillatory. There are several ways to resist undesirable hourglass modes such as use of higher integration elements, or a viscous damping. For the purpose of this research, energy related to hourglass modes is shown in the energy plots provided for each run in sections 5.1 through 5.4. These plots show that for most runs, the energy associated with hourglassing modes are low or negligible, hence hourglassing is not an issue for the single block model. However, to ensure coverage of important issues related with structural behavior related to blast, runs were made using higher integration elements. The results agree with the LS-DYNA predictions in that the runs consume longer processing time, but the energy related to hourglass modes go to zero for the higher integration elements, and certain variations are detected in the energy and displacement plots. However, the overall failure behavior of the block remains the same as shown by the single point integration models. Figure 5.6-1 shows the energy plots for the 500 lbs. ANFO at 10 feet where a small amount of hourglass energy is present using single point integration. This is in contrast with Figure 5.6-2 where energy plots of the same model and loading condition shows zero hourglass energy using higher integration elements. Figures 5.6-3 and 5.6-4 show the displacement histories for the two runs closely agree.

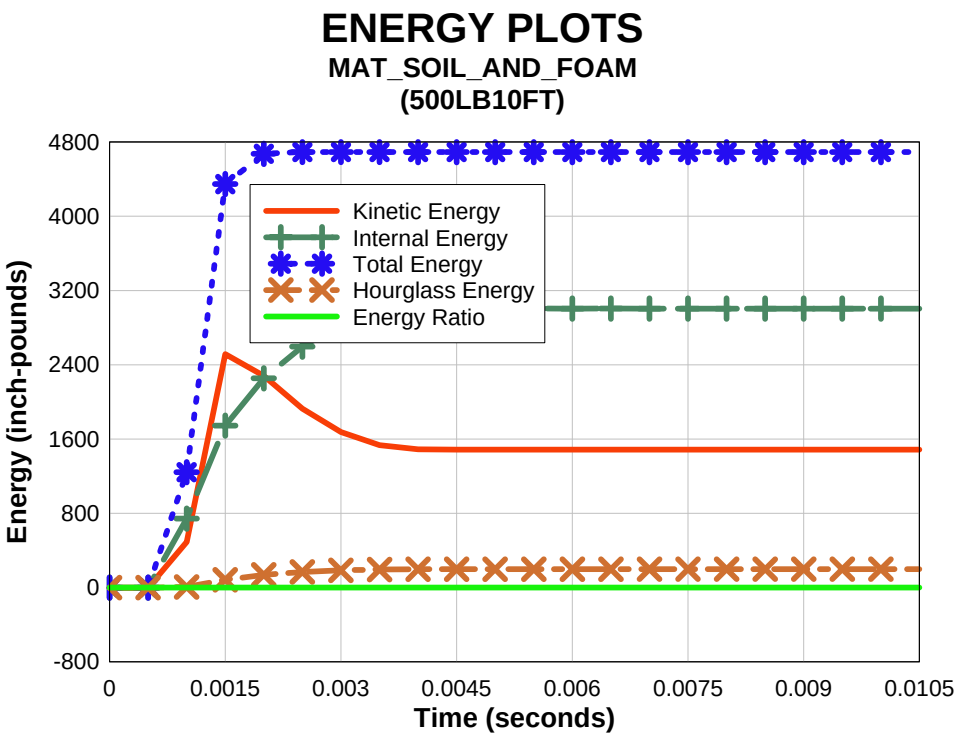

Figure 5.6 -1 MAT_SOIL_AND_FOAM Energy Plots

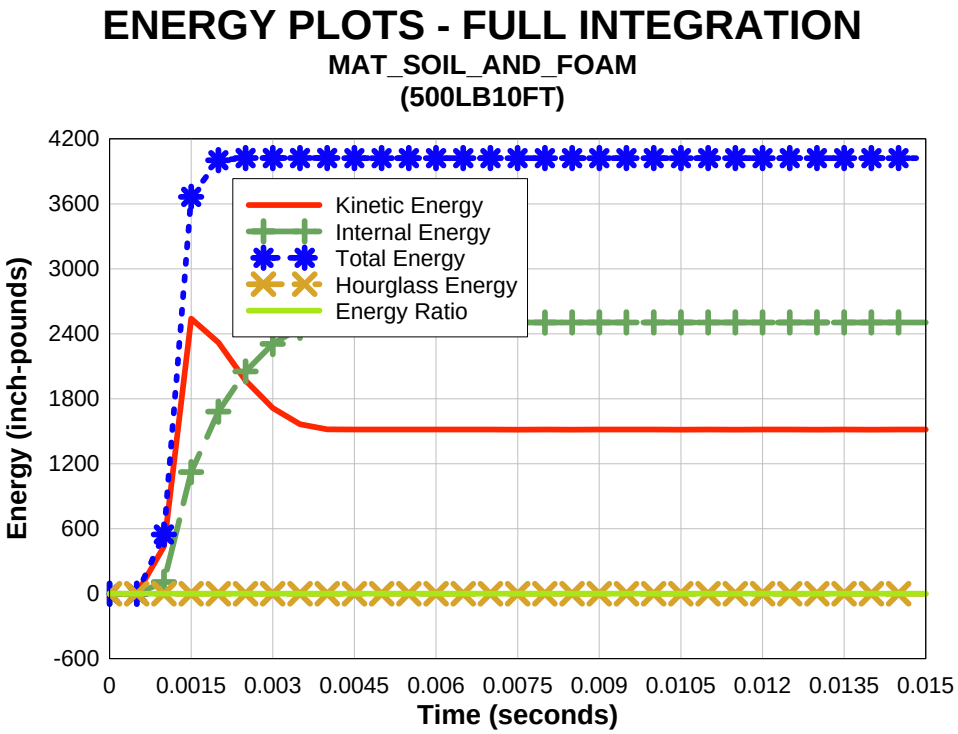

Figure 5.6 - 2 MAT_SOIL_AND_FOAM Energy Plots – Full Integration

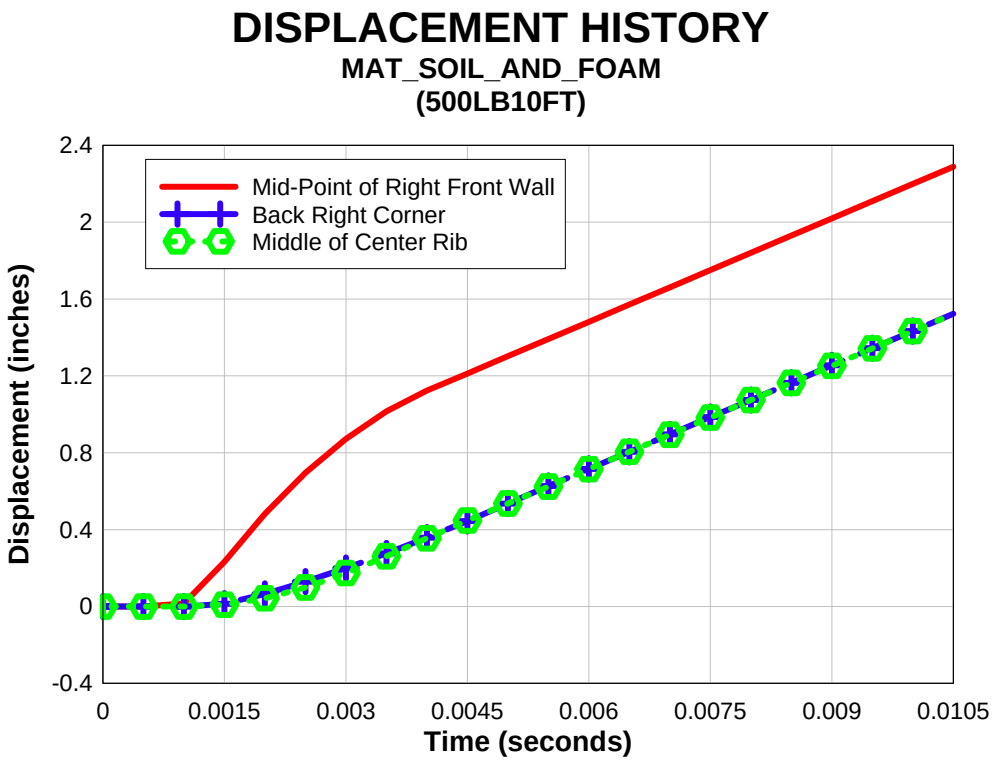

Figure 5.6 - 3 MAT_SOIL_AND_FOAM Displacement History Plots

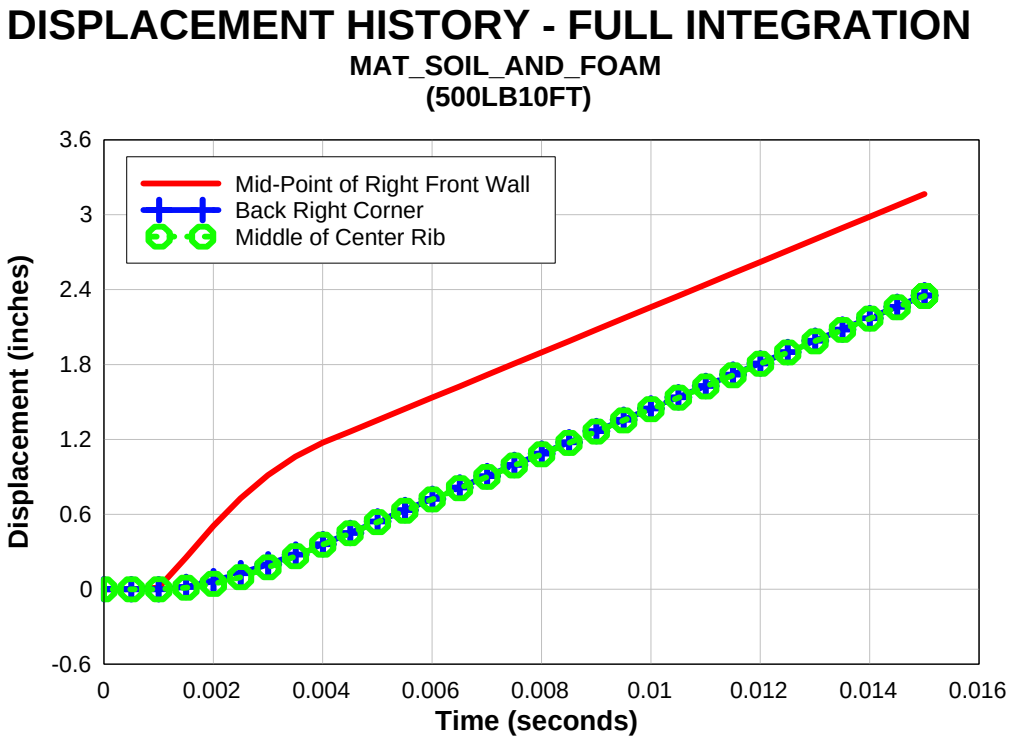

Figure 5.6 - 4 MAT_SOIL_AND_FOAM Displacement History Plots – Full Integration

5.7 Effect of Rigid Boundary Conditions

The real interest behind this research is to establish the correct behavior of single blocks of CMU that make up elements of infill masonry walls. In the blast tests, the CMUs making up elements of a wall failed at greater distances from the blast source than the single blocks resting freely on a support. Walls are constructed by stacking CMU blocks next to each other and on top of one another with the use of mortar as joint material. The boundary conditions provided to each block by the manner of wall construction are far more rigid than the free-free conditions assumed for the effort reported so far. While it is important to remember that the free-free boundary condition was used correctly to compare the analyses results to the test conditions set up for this effort, it is equally important to examine the effect of the more rigid boundary conditions imposed by the surrounding CMUs. Will the addition of rigid boundary conditions cause the CMU to fail at greater distances than those with the free-free boundary conditions?

Full wall models are currently under investigation by UAB. These models examine the wall and the impact of the mortar joints in great detail. Therefore, this section will briefly examine the impact of rigid boundary conditions on the single block model. All nodes on the outside surface of the back face of the single block were constrained in the three translational directions. The blast pressure is applied to the outside front face of the single block. The MAT_SOIL_AND_FOAM model was used for this effort, and loading condition of 500 lbs of ANFO was used at distances beyond 32 feet. Both the model and the actual tests had shown that the CMU was not failing at greater distances than 32 feet from the blast source. Two runs were made at the distances of 35 feet and 40 feet from the source. Both runs show failure in the front wall as indicated by the stress and displacement fringes shown in the figures on the following pages. Figures 5.7-1 and 5.7-2 are the stress and displacement fringes for the 35-ft distance, while Figure 5.7-3 is the energy plots, and Figure 5.7-4 is the displacement history for three selected nodes on the CMU. Figures 5.7-5 and 5.7-6 are the stress and displacement fringes for the 40-ft distance, while Figure 5.7-7 is the energy plot, and Figure 5.7-8 is the displacement history for three selected nodes on the CMU.

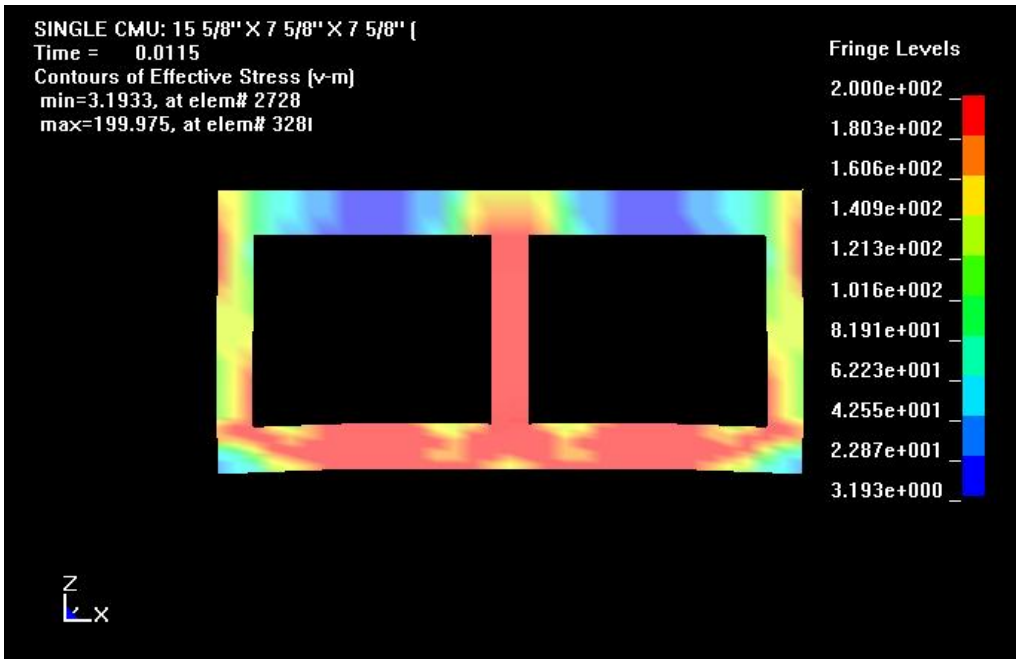

Figure 5.7 -1 MAT_SOIL_AND_FOAM Stress Fringes for 500 lb ANFO at 35 ft

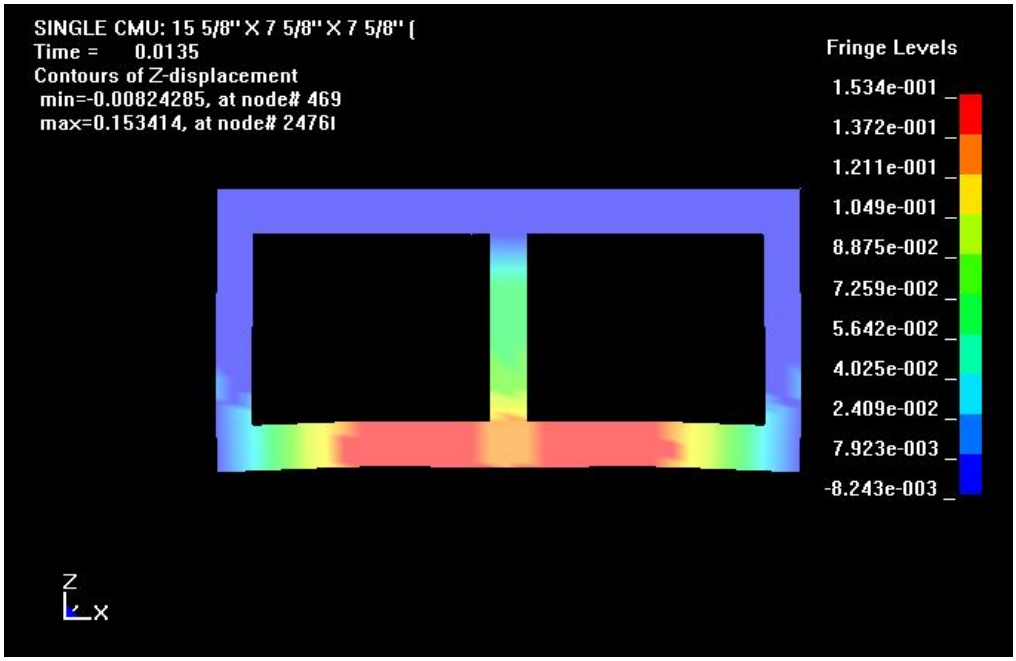

Figure 5.7 -2 MAT_SOIL_AND_FOAM Displacement Fringes for 500 lb ANFO at 35 ft

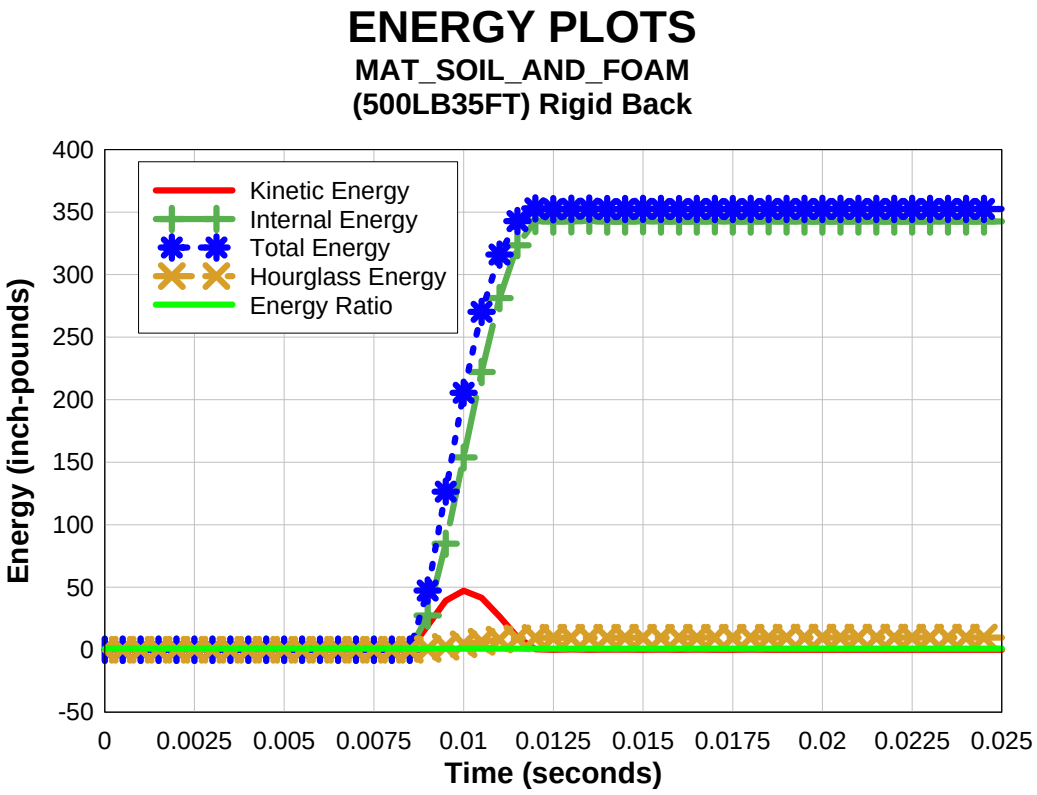

Figure 5.7 - 3 MAT_SOIL_AND_FOAM Rigid Back Energy Plots

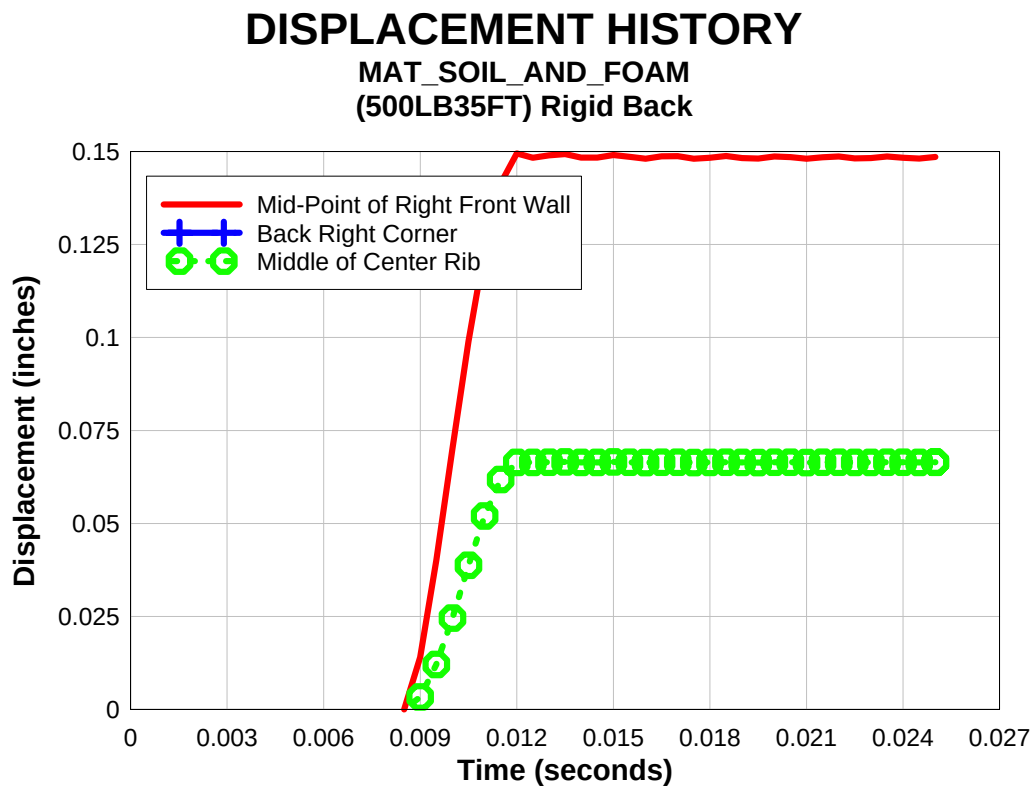

Figure 5.7 - 4 MAT_SOIL_AND_FOAM Rigid Back Displacement History Plots

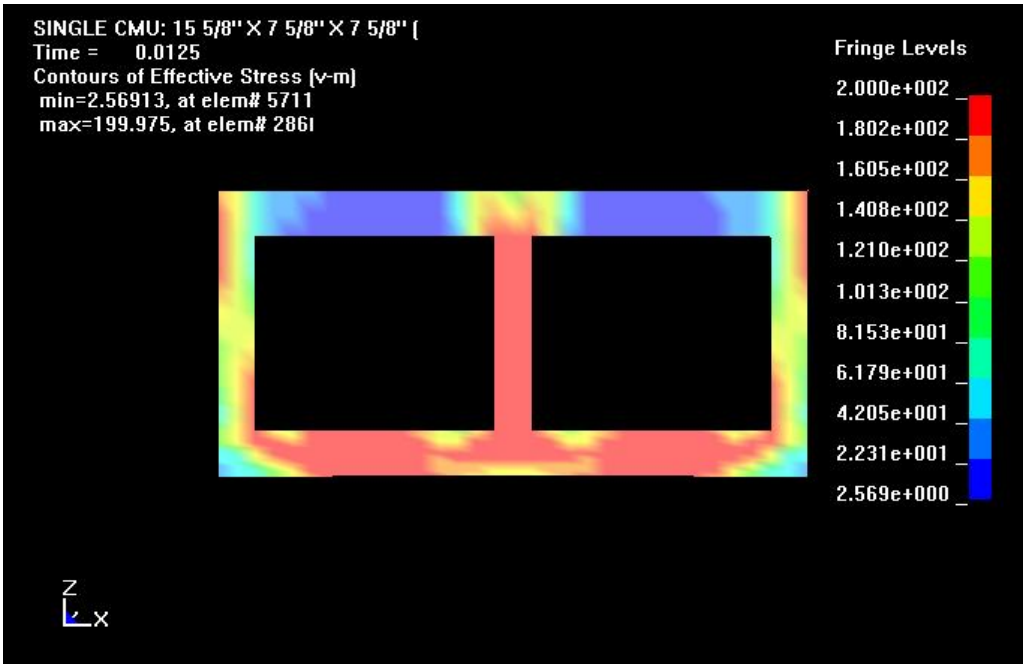

Figure 5.7 -5 MAT_SOIL_AND_FOAM Stress Fringes for 500 lb ANFO at 40 ft

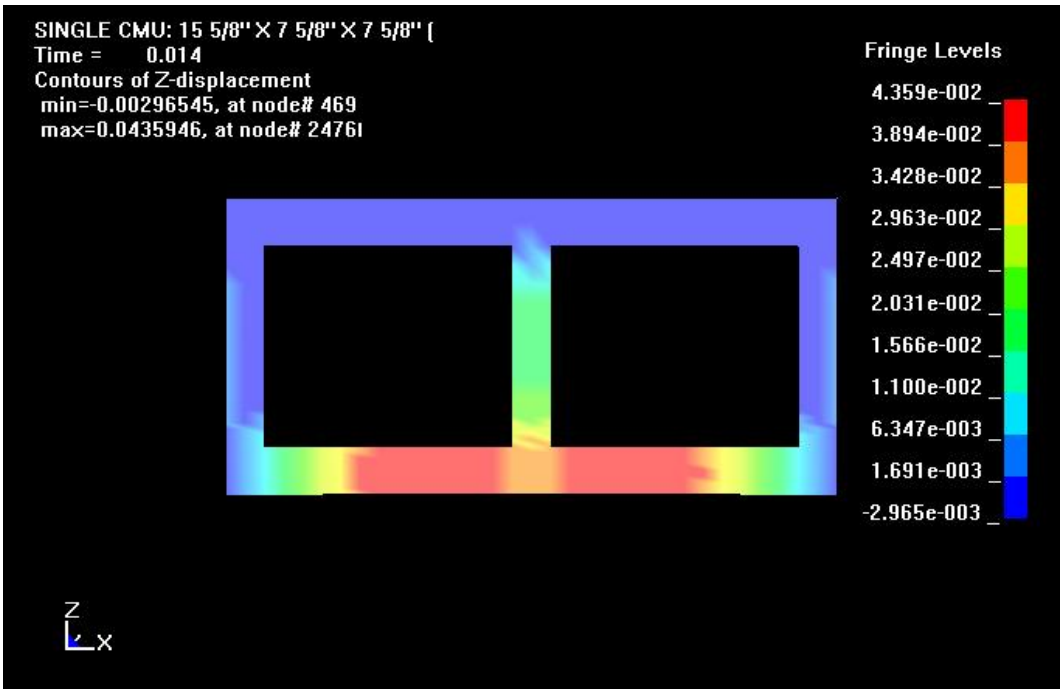

Figure 5.7 -6 MAT_SOIL_AND_FOAM Displacement Fringes for 500 lb ANFO at 40 ft

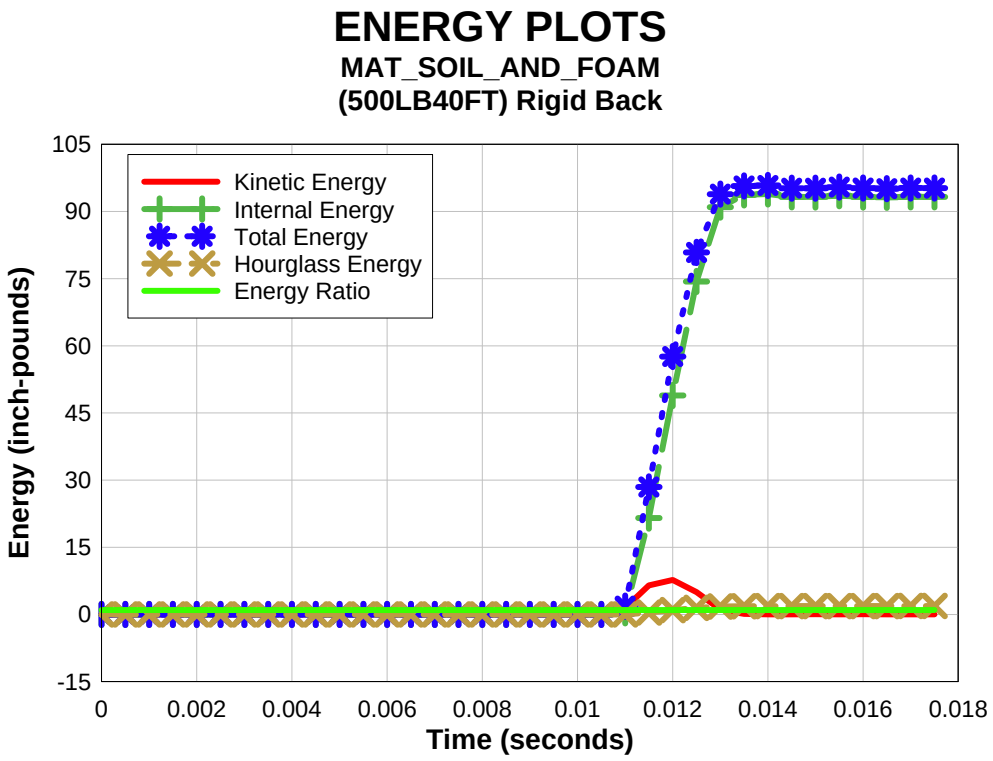

Figure 5.7 - 7 MAT_SOIL_AND_FOAM Rigid Back Energy Plots

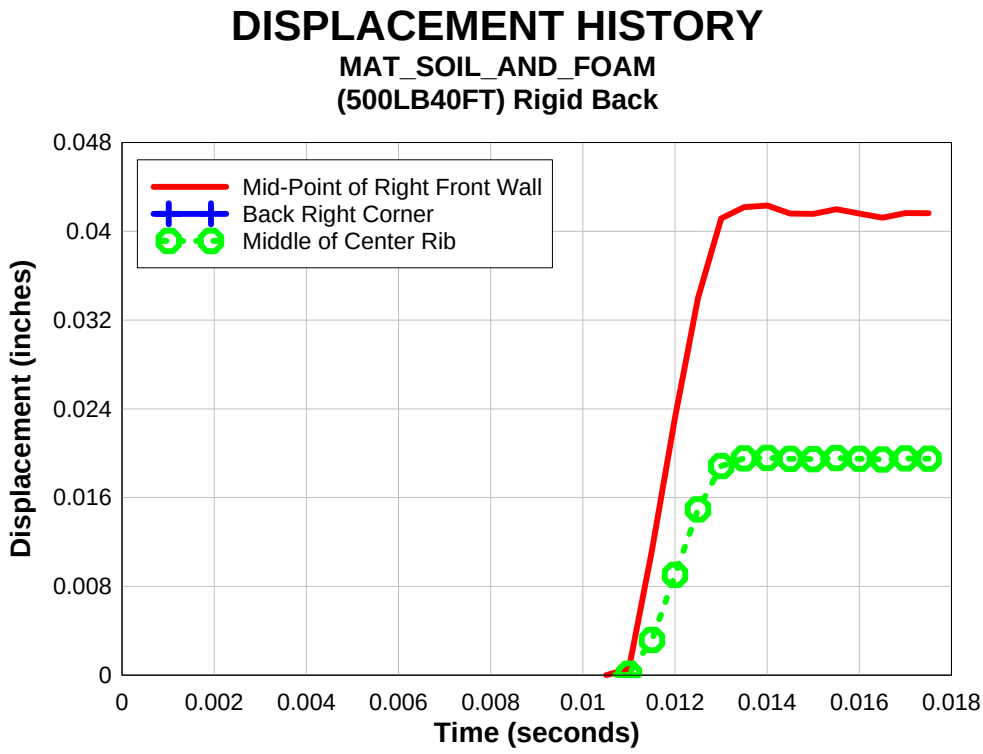

Figure 5.7 - 8 MAT_SOIL_AND_FOAM Rigid Back Displacement History Plots

CHAPTER 6

SUMMARY AND CONCLUSIONS

A fine mesh finite element model was used to examine the behavior of a single CMU exposed to blast loads. The main objective of this research was to determine the most suitable DYNA-3D material model for CMU blocks so that the decided material model could be used with confidence in full polymer-retrofit wall models. The objective was achieved by comparing the analytical results with actual blast test results conducted by AFRL at Tyndall AFB. After some initial consideration, four DYNA-3D material models were evaluated.

MAT_SOIL_AND_FOAM: The stress fringe levels indicate that the exposed wall of the CMU reaches its ultimate strength within the first few milliseconds. Stresses remain at this level as the elements of the exposed wall experience large displacements in the following m-seconds of the blast. At greater distances the CMU experiences rigid body movement as indicated by the displacement fringe plots at 35 and 40 ft. In these cases, the stress level may reach the ultimate strength but fracture does not occur. Displacement time histories show clearly that the front wall displaces more and at earlier time steps than the middle rib or the back corners of the CMU. It is also observed that the latter two points move exactly the same distance and at the same time step indicating a rigid body movement of the rest of the block. Energy plots indicate significant kinetic and internal energy are present during the blast event, and the hourglass energy and energy ratio seem to be negligible. Results indicate fracture failure in the CMU for 500 lb ANFO at distances of 32 ft and less. At greater distances, fracture is not detected and the CMU seems to move as a rigid body. Similar results are noted for the 1000 lb ANFO where fracture is noticed at 40 ft or less, but rigid body movement in noticed at 45 ft or more. These results closely match those obtained from the actual blast test conducted at by AFRL at Tyndall AFB.

MAT_BRITTLE_DAMAGE: The stress fringe levels indicate that most sections of the CMU reach their ultimate strength within the first few m-seconds. However, examination of the displacement fringes and time histories show that most points on the CMU move at the same level and at the same time. For the 500 lbs ANFO at 10 ft, the middle of the center rib seem to displace larger than the mid-point of the right front wall. Displacements seem to be significantly less than the MAT_SOIL_AND_FOAM case for the same loading conditions. The energy plots exhibits significantly low strain energy for all loading conditions except for the 500 lb ANFO at 10 ft. The kinetic energy is by far the dominant factor in the MAT_BRITTLE_DAMAGE constitutive model, and the hourglass energy and energy ratio appear to be at negligible levels. Results of the analysis indicate fracture failure for the 500 lb ANFO at distances less than 30 ft, but rigid body movements at greater distances. Similar results are noted for the 1000 lb ANFO where fracture is noticed at 20 ft, but rigid body movement in noticed at 40 ft or more. The results match those obtained from the actual blast test conducted by AFRL at Tyndall AFB fairly closely for the 500 lbs ANFO at most distances, but fail to match those for the 1000 lb ANFO at 40 ft.

MAT_PSEUDO_TENSOR: The stress fringe levels indicate that the exposed front wall of the CMU reaches its ultimate strength within the first few m-seconds. Stress

levels tend to remain at this level as the elements of the exposed wall experience large displacements in the following m-seconds of the blast. Examination of the displacement fringes and time histories show that the mid-point of the right front wall of the CMU moves at significantly greater levels than the rear corner or a point on the middle rib of the CMU. The energy plots show that the CMU exhibits significantly low strain energy for all loading conditions, and the kinetic energy is the dominant factor in this case. The hourglass energy seems to be significantly higher than the MAT_SOIL_AND_FOAM and MAT_BRITTLE_DAMAGE cases. Results of the analysis show that the CMU experiences fracture for 500 lb ANFO at 28 ft or less. However, at 29 ft or more the CMU seems to experience more of a rigid body movement. In these cases, the stress level may reach the ultimate strength but fracture does not seem to occur. Similar results are noted for the 1000 lbs ANFO where fracture is noticed at 37 ft or less, but rigid body movement in noticed at 38 ft or more.

MAT_WINFRITH_CONCRETE: The stress fringe levels indicate that the exposed front wall of the CMU reaches its ultimate strength within the first few m-seconds. Stress levels tend to remain at this level as the elements of the exposed wall experience large displacements in the following m-seconds of the blast. Examination of the displacement fringes and time histories show that the mid-point of the right front wall of the CMU displaces more than the other two points of interest. Examination of the energy plots show that, for the exception of 500 lb ANFO at 10 ft, the CMU exhibits significantly low strain energy for all loading conditions, and the kinetic energy is the dominant factor in this case. The hourglass energy and energy ratio seem to be negligible for this constitutive model. The results show that the CMU experiences fracture failure for 500 lb ANFO at 30 ft or less, but rigid body movement for greater distances. In these cases, the stress level may reach the ultimate strength but fracture does not seem to occur. No analysis is performed for the 1000 lbs ANFO, but similar results are expected. It was observed that changing of the initial crack size made little difference in the results of the analysis for this material card. Another observation is the three nodes of interest move more in unison as the distance from the blast source increases from 10 ft to 30 ft. This is most visible in Figure 4.4-11 where the displacement history is plotted for 500 lb ANFO at 30 feet. Comparing Figure 5.4-11 to Figure 5.1-12 shows that the MAT_SOIL_AND_FOAM model makes better distinction between the three nodes of interest than MAT_WINFRITH_CONCRETE. The conclusion drawn is that although the MAT_WINFRITH_CONCRETE constitutive model predicts stress fracture fairly accurately, it seems to have difficulties predicting displacements.

6.1 Conclusions

The results of the analyses for the four selected constitutive models closely match results of the blast tests conducted by AFRL at Tyndall AFB. The analytical results for the MAT_SOIL_AND_FOAM constitutive model are the closest match of the four candidates. It predicts the failure mode for all cases tested at AFRL in the 500 lb ANFO as well as the 1000 lb ANFO blast charges. The MAT_BRITTLE_DAMAGE constitutive model predicted the failure modes of the CMU well for the 500 lb ANFO at distances of 30 ft and less, but failed to predict fracture in the 1000 lb ANFO at 40 ft. Another major shortcoming of the MAT_BRITTLE_DAMAGE constitutive model is in the prediction of the displacement results where the front wall of the CMU displaces less

than the rib. The MAT_PSEUDO_TENSOR constitutive model predicted fracture failure for the 500 lb ANFO at 28 ft and less, and for the 1000 lb ANFO at 37 ft and less. The MAT_WINFRITH_CONCRETE constitutive model predicted fracture failure for the 500 lb ANFO at 30 ft and less, and for the 1000 lb ANFO similar results are expected as in the MAT_PSEUDO_TENSOR case.

Overall, the MAT_SOIL_AND_FOAM constitutive model provided better prediction than the other models. This model is also the simplest of the three and was developed for cases of plane soils, foams, and concrete. This closely matches the make-up of a common CMU composed of plain concrete material exhibiting simple fracture modes. The other three constitutive models were developed for more complex concrete and reinforced concrete structures. The MAT_PSEUDO_TENSOR model was used for buried steel reinforced concrete structures subjected to impulsive loads. This report therefore, recommends the use MAT_SOIL_AND_FOAM for analytical investigations of effects of blast on CMU walls.

Agreement between computation models and explosive tests could be improved by conducting laboratory tests as described in Section 4.3 to derive the constitutive characteristic parameters specific for CMUs. Many of the parameters in this effort were estimated based on available data, most often, high strength concrete. CMUs are constructed from low to moderate strength concrete, and the constituents are often different from those of high strength concrete. Actual tests based on concrete mixes for CMU construction would yield valuable information on bulk unloading modulus, volume strains, ultimate unconfined strength, etc. This information would be used to identify the best constitutive model for use in computational analysis of CMU construction, as well as, provide accurate results in the failure analysis of CMUs structures. Furthermore, since the load input to the finite element model does not exactly simulate the complex loading of a blast environment, the comparison between finite element results and the outcome of the blast tests can only be considered approximate.

REFERENCES

Barbero, E. J., Davalos, J. F., Kiger, S. A., and Shore, J. S. (1997). "Reinforcement with advanced composite materials for blast loads." *Proc., Structures Congress XV*, Portland, Oregon.

Biggs (1964), "Introduction to Structural Dynamics", McGraw-Hill Book Company, New York.

Connell (2002), "Evaluation of Elastomeric Polymer for Retrofit of Unreinforced Masonry Walls Subjected to Blast", MS Thesis, University of Alabama at Birmingham, Birmingham, Alabama, U.S.A.

Crawford, J. E., Bogosian, D. D., and Wesevich, J. W. (1997a). "Evaluation of the effects of explosive loads on masonry walls and an assessment of retrofit techniques for increasing their strength." *Proc., 8th International Symposium on Interaction of the Effects of Munitions with Structures*, McLean, Virginia.

Crawford, J. E., Malvar, L. J., Wesevich, J. W., Valancius, J., and Reynolds, A. D. (1997b). "Retrofit of reinforced concrete structures to resist blast effects." Technical paper, *Title No. 94-S34*, ACI Structural Journal, 94(4), 371-377.

Dennis, S. T. (1999). "Masonry walls subjected to blast loading-DYNA3D analysis." U.S. Army Engineer Waterways Experiment Station, Vicksburg, Mississippi.

Dennis, S. T., Baylot, J. T., and Woodson, S. C. (2000). "Response of ¼ scale concrete masonry unit (CMU) walls to blast." *Proc., ASME Pressure Vessels and Piping Conference*, Seattle, Washington.

Drysdale, R. G., Hamid A. A., and Baker L. R. (1999). *Masonry structures: behavior and design*. The Masonry Society, Boulder, Colorado.

Effects of Airblast, Cratering, Ground Shock and Radiation on Hardened Structures, (1976), Air Force Systems Command Manual, AFSCM 500-6, United States Air Force, Andrews Air Force Base, Washington, DC.

Engineering Technical Letter (ETL) 02-4 (2002): "Airblast Protection Polymer Retrofit of Unreinforced Concrete Masonry Walls", HQ AFCESA/CES, Department of the Air Force, Tyndall Air Force Base, Florida.

Fintel (1974), "Handbook of Concrete Engineering", Van Nostrand Reinhold Company, New York.

Hornbostel (1978), "Construction Manual", John Wiley and Sons Inc., New York.

Knox, K. J., Hammons, M. I., Lewis, T. T., and Porter, J. R. (2000). “Polymer materials for structural retrofit.” Force Protection Branch, Air Expeditionary Forces Technology Division, Air Force Research Laboratory, Tyndall AFB, Florida.

Laursen, P. T., Seible, F., and Hegemeir, G. A. (1995). “Seismic retrofit and repair of reinforced concrete with carbon overlays.” *Rep. No. SSRP-95/01*, Structural Systems Research Project, University of California, San Diego, California.

Len Schwer (2001) Draft, “Laboratory Tests for Characterizing Geomaterials”, Livermore Software Technology Corporation, Livermore, California.

LS-DYNA keyword user’s manual: nonlinear dynamic analysis of structures. (1999). Livermore Software Technology Corporation, Livermore, California.

LS-DYNA keyword user’s and Theoretical Manuals: Version 960 (2001). Livermore Software Technology Corporation, Livermore, California.

Martini, K. (1996). “Research in the out-of-plane behavior of unreinforced masonry.” Ancient Reconstruction of the Pompeii Forum, School of Architecture, University of Virginia.

Purcell, M. R., Muszynski, L. C., and Taun, C. Y. (1995). "Explosive field tests to evaluate composite reinforcement of concrete and masonry walls." Applied Research Associates, Inc., Gulf Coast Division, Tyndall AFB, Florida.

Roark and Young (1975), “Formulas for Stress and Strains”, Fifth Edition, McGraw Hill, Inc., New York.

Ross, C. A., Jerome, D. M., and Hughes, M. L. (1994). “Hardening and rehabilitation of concrete structures using carbon fiber reinforced plastics (CFRP).” *Rep. No. WL-TR-94-7100*, Wright Laboratory Armament Di 157 Eglin AFB, Florida.

Seible, F., and Karbhari, V. M. (1996). “Seismic retrofit of bridge columns using advanced composite materials.” Division of Structural Engineering, University of California, San Diego, La Jolla, California.

Shope, R., and Frank, R. (1998). “Preliminary finite element analysis of masonry walls.” Applied Research Associates, Inc., Raleigh, North Carolina.

Slawson, T. R., Coltharp, D. R., Dennis, S. T., and Mosher, R. (1999). “Evaluation of anchored fabric retrofits for reducing masonry wall debris hazard.” *Proc., 9th International Symposium on Interaction of the Effects of Munitions with Structures*, Berlin-Strausberg, Federal Republic of Germany.

Taun, C. Y., Muszynski, L. C., and Dass, W. C. (1995). “Explosive test of an externally-reinforced multi-story concrete structure at Eglin AFB, FL.” Applied Research Associates, Inc., Gulf Coast Division, Tyndall AFB, Florida.
W. F. Chen (1982), “Plasticity in Reinforced Concrete”, McGraw-Hill, Inc., New York.

Wall response to airblast loads: the wall analysis code (WAC). (1995). U.S. Army Engineer Waterways Experiment Station, Vicksburg, Mississippi.

Weeks, J., Seible, F., Hegemeir, G., and Priestly, M. J. N. (1994). “The U.S.-TCCMAR full-scale five-story masonry research building test: part V – repair and retest.” *Rep. No. SSRP-94/05,* Structural Systems Research Project, University of California, San Diego.

Wesevich, J. W., and Crawford, J. E. (1996). “Candidate retrofit designs for increasing the blast resistance of conventional wall panels.” *Technical report, TR-96-32.1,* Karagozian & Case, Glendale, California.

Whiting, W. D., and Coltharp, D. R. (1996). “Retrofit measures for conventional concrete masonry unit building subject to terrorist threat.” U.S. Army Engineer Waterways Experiment Station, Vicksburg, Mississippi.

Yokel, F. Y., and Dikkers, R. D. (1971). “Strength of load bearing masonry walls.” *Proc., American Society of Civil Engineers,* Journal of the Structural Division, 97, 1593 – 1609.

APPENDIX A

INPUT FILE FOR THE MAT_SOIL_AND_FOAM CONSTITUTIVE MODEL

```
$$ SOIL_FOAM
$$
*KEYWORD
*TITLE
Single CMU: 15 5/8" x 7 5/8" x 7 5/8" (no backing material)
$500lb ANFO at 10 ft
$---+----1----+----2----+----3----+----4----+----5----+----6----+----7----+----8
*CONTROL_TERMINATION
$   ENDTIM    ENDCYC     DTMIN    ENDNEG    ENDMAS
  .015E+00         0      .000      .000      .000
*CONTROL_TIMESTEP
$   DTINIT      SCFT      ISDO    TSLIMT      DTMS      LCTM     ERODE     MS1ST
   0.0E-00      .670         0
*CONTROL_HOURGLASS
$      IHQ        QH
         1      .100
*CONTROL_BULK_VISCOSITY
$       Q2        Q1
     1.500      .060
*CONTROL_SHELL
$   WRPANG    ITRIST     IRNXX    ISTUPD    THEORY       BWC     MITER
    20.000         2        -1         0         2         2         1
*CONTROL_CONTACT
$   SLSFAC    RWPNAL    ISLCHK    SHLTHK    PENOPT    THKCHG     ORIEN
      .100
$   USRSTR    USRFAC     NSBCS    INTERM     XPENE
         0         0        10         0     4.000
*CONTROL_ENERGY
$     HGEN      RWEN    SLNTEN     RYLEN
         2         2         2         2
*CONTROL_OUTPUT
$    NPOPT    NEECHO    NREFUP    IACCOP     OPIFS    IPNINT    IKEDIT
         0         0         0         0      .000         0       100
$---+----1----+----2----+----3----+----4----+----5----+----6----+----7----+----8
*DAMPING_GLOBAL
$     lcid    valdmp       stx       sty       stz       srx       sry       srz
         0        50       0.0       0.0       0.0       0.0       0.0       0.0
$
```

```
$---+----1----+----2----+----3----+----4----+----5----+----6----+----7----+----8
$                    (3) DATABASE CONTROL CARDS - ASCII HISTORY FILE
$---+----1----+----2----+----3----+----4----+----5----+----6----+----7----+----8
$*DATABASE_HISTORY_OPTION
$      ID1       ID2       ID3       ID4       ID5       ID6       ID7       ID8
$
$OPTION : BEAM    BEAM_SET   NODE   NODE_SET
$         SHELL   SHELL_SET  SOLID  SOLID_SET
$         TSHELL  TSHELL_SET
$---+----1----+----2----+----3----+----4----+----5----+----6----+----7----+----8
$                    (4) DATABASE CONTROL CARDS FOR ASCII FILE
$---+----1----+----2----+----3----+----4----+----5----+----6----+----7----+----8
$---+----1----+----2----+----3----+----4----+----5----+----6----+----7----+----8
$*DATABASE_OPTION
$       DT
$
$OPTION : SECFORC RWFORC NODOUT ELOUT  GLSTAT
$         DEFORC  MATSUM NCFORC RCFORC DEFGEO
$         SPCFORC SWFORC ABSTAT NODFOR BNDOUT
$         RBDOUT  GCEOUT SLEOUT MPGS   SBTOUT
$         JNTFORC AVSFLT MOVIE
*DATABASE_NODOUT
  .050E-02
*DATABASE_ELOUT
  .050E-02
*DATABASE_SPCFORC
  .050E-02
*DATABASE_GLSTAT
    0.0005
$---+----1----+----2----+----3----+----4----+----5----+----6----+----7----+----8
$                    (5) DATABASE CONTROL CARDS FOR BINARY FILE
$---+----1----+----2----+----3----+----4----+----5----+----6----+----7----+----8
*DATABASE_BINARY_D3PLOT
$  DT/CYCL      LCDT    NOBEAM
  .050E-02
*DATABASE_BINARY_D3THDT
$  DT/CYCL      LCDT    NOBEAM
  .050E-02
```

```
$*DATABASE_BINARY_OPTION
$  DT/CYCL      LCDT    NOBEAM
$
$OPTION : D3DRFL D3DUMP RUNRSF INTFOR
$---+----1----+----2----+----3----+----4----+----5----+----6----+----7----+----8
*DATABASE_EXTENT_BINARY
         0         0         3         0         1         1         1         1
         0         0         0         0         0         0
$---+----1----+----2----+----3----+----4----+----5----+----6----+----7----+----8
$
*MAT_SOIL_AND_FOAM
$      mid        ro         g      bulk        a0        a1        a2        pc
         1 2.22470-4 7.88000+5 6.00000+6   13333.3       0.0       0.0 -200.0000
$      vcr       ref
 0.0000000 0.0000000
$     eps1      eps2      eps3      eps4      eps5      eps6      eps7      eps8
 0.0000000-0.0200000-0.0377000-0.0418000-0.0513000-0.1000000-0.5000000 0.0000000
$     eps9     eps10
 0.0000000 0.0000000
$       p1        p2        p3        p4        p5        p6        p7        p8
 0.0000000 21000.000 34800.000 45000.000 58000.000 1.25000+5 9.44500+5 0.0000000
$       p9       p10
 0.0000000 0.0000000
$
$---+----1----+----2----+----3----+----4----+----5----+----6----+----7----+----8
*SECTION_SOLID
$    secid    elform
         1         1
*PART
Block
$      pid       sid       mid     eosid      hgid      grav    adpopt      tmid
         1         1         1         0         0         0         0         0
$
*NODE
       1 0.000000000E+00 0.000000000E+00 0.000000000E+00       0       0
       2 5.000000000E-01 0.000000000E+00 0.000000000E+00       0       0
       3 1.000000000E+00 0.000000000E+00 0.000000000E+00       0       0
       4 0.000000000E+00 4.765625298E-01 0.000000000E+00       0       0
```

```
       5 5.000000000E-01 4.765625298E-01 0.000000000E+00       0       0



*ELEMENT_SOLID
       1       1       1       2       5       4      52      53      56      55
       2       1       2       3       6       5      53      54      57      56
       3       1       4       5       8       7      55      56      59      58
       4       1       5       6       9       8      56      57      60      59
       5       1       7       8      11      10      58      59      62      61
       6       1       8       9      12      11      59      60      63      62
       7       1      10      11      14      13      61      62      65      64
       8       1      11      12      15      14      62      63      66      65
       9       1      13      14      17      16      64      65      68      67
      10       1      14      15      18      17      65      66      69      68



$
$---+----1----+----2----+----3----+----4----+----5----+----6----+----7----+----8
$                                                                             $
$                              LOAD SEGMENT CARDS                             $
$                                                                             $
$---+----1----+----2----+----3----+----4----+----5----+----6----+----7----+----8
*LOAD_SEGMENT_SET
$^SEGMENT
$     SSID      LCID        SF        AT
         1        -2         1         0
$---+----1----+----2----+----3----+----4----+----5----+----6----+----7----+----8
$                                                                             $
$                               LOAD BLAST CARDS                              $
$                                                                             $
$---+----1----+----2----+----3----+----4----+----5----+----6----+----7----+----8
*LOAD_BLAST
$^BLAST
$      WGT       XBO       YBO       ZBO       TBO     IUNIT     ISURF
```

```
    1.074       0.0       0.0     120.0                    3         1
$      CFM       CFL       CFT       CFP
       0.0       0.0       0.0       0.0
*DEFINE_CURVE
$     lcid      sidr       sfa       sfo      offa      offo
         1         0      .001       1.0 0.0000000 0.0000000
$---+----1----+----2----+----3----+----4----+----5----+----6----+----7----+----8
$     abcissa values     ordinate values
0.00                0.00
$0.06                15.21
$0.12                30.42
$0.18                45.64
$0.24                60.85
$0.30                76.06
$0.36                91.27
$0.42                106.48
$0.48                121.70
$0.54                136.91
$1.00                152.12
$1.06                167.33
$1.12                182.54
$1.18                197.76
$1.24                212.97
$1.30                228.18
$1.36                243.39
$1.42                258.60
$1.48                273.81
$1.54                289.02
2.00                304.24
2.06                290.79
2.12                277.92
2.18                265.62
2.30                242.61
2.42                221.57
2.54                202.33
2.66                184.74
2.79                168.66
2.91                153.97
```

3.03	140.53
3.15	128.26
3.27	117.04
3.39	106.79
3.51	97.43
3.63	88.87
3.75	81.06
3.87	73.92
3.99	67.40
4.11	61.45
4.24	56.01
4.36	51.05
4.48	46.52
4.60	42.39
4.72	38.61
4.84	35.17
4.96	32.03
5.08	29.16
5.20	26.55
5.32	24.16
5.44	21.99
5.56	20.01
5.69	18.20
5.81	16.55
5.93	15.05
6.05	13.68
6.17	12.43
6.29	11.30
6.41	10.26
6.53	9.32
6.65	8.46
6.77	7.68
6.89	6.97
7.01	6.32
7.14	5.74
7.26	5.20
7.38	4.71
7.50	4.27

7.62	3.87
7.74	3.50
7.86	3.17
7.98	2.87
8.10	2.60
8.22	2.35
8.34	2.12
8.46	1.92
8.59	1.73
8.71	1.56
8.83	1.41
8.95	1.27
9.07	1.14
9.19	1.03
9.31	0.93
9.43	0.83
9.55	0.75
9.67	0.67
9.79	0.60
9.91	0.54
10.04	0.49
10.16	0.43
10.28	0.39
10.40	0.31
10.64	0.28
10.76	0.25
10.88	0.22
11.00	0.19
11.12	0.17
11.24	0.15
11.36	0.13
11.49	0.12
11.61	0.10
11.73	0.09
11.85	0.08
11.97	0.07
12.09	0.06
12.21	0.05

```
12.33                0.05
12.45                0.04
12.57                0.03
12.69                0.03
12.81                0.02
12.94                0.02
13.06                0.02
13.18                0.01
13.30                0.01
13.42                0.01
13.54                0.01
13.66                0.00
13.78                0.00
13.90                0.00
14.02                0.00
100.00               0.00
$
*DEFINE_CURVE
$     lcid      sidr       sfa       sfo      offa      offo
         2         0      .001       1.0 0.0000000 0.0000000
$---+----1----+----2----+----3----+----4----+----5----+----6----+----7----+----8
$     abcissa values     ordinate values
0.00                 0.00
2.00                 190.38
2.06                 184.27
2.12                 178.36
2.18                 172.63
2.29                 161.71
2.41                 151.46
2.53                 141.85
2.64                 132.83
2.76                 124.38
2.88                 116.44
2.99                 109.00
3.11                 102.03
3.23                 95.48
3.34                 89.35
3.46                 83.60
```

3.58	78.21
3.69	73.16
3.81	68.42
3.93	63.99
4.04	59.83
4.16	55.93
4.28	52.28
4.39	48.86
4.51	45.66
4.63	42.66
4.74	39.85
4.86	37.21
4.98	34.75
5.09	32.45
5.21	30.29
5.33	28.27
5.45	26.38
5.56	24.61
5.68	22.95
5.80	21.40
5.91	19.95
6.03	18.60
6.15	17.33
6.26	16.15
6.38	15.04
6.50	14.01
6.61	13.04
6.73	12.14
6.85	11.29
6.96	10.50
7.08	9.77
7.20	9.08
7.31	8.44
7.43	7.84
7.55	7.28
7.66	6.76
7.78	6.27
7.90	5.82

8.01	5.39
8.13	5.00
8.25	4.63
8.36	4.29
8.48	3.97
8.60	3.67
8.72	3.39
8.83	3.14
8.95	2.90
9.07	2.67
9.18	2.47
9.30	2.27
9.42	2.09
9.53	1.93
9.65	1.77
9.77	1.63
9.88	1.50
10.00	1.37
10.12	1.26
10.23	1.15
10.35	1.05
10.47	0.96
10.58	0.88
10.70	0.80
10.82	0.72
10.93	0.66
11.05	0.60
11.17	0.54
11.28	0.49
11.40	0.44
11.52	0.39
11.63	0.35
11.75	0.31
11.87	0.28
11.99	0.25
12.10	0.22
12.22	0.19
12.34	0.17

```
12.45               0.14
12.57               0.12
12.69               0.10
12.80               0.09
12.92               0.07
13.04               0.06
13.15               0.04
13.27               0.03
13.39               0.02
13.50               0.01
13.62               0.00
13.74               0.00
13.85               0.00
13.97               0.00
14.09               0.00
100.00              0.00
$
*SET_SEGMENT
         1
$  No.of items in set =    512
         1         4         5         2
         2         5         6         3
         4         7         8         5
         5         8         9         6
         7        10        11         8
         8        11        12         9
        10        13        14        11
        11        14        15        12
        13        16        17        14
        14        17        18        15
        16        19        20        17
        17        20        21        18
        19        22        23        20
        20        23        24        21
        22        25        26        23
        23        26        27        24
        25        28        29        26
        26        29        30        27
```

28	31	32	29
29	32	33	30
31	34	35	32
32	35	36	33
34	37	38	35
35	38	39	36
37	40	41	38
38	41	42	39
40	43	44	41
41	44	45	42
43	46	47	44
44	47	48	45
46	49	50	47
47	50	51	48
3	6	1391	1378
1378	1391	1392	1379
1379	1392	1393	1380
1380	1393	1394	1381
1381	1394	1395	1382
1382	1395	1396	1383
1383	1396	1397	1384
1384	1397	1398	1385
1385	1398	1399	1386
1386	1399	1400	1387
1387	1400	1401	1388
1388	1401	1402	1389
1389	1402	1403	1390
6	9	1404	1391
1391	1404	1405	1392
1392	1405	1406	1393
1393	1406	1407	1394
1394	1407	1408	1395
1395	1408	1409	1396
1396	1409	1410	1397
1397	1410	1411	1398
1398	1411	1412	1399
1399	1412	1413	1400
1400	1413	1414	1401

```
1401      1414      1415      1402
1402      1415      1416      1403
   9        12      1417      1404
1404      1417      1418      1405
1405      1418      1419      1406
1406      1419      1420      1407
1407      1420      1421      1408
1408      1421      1422      1409
1409      1422      1423      1410
1410      1423      1424      1411
1411      1424      1425      1412
1412      1425      1426      1413
1413      1426      1427      1414
1414      1427      1428      1415
1415      1428      1429      1416
  12        15      1430      1417
1417      1430      1431      1418
1418      1431      1432      1419
1419      1432      1433      1420
1420      1433      1434      1421
1421      1434      1435      1422
1422      1435      1436      1423
1423      1436      1437      1424
1424      1437      1438      1425
1425      1438      1439      1426
1426      1439      1440      1427
1427      1440      1441      1428
1428      1441      1442      1429
  15        18      1443      1430
1430      1443      1444      1431
1431      1444      1445      1432
1432      1445      1446      1433
1433      1446      1447      1434
1434      1447      1448      1435
1435      1448      1449      1436
1436      1449      1450      1437
1437      1450      1451      1438
1438      1451      1452      1439
```

```
1439      1452      1453      1440
1440      1453      1454      1441
1441      1454      1455      1442
  18        21      1456      1443
1443      1456      1457      1444
1444      1457      1458      1445
1445      1458      1459      1446
1446      1459      1460      1447
1447      1460      1461      1448
1448      1461      1462      1449
1449      1462      1463      1450
1450      1463      1464      1451
1451      1464      1465      1452
1452      1465      1466      1453
1453      1466      1467      1454
1454      1467      1468      1455
  21        24      1469      1456
1456      1469      1470      1457
1457      1470      1471      1458
1458      1471      1472      1459
1459      1472      1473      1460
1460      1473      1474      1461
1461      1474      1475      1462
1462      1475      1476      1463
1463      1476      1477      1464
1464      1477      1478      1465
1465      1478      1479      1466
1466      1479      1480      1467
1467      1480      1481      1468
  24        27      1482      1469
1469      1482      1483      1470
1470      1483      1484      1471
1471      1484      1485      1472
1472      1485      1486      1473
1473      1486      1487      1474
1474      1487      1488      1475
1475      1488      1489      1476
1476      1489      1490      1477
```

1477	1490	1491	1478
1478	1491	1492	1479
1479	1492	1493	1480
1480	1493	1494	1481
27	30	1495	1482
1482	1495	1496	1483
1483	1496	1497	1484
1484	1497	1498	1485
1485	1498	1499	1486
1486	1499	1500	1487
1487	1500	1501	1488
1488	1501	1502	1489
1489	1502	1503	1490
1490	1503	1504	1491
1491	1504	1505	1492
1492	1505	1506	1493
1493	1506	1507	1494
30	33	1508	1495
1495	1508	1509	1496
1496	1509	1510	1497
1497	1510	1511	1498
1498	1511	1512	1499
1499	1512	1513	1500
1500	1513	1514	1501
1501	1514	1515	1502
1502	1515	1516	1503
1503	1516	1517	1504
1504	1517	1518	1505
1505	1518	1519	1506
1506	1519	1520	1507
33	36	1521	1508
1508	1521	1522	1509
1509	1522	1523	1510
1510	1523	1524	1511
1511	1524	1525	1512
1512	1525	1526	1513
1513	1526	1527	1514
1514	1527	1528	1515

1515	1528	1529	1516
1516	1529	1530	1517
1517	1530	1531	1518
1518	1531	1532	1519
1519	1532	1533	1520
36	39	1534	1521
1521	1534	1535	1522
1522	1535	1536	1523
1523	1536	1537	1524
1524	1537	1538	1525
1525	1538	1539	1526
1526	1539	1540	1527
1527	1540	1541	1528
1528	1541	1542	1529
1529	1542	1543	1530
1530	1543	1544	1531
1531	1544	1545	1532
1532	1545	1546	1533
39	42	1547	1534
1534	1547	1548	1535
1535	1548	1549	1536
1536	1549	1550	1537
1537	1550	1551	1538
1538	1551	1552	1539
1539	1552	1553	1540
1540	1553	1554	1541
1541	1554	1555	1542
1542	1555	1556	1543
1543	1556	1557	1544
1544	1557	1558	1545
1545	1558	1559	1546
42	45	1560	1547
1547	1560	1561	1548
1548	1561	1562	1549
1549	1562	1563	1550
1550	1563	1564	1551
1551	1564	1565	1552
1552	1565	1566	1553

1553	1566	1567	1554
1554	1567	1568	1555
1555	1568	1569	1556
1556	1569	1570	1557
1557	1570	1571	1558
1558	1571	1572	1559
45	48	1573	1560
1560	1573	1574	1561
1561	1574	1575	1562
1562	1575	1576	1563
1563	1576	1577	1564
1564	1577	1578	1565
1565	1578	1579	1566
1566	1579	1580	1567
1567	1580	1581	1568
1568	1581	1582	1569
1569	1582	1583	1570
1570	1583	1584	1571
1571	1584	1585	1572
48	51	1586	1573
1573	1586	1587	1574
1574	1587	1588	1575
1575	1588	1589	1576
1576	1589	1590	1577
1577	1590	1591	1578
1578	1591	1592	1579
1579	1592	1593	1580
1580	1593	1594	1581
1581	1594	1595	1582
1582	1595	1596	1583
1583	1596	1597	1584
1584	1597	1598	1585
1390	1403	4032	4030
4030	4032	4033	4031
1403	1416	4034	4032
4032	4034	4035	4033
1416	1429	4036	4034
4034	4036	4037	4035

1429	1442	4038	4036
4036	4038	4039	4037
1442	1455	4040	4038
4038	4040	4041	4039
1455	1468	4042	4040
4040	4042	4043	4041
1468	1481	4044	4042
4042	4044	4045	4043
1481	1494	4046	4044
4044	4046	4047	4045
1494	1507	4048	4046
4046	4048	4049	4047
1507	1520	4050	4048
4048	4050	4051	4049
1520	1533	4052	4050
4050	4052	4053	4051
1533	1546	4054	4052
4052	4054	4055	4053
1546	1559	4056	4054
4054	4056	4057	4055
1559	1572	4058	4056
4056	4058	4059	4057
1572	1585	4060	4058
4058	4060	4061	4059
1585	1598	4062	4060
4060	4062	4063	4061
4031	4033	5216	5203
5203	5216	5217	5204
5204	5217	5218	5205
5205	5218	5219	5206
5206	5219	5220	5207
5207	5220	5221	5208
5208	5221	5222	5209
5209	5222	5223	5210
5210	5223	5224	5211
5211	5224	5225	5212
5212	5225	5226	5213
5213	5226	5227	5214

5214	5227	5228	5215
4033	4035	5229	5216
5216	5229	5230	5217
5217	5230	5231	5218
5218	5231	5232	5219
5219	5232	5233	5220
5220	5233	5234	5221
5221	5234	5235	5222
5222	5235	5236	5223
5223	5236	5237	5224
5224	5237	5238	5225
5225	5238	5239	5226
5226	5239	5240	5227
5227	5240	5241	5228
4035	4037	5242	5229
5229	5242	5243	5230
5230	5243	5244	5231
5231	5244	5245	5232
5232	5245	5246	5233
5233	5246	5247	5234
5234	5247	5248	5235
5235	5248	5249	5236
5236	5249	5250	5237
5237	5250	5251	5238
5238	5251	5252	5239
5239	5252	5253	5240
5240	5253	5254	5241
4037	4039	5255	5242
5242	5255	5256	5243
5243	5256	5257	5244
5244	5257	5258	5245
5245	5258	5259	5246
5246	5259	5260	5247
5247	5260	5261	5248
5248	5261	5262	5249
5249	5262	5263	5250
5250	5263	5264	5251
5251	5264	5265	5252

5252	5265	5266	5253
5253	5266	5267	5254
4039	4041	5268	5255
5255	5268	5269	5256
5256	5269	5270	5257
5257	5270	5271	5258
5258	5271	5272	5259
5259	5272	5273	5260
5260	5273	5274	5261
5261	5274	5275	5262
5262	5275	5276	5263
5263	5276	5277	5264
5264	5277	5278	5265
5265	5278	5279	5266
5266	5279	5280	5267
4041	4043	5281	5268
5268	5281	5282	5269
5269	5282	5283	5270
5270	5283	5284	5271
5271	5284	5285	5272
5272	5285	5286	5273
5273	5286	5287	5274
5274	5287	5288	5275
5275	5288	5289	5276
5276	5289	5290	5277
5277	5290	5291	5278
5278	5291	5292	5279
5279	5292	5293	5280
4043	4045	5294	5281
5281	5294	5295	5282
5282	5295	5296	5283
5283	5296	5297	5284
5284	5297	5298	5285
5285	5298	5299	5286
5286	5299	5300	5287
5287	5300	5301	5288
5288	5301	5302	5289
5289	5302	5303	5290

5290	5303	5304	5291
5291	5304	5305	5292
5292	5305	5306	5293
4045	4047	5307	5294
5294	5307	5308	5295
5295	5308	5309	5296
5296	5309	5310	5297
5297	5310	5311	5298
5298	5311	5312	5299
5299	5312	5313	5300
5300	5313	5314	5301
5301	5314	5315	5302
5302	5315	5316	5303
5303	5316	5317	5304
5304	5317	5318	5305
5305	5318	5319	5306
4047	4049	5320	5307
5307	5320	5321	5308
5308	5321	5322	5309
5309	5322	5323	5310
5310	5323	5324	5311
5311	5324	5325	5312
5312	5325	5326	5313
5313	5326	5327	5314
5314	5327	5328	5315
5315	5328	5329	5316
5316	5329	5330	5317
5317	5330	5331	5318
5318	5331	5332	5319
4049	4051	5333	5320
5320	5333	5334	5321
5321	5334	5335	5322
5322	5335	5336	5323
5323	5336	5337	5324
5324	5337	5338	5325
5325	5338	5339	5326
5326	5339	5340	5327
5327	5340	5341	5328

5328	5341	5342	5329
5329	5342	5343	5330
5330	5343	5344	5331
5331	5344	5345	5332
4051	4053	5346	5333
5333	5346	5347	5334
5334	5347	5348	5335
5335	5348	5349	5336
5336	5349	5350	5337
5337	5350	5351	5338
5338	5351	5352	5339
5339	5352	5353	5340
5340	5353	5354	5341
5341	5354	5355	5342
5342	5355	5356	5343
5343	5356	5357	5344
5344	5357	5358	5345
4053	4055	5359	5346
5346	5359	5360	5347
5347	5360	5361	5348
5348	5361	5362	5349
5349	5362	5363	5350
5350	5363	5364	5351
5351	5364	5365	5352
5352	5365	5366	5353
5353	5366	5367	5354
5354	5367	5368	5355
5355	5368	5369	5356
5356	5369	5370	5357
5357	5370	5371	5358
4055	4057	5372	5359
5359	5372	5373	5360
5360	5373	5374	5361
5361	5374	5375	5362
5362	5375	5376	5363
5363	5376	5377	5364
5364	5377	5378	5365
5365	5378	5379	5366

5366	5379	5380	5367
5367	5380	5381	5368
5368	5381	5382	5369
5369	5382	5383	5370
5370	5383	5384	5371
4057	4059	5385	5372
5372	5385	5386	5373
5373	5386	5387	5374
5374	5387	5388	5375
5375	5388	5389	5376
5376	5389	5390	5377
5377	5390	5391	5378
5378	5391	5392	5379
5379	5392	5393	5380
5380	5393	5394	5381
5381	5394	5395	5382
5382	5395	5396	5383
5383	5396	5397	5384
4059	4061	5398	5385
5385	5398	5399	5386
5386	5399	5400	5387
5387	5400	5401	5388
5388	5401	5402	5389
5389	5402	5403	5390
5390	5403	5404	5391
5391	5404	5405	5392
5392	5405	5406	5393
5393	5406	5407	5394
5394	5407	5408	5395
5395	5408	5409	5396
5396	5409	5410	5397
4061	4063	5411	5398
5398	5411	5412	5399
5399	5412	5413	5400
5400	5413	5414	5401
5401	5414	5415	5402
5402	5415	5416	5403
5403	5416	5417	5404

5404	5417	5418	5405
5405	5418	5419	5406
5406	5419	5420	5407
5407	5420	5421	5408
5408	5421	5422	5409
5409	5422	5423	5410
5215	5228	7857	7855
7855	7857	7858	7856
5228	5241	7859	7857
7857	7859	7860	7858
5241	5254	7861	7859
7859	7861	7862	7860
5254	5267	7863	7861
7861	7863	7864	7862
5267	5280	7865	7863
7863	7865	7866	7864
5280	5293	7867	7865
7865	7867	7868	7866
5293	5306	7869	7867
7867	7869	7870	7868
5306	5319	7871	7869
7869	7871	7872	7870
5319	5332	7873	7871
7871	7873	7874	7872
5332	5345	7875	7873
7873	7875	7876	7874
5345	5358	7877	7875
7875	7877	7878	7876
5358	5371	7879	7877
7877	7879	7880	7878
5371	5384	7881	7879
7879	7881	7882	7880
5384	5397	7883	7881
7881	7883	7884	7882
5397	5410	7885	7883
7883	7885	7886	7884
5410	5423	7887	7885
7885	7887	7888	7886

```
$
$*LOAD_SEGMENT_SET
$     ssid      lcid        sf        at
$         1         1         1       0.0
$
*END
```

APPENDIX B

INPUT FILE FOR THE MAT_BRITTLE_DAMAGE CONSTITUTIVE MODEL

```
$$ BRITTLE_DAMAGE
$$
*KEYWORD
*TITLE
Single CMU: 15 5/8" x 7 5/8" x 7 5/8" (no backing material)
$500lb ANFO at 20 ft
$---+----1----+----2----+----3----+----4----+----5----+----6----+----7----+----8
*CONTROL_TERMINATION
$   ENDTIM    ENDCYC     DTMIN    ENDNEG    ENDMAS
  .015E+00         0      .000      .000      .000
*CONTROL_TIMESTEP
$   DTINIT      SCFT      ISDO    TSLIMT      DTMS      LCTM     ERODE     MS1ST
   0.0E-00      .670         0
*CONTROL_HOURGLASS
$      IHQ        QH
         1      .100
*CONTROL_BULK_VISCOSITY
$       Q2        Q1
     1.500      .060
*CONTROL_SHELL
$   WRPANG    ITRIST     IRNXX    ISTUPD    THEORY       BWC     MITER
    20.000         2        -1         0         2         2         1
*CONTROL_CONTACT
$   SLSFAC    RWPNAL    ISLCHK    SHLTHK    PENOPT    THKCHG     ORIEN
      .100
$   USRSTR    USRFAC     NSBCS    INTERM     XPENE
         0         0        10         0     4.000
*CONTROL_ENERGY
$     HGEN      RWEN    SLNTEN     RYLEN
         2         2         2         2
*CONTROL_OUTPUT
$    NPOPT    NEECHO    NREFUP    IACCOP     OPIFS    IPNINT    IKEDIT
         0         0         0         0      .000         0       100
$---+----1----+----2----+----3----+----4----+----5----+----6----+----7----+----8
*DAMPING_GLOBAL
$     lcid    valdmp       stx       sty       stz       srx       sry       srz
         0        50       0.0       0.0       0.0       0.0       0.0       0.0
$
```

```
$---+----1----+----2----+----3----+----4----+----5----+----6----+----7----+----8
$                    (3) DATABASE CONTROL CARDS - ASCII HISTORY FILE
$---+----1----+----2----+----3----+----4----+----5----+----6----+----7----+----8
$*DATABASE_HISTORY_OPTION
$      ID1       ID2       ID3       ID4       ID5       ID6       ID7       ID8
$
$OPTION : BEAM    BEAM_SET   NODE   NODE_SET
$         SHELL   SHELL_SET  SOLID  SOLID_SET
$         TSHELL  TSHELL_SET
$---+----1----+----2----+----3----+----4----+----5----+----6----+----7----+----8
$                    (4) DATABASE CONTROL CARDS FOR ASCII FILE
$---+----1----+----2----+----3----+----4----+----5----+----6----+----7----+----8
$---+----1----+----2----+----3----+----4----+----5----+----6----+----7----+----8
$*DATABASE_OPTION
$       DT
$
$OPTION : SECFORC RWFORC NODOUT ELOUT  GLSTAT
$         DEFORC  MATSUM NCFORC RCFORC DEFGEO
$         SPCFORC SWFORC ABSTAT NODFOR BNDOUT
$         RBDOUT  GCEOUT SLEOUT MPGS   SBTOUT
$         JNTFORC AVSFLT MOVIE
*DATABASE_NODOUT
  .050E-02
*DATABASE_ELOUT
  .050E-02
*DATABASE_SPCFORC
  .050E-02
*DATABASE_GLSTAT
    0.0005
$---+----1----+----2----+----3----+----4----+----5----+----6----+----7----+----8
$                    (5) DATABASE CONTROL CARDS FOR BINARY FILE
$---+----1----+----2----+----3----+----4----+----5----+----6----+----7----+----8
*DATABASE_BINARY_D3PLOT
$  DT/CYCL      LCDT    NOBEAM
  .050E-02
*DATABASE_BINARY_D3THDT
$  DT/CYCL      LCDT    NOBEAM
  .050E-02
```

```
$*DATABASE_BINARY_OPTION
$  DT/CYCL      LCDT    NOBEAM
$
$OPTION : D3DRFL D3DUMP RUNRSF INTFOR
$---+----1----+----2----+----3----+----4----+----5----+----6----+----7----+----8
*DATABASE_EXTENT_BINARY
         0         0         3         0         1         1         1         1
         0         0         0         0         0         0
$---+----1----+----2----+----3----+----4----+----5----+----6----+----7----+----8
$
$---+----1----+----2----+----3----+----4----+----5----+----6----+----7----+----8
*MAT_BRITTLE_DAMAGE
$^M-1
$      MID        RO         E        PR    TLIMIT    SLIMIT    FTOUGH    SRETEN
         1 0.00022247 2000000.0      0.15     200.0     100.0      0.80     0.030
$     VISC    FRA_RF      E_RF     YS_RF     EH_RF     FS_RF      SIGY
     104.0       0.0       0.0       0.0       0.0       0.0         0
$
$
$---+----1----+----2----+----3----+----4----+----5----+----6----+----7----+----8
*SECTION_SOLID
$    secid    elform
         1         1
*PART
Block
$      pid       sid       mid     eosid      hgid      grav    adpopt      tmid
         1         1         1         0         0         0         0         0
$
*NODE
```

APPENDIX C

INPUT FILE FOR THE MAT_PSEUDO_TENSOR CONSTITUTIVE MODEL

```
$$ PSEUDOTENSOR
$$
*KEYWORD
*TITLE
Single CMU: 15 5/8" x 7 5/8" x 7 5/8" (no backing material)
$500lb ANFO at 20 ft
$---+----1----+----2----+----3----+----4----+----5----+----6----+----7----+----8
*CONTROL_TERMINATION
$   ENDTIM    ENDCYC     DTMIN    ENDNEG    ENDMAS
  .025E+00         0      .000      .000      .000
*CONTROL_TIMESTEP
$   DTINIT      SCFT      ISDO    TSLIMT      DTMS      LCTM     ERODE     MS1ST
   0.0E-00      .670         0
*CONTROL_HOURGLASS
$      IHQ        QH
         1      .100
*CONTROL_BULK_VISCOSITY
$       Q2        Q1
     1.500      .060
*CONTROL_SHELL
$   WRPANG    ITRIST     IRNXX    ISTUPD    THEORY       BWC     MITER
    20.000         2        -1         0         2         2         1
*CONTROL_CONTACT
$   SLSFAC    RWPNAL    ISLCHK    SHLTHK    PENOPT    THKCHG     ORIEN
      .100
$   USRSTR    USRFAC     NSBCS    INTERM     XPENE
         0         0        10         0     4.000
*CONTROL_ENERGY
$     HGEN      RWEN    SLNTEN     RYLEN
         2         2         2         2
*CONTROL_OUTPUT
$    NPOPT    NEECHO    NREFUP    IACCOP     OPIFS    IPNINT    IKEDIT
         0         0         0         0      .000         0       100
$---+----1----+----2----+----3----+----4----+----5----+----6----+----7----+----8
*DAMPING_GLOBAL
$     lcid    valdmp       stx       sty       stz       srx       sry       srz
         0        50       0.0       0.0       0.0       0.0       0.0       0.0
$
```

```
$---+----1----+----2----+----3----+----4----+----5----+----6----+----7----+----8
$                    (3) DATABASE CONTROL CARDS - ASCII HISTORY FILE
$---+----1----+----2----+----3----+----4----+----5----+----6----+----7----+----8
$*DATABASE_HISTORY_OPTION
$      ID1       ID2       ID3       ID4       ID5       ID6       ID7       ID8
$
$OPTION : BEAM    BEAM_SET   NODE   NODE_SET
$         SHELL   SHELL_SET  SOLID  SOLID_SET
$         TSHELL  TSHELL_SET
$---+----1----+----2----+----3----+----4----+----5----+----6----+----7----+----8
$                    (4) DATABASE CONTROL CARDS FOR ASCII FILE
$---+----1----+----2----+----3----+----4----+----5----+----6----+----7----+----8
$---+----1----+----2----+----3----+----4----+----5----+----6----+----7----+----8
$*DATABASE_OPTION
$       DT
$
$OPTION : SECFORC RWFORC NODOUT ELOUT  GLSTAT
$         DEFORC  MATSUM NCFORC RCFORC DEFGEO
$         SPCFORC SWFORC ABSTAT NODFOR BNDOUT
$         RBDOUT  GCEOUT SLEOUT MPGS   SBTOUT
$         JNTFORC AVSFLT MOVIE
*DATABASE_NODOUT
  .050E-02
*DATABASE_ELOUT
  .050E-02
*DATABASE_SPCFORC
  .050E-02
*DATABASE_GLSTAT
    0.0005
$---+----1----+----2----+----3----+----4----+----5----+----6----+----7----+----8
$                    (5) DATABASE CONTROL CARDS FOR BINARY FILE
$---+----1----+----2----+----3----+----4----+----5----+----6----+----7----+----8
*DATABASE_BINARY_D3PLOT
$  DT/CYCL      LCDT    NOBEAM
  .050E-02
*DATABASE_BINARY_D3THDT
$  DT/CYCL      LCDT    NOBEAM
  .050E-02
```

```
$*DATABASE_BINARY_OPTION
$  DT/CYCL      LCDT    NOBEAM
$
$OPTION : D3DRFL D3DUMP RUNRSF INTFOR
$---+----1----+----2----+----3----+----4----+----5----+----6----+----7----+----8
*DATABASE_EXTENT_BINARY
         0         0         3         0         1         1         1         1
         0         0         0         0         0         0
$---+----1----+----2----+----3----+----4----+----5----+----6----+----7----+----8
$
*MAT_PSEUDO_TENSOR
$      mid        ro         g        pr
         1 0.0002247  833333.0      0.20
$     sigf        a0        a1        a2       a0f       a1f        b1       per
    2000.0        -1
$       er       prr      sigy      etan       lcp       lcr

$       x1        x2        x3        x4        x5        x6        x7        x8

$       x9       x10       x11       x12       x13       x14       x15       x16

$      ys1       ys2       ys3       ys4       ys5       ys6       ys7       ys8

$      ys9      ys10      ys11      ys12      ys13      ys14      ys15      ys16

$
*SECTION_SOLID
$    secid    elform
         1         1
*PART
Block
$      pid       sid       mid     eosid      hgid      grav    adpopt      tmid
         1         1         1         0         0         0         0         0
$
*NODE
```

APPENDIX D

INPUT FILE FOR THE MAT_WINFRITH_CONCRETE CONSTITUTIVE MODEL

```
$$ WINFRITH CONCRETE
$$
*KEYWORD
*TITLE
Single CMU: 15 5/8" x 7 5/8" x 7 5/8" (no backing material)
$500lb ANFO at 30 ft
$---+----1----+----2----+----3----+----4----+----5----+----6----+----7----+----8
*CONTROL_TERMINATION
$   ENDTIM    ENDCYC     DTMIN    ENDNEG    ENDMAS
  .020E+00         0      .000      .000      .000
*CONTROL_TIMESTEP
$   DTINIT      SCFT      ISDO    TSLIMT      DTMS      LCTM     ERODE     MS1ST
   0.0E-00       .67         0
*CONTROL_HOURGLASS
$      IHQ        QH
         1      .100
*CONTROL_BULK_VISCOSITY
$       Q2        Q1
     1.500      .060
*CONTROL_SHELL
$   WRPANG    ITRIST     IRNXX    ISTUPD    THEORY       BWC     MITER
    20.000         2        -1         0         2         2         1
*CONTROL_CONTACT
$   SLSFAC    RWPNAL    ISLCHK    SHLTHK    PENOPT    THKCHG     ORIEN
      .100
$   USRSTR    USRFAC     NSBCS    INTERM     XPENE
         0         0        10         0     4.000
*CONTROL_ENERGY
$     HGEN      RWEN    SLNTEN     RYLEN
         2         2         2         2
*CONTROL_OUTPUT
$    NPOPT    NEECHO    NREFUP    IACCOP     OPIFS    IPNINT    IKEDIT
         0         0         0         0      .000         0       100
$---+----1----+----2----+----3----+----4----+----5----+----6----+----7----+----8
*DAMPING_GLOBAL
$     lcid    valdmp       stx       sty       stz       srx       sry       srz
         0        50       0.0       0.0       0.0       0.0       0.0       0.0
$
```

```
$---+----1----+----2----+----3----+----4----+----5----+----6----+----7----+----8
$                    (3) DATABASE CONTROL CARDS - ASCII HISTORY FILE
$---+----1----+----2----+----3----+----4----+----5----+----6----+----7----+----8
$*DATABASE_HISTORY_OPTION
$      ID1       ID2       ID3       ID4       ID5       ID6       ID7       ID8
$
$OPTION : BEAM    BEAM_SET   NODE   NODE_SET
$         SHELL   SHELL_SET  SOLID  SOLID_SET
$         TSHELL  TSHELL_SET
$---+----1----+----2----+----3----+----4----+----5----+----6----+----7----+----8
$                    (4) DATABASE CONTROL CARDS FOR ASCII FILE
$---+----1----+----2----+----3----+----4----+----5----+----6----+----7----+----8
$---+----1----+----2----+----3----+----4----+----5----+----6----+----7----+----8
$*DATABASE_OPTION
$       DT
$
$OPTION : SECFORC RWFORC NODOUT ELOUT  GLSTAT
$         DEFORC  MATSUM NCFORC RCFORC DEFGEO
$         SPCFORC SWFORC ABSTAT NODFOR BNDOUT
$         RBDOUT  GCEOUT SLEOUT MPGS   SBTOUT
$         JNTFORC AVSFLT MOVIE
*DATABASE_NODOUT
  .050E-02
*DATABASE_ELOUT
  .050E-02
*DATABASE_SPCFORC
  .050E-02
*DATABASE_GLSTAT
    0.0005
$---+----1----+----2----+----3----+----4----+----5----+----6----+----7----+----8
$                    (5) DATABASE CONTROL CARDS FOR BINARY FILE
$---+----1----+----2----+----3----+----4----+----5----+----6----+----7----+----8
*DATABASE_BINARY_D3PLOT
$  DT/CYCL      LCDT    NOBEAM
  .050E-02
*DATABASE_BINARY_D3THDT
$  DT/CYCL      LCDT    NOBEAM
  .050E-02
```

```
$*DATABASE_BINARY_OPTION
$  DT/CYCL      LCDT    NOBEAM
$
$OPTION : D3DRFL D3DUMP RUNRSF INTFOR
$---+----1----+----2----+----3----+----4----+----5----+----6----+----7----+----8
*DATABASE_EXTENT_BINARY
         0         0         3         0         1         1         1         1
         0         0         0         0         0         0
$---+----1----+----2----+----3----+----4----+----5----+----6----+----7----+----8
$
*MAT_WINFRITH_CONCRETE
$      mid        ro        tm        pr       ucs       uts        fe     asize
         1 2.22470-4 3000000.0       0.20    2000.0     200.0       .15    0.0625
$        e        ys        eh    uelong      rate      conm      conl      cont
     30.+6   60000.0      4.+7     0.003       1.0        -1
$     eps1      eps2      eps3      eps4      eps5      eps6      eps7      eps8
$ 0.0000000 0.0200000 0.0377000 0.0418000 0.0513000 0.1000000 0.5000000 0.0000000

$       p1        p2        p3        p4        p5        p6        p7        p8
$ 0.0000000 210.00000 348.00000 450.00000 580.00000 1.25000+3 9.44500+3 0.0000000

$---+----1----+----2----+----3----+----4----+----5----+----6----+----7----+----8
*SECTION_SOLID
$    secid    elform
         1         1
*PART
Block
$      pid       sid       mid     eosid      hgid      grav    adpopt      tmid
         1         1         1         0         0         0         0         0
$
*NODE
```

APPENDIX E

CALCULATIONS AND MISCELLANEOUS ANALYSIS

SINGLE CMU: 15 5/8" X 7 5/8" X 7 5/8" (NO BACKING MATERIAL)
ls-dyna (version 960) date 01/28/2002

r e s u l t s o f e i g e n v a l u e a n a l y s i s:
Problem time = 1.50000E-02
(all frequencies de-shifted)
Frequencies of modes:

Number = 1: (radians)= -0.44046E+02 (hertz)= -0.70102E+01 period= -0.14265E+00
Number = 2: (radians)= -0.37413E+02 (hertz)= -0.59545E+01 period= -0.16794E+00
Number = 3: (radians)= -0.19631E+02 (hertz)= -0.31243E+01 period= -0.32007E+00
Number = 4: (radians)= -0.12670E+02 (hertz)= -0.20165E+01 period= -0.49591E+00
Number = 5: (radians)= 0.16948E+02 (hertz)= 0.26974E+01 period= 0.37073E+00
Number = 6: (radians)= 0.41999E+02 (hertz)= 0.66843E+01 period= 0.14960E+00
Number = 7: (radians)= 0.27251E+04 (hertz)= 0.43372E+03 period= 0.23057E-02
Number = 8: (radians)= 0.28590E+04 (hertz)= 0.45502E+03 period= 0.21977E-02
Number = 9: (radians)= 0.34253E+04 (hertz)= 0.54516E+03 period= 0.18343E-02
Number = 10: (radians)= 0.56944E+04 (hertz)= 0.90629E+03 period= 0.11034E-02
Number = 11: (radians)= 0.74593E+04 (hertz)= 0.11872E+04 period= 0.84233E-03
Number = 12: (radians)= 0.86001E+04 (hertz)= 0.13688E+04 period= 0.73059E-03
Number = 13: (radians)= 0.88491E+04 (hertz)= 0.14084E+04 period= 0.71004E-03
Number = 14: (radians)= 0.92573E+04 (hertz)= 0.14734E+04 period= 0.67872E-03
Number = 15: (radians)= 0.98423E+04 (hertz)= 0.15665E+04 period= 0.63839E-03
Number = 16: (radians)= 0.10413E+05 (hertz)= 0.16573E+04 period= 0.60338E-03
Number = 17: (radians)= 0.11156E+05 (hertz)= 0.17755E+04 period= 0.56321E-03
Number = 18: (radians)= 0.11974E+05 (hertz)= 0.19057E+04 period= 0.52474E-03

Damping Ratio for Single CMU

Weight = 32 lb
E = 2,000,000 psi
Volume = 15.625” x 7.625” x 7.625” – 2(7.625”)(5.625”)(15.625”/2 – 1” - 0.5”)
= 367.0 in^3

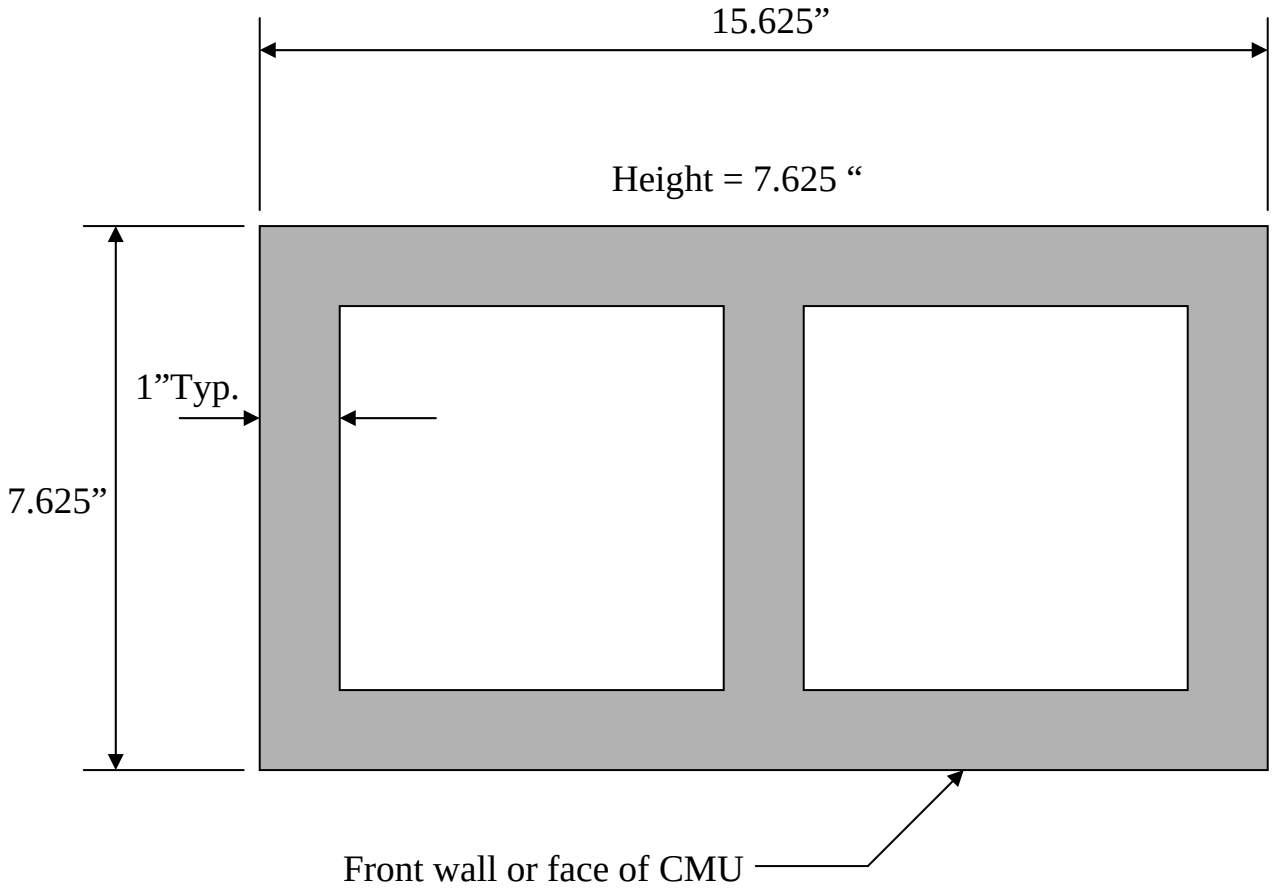

As shown in Section 4.2 of the text, the first six modes of the CMU are rigid body modes. Mode 7 is a bending mode of the four corners, while mode 8 is a torsional mode. Both are due to the flexibility of the four corners of the CMU. Mode 9 shows bending of the front and back walls of the CMU. Damping ratios are calculated for all three modes.

Biggs and Fintel provide a formula for critical damping as:

$C_{cr} = 2\ \omega_{min}\ M$ $\quad$ $M = 32\ lb / 386.4\ in/sec^2 = 0.083\ lb.sec^2/in$

Mode #7	$\omega = 2725$ rad/sec	$C_{cr} = 452.35$
Mode #8	$\omega = 2859$ rad/sec	$C_{cr} = 474.59$
Node #9	$\omega = 3425$ rad/sec	$C_{cr} = 568.55$

β = Damping Ratio = C/C_{cr}

Fintel recommends β to range from 0.02 to 0.20 for most civil engineering structures. Other references and tests on reinforced concrete structures indicate lower values of 0.01 to 0.03.

$\beta = 0.01$	C = 4.5 – 5.7
$\beta = 0.05$	C = 22.5 – 28.4
$\beta = 0.1$	C = 45.2 – 56.9
$\beta = 0.15$	C = 67.8 – 85.2
$\beta = 0.20$	C = 90.4-113.8

NOTICE

Using Government drawings, specifications, or other data included in this document for any purpose other than Government procurement does not in any way obligate the U.S. Government. The fact that the Government formulated or supplied the drawings, specifications, or other data does not license the holder or any other person or corporation; or convey any rights or permission to manufacture, use, or sell any patented invention that may relate to them.

This technical report was reviewed and cleared for public release by the Air Force Research Laboratory Tyndall Site (AFRL/MLQ) Public Affairs Office (PAO) and is releasable to the National Technical Information Service (NTIS). Reference PAO Case Number:

This report is releasable to the National Technical Information Service (NTIS) where it will be available to the general public, including foreign nationals.

5285 Port Royal Road
Springfield VA 22161
Telephone (703) 487-4650, (703) 487-4639 (TDD for the hearing impaired)
e-mail: orders@ntis.fedworld.gov
http://www.ntis.gov/index.html

This technical report is approved for publication.

/s/
ELIZABETH TRAWINSKI, 1st Lt, USAF
Work Unit Manager

/s/
AL D. NEASE
Chief, Force Protection Branch

/s/
JIMMY L. POLLARD, Colonel, USAF
Chief, Airbase Technologies Division

This report is published in the interest of scientific and technical information exchange and its publication does not constitute the Government's approval or disapproval of its ideas or findings.